ISSN 1408-7073

RMZ – MATERIALS AND GEOENVIRONMENT

PERIODICAL FOR MINING, METALLURGY AND GEOLOGY

RMZ – MATERIALI IN GEOOKOLJE

REVIJA ZA RUDARSTVO, METALURGIJO IN GEOLOGIJO

RMZ-M&G, Vol. 57, No. 4 pp. 441–584 (2010)

Ljubljana, December 2010

Historical Rewiev

More than 80 years have passed since in 1919 the University Ljubljana in Slovenia was founded. Technical fields were joint in the School of Engineering that included the Geologic and Mining Division while the Metallurgy Division was established in 1939 only. Today the Departments of Geology, Mining and Geotechnology, Materials and Metallurgy are part of the Faculty of Natural Sciences and Engineering, University of Ljubljana.

Before War II the members of the Mining Section together with the Association of Yugoslav Mining and Metallurgy Engineers began to publish the summaries of their research and studies in their technical periodical Rudarski zbornik (Mining Proceedings). Three volumes of Rudarski zbornik (1937, 1938 and 1939) were published. The War interrupted the publication and not untill 1952 the first number of the new journal Rudarsko-metalurški zbornik - RMZ (Mining and Metallurgy Quarterly) has been published by the Division of Mining and Metallurgy, University of Ljubljana. Later the journal has been regularly published quarterly by the Departments of Geology, Mining and Geotechnology, Materials and Metallurgy, and the Institute for Mining, Geotechnology and Environment.

On the meeting of the Advisory and the Editorial Board on May 22nd 1998 Rudarsko-metalurški zbornik has been renamed into "RMZ - Materials and Geoenvironment (RMZ -Materiali in Geookolje)" or shortly RMZ - M&G.

RMZ - M&G is managed by an international advisory and editorial board and is exchanged with other world-known periodicals. All the papers are reviewed by the corresponding professionals and experts.

RMZ - M&G is the only scientific and professional periodical in Slovenia, which is published in the same form nearly 50 years. It incorporates the scientific and professional topics in geology, mining, and geotechnology, in materials and in metallurgy.

The wide range of topics inside the geosciences are wellcome to be published in the RMZ -Materials and Geoenvironment. Research results in geology, hydrogeology, mining, geotechnology, materials, metallurgy, natural and antropogenic pollution of environment, biogeochemistry are proposed fields of work which the journal will handle. RMZ - M&G is co-issued and co-financed by the Faculty of Natural Sciences and Engineering Ljubljana, and the Institute for Mining, Geotechnology and Environment Ljubljana. In addition it is financially supported also by the Ministry of Higher Education, Science and Technology of Republic of Slovenia.

Editor in chief

Table of Contents – Kazalo

Original Scientific Papers – Izvirni znanstveni članki

Professional Papers – Strokovni članki

Comparison between Sn–Ni–Zn liquid phase thermodynamic assessments performed by the CALPHAD method and by geometrical models

Primerjava med termodinamskim ovrednotenjem taline Sn–Ni–Zn z metodo CALPHAD in geometrijskimi modeli

V. Gandova [1], J. Romanowska[2], G. Vassilev [1,*]

[1]University of Plovdiv, Faculty of Chemistry, Plovdiv, Bulgaria
[2]Technical University of Rzeszow, Rzeszow, Poland

*Corresponding author. E-mail: gpvassilev@gmail.com

Received: May 25, 2010 **Accepted:** September 1, 2010

Abstract: Estimation of the thermodynamic properties of the Sn–Ni–Zn systems has been performed using the general solution model and by other geometric models. Description of the ternary liquid phase (Gibbs excess energy dependence on the temperature and the composition) was achieved using the available thermodynamic data of the constitutive binary systems (Ni–Zn, Sn–Zn, Sn–Ni). The validity of the geometric models was checked. The calculations have been performed in a wide temperature range (1000–2000 K). The calculated quantities were compared with the available literature data. Good agreement of the present assessment with thermodynamically optimized values of the system Sn–Ni–Zn (obtained by the CALPHAD approach) was observed.

Povzetek: Termodinamske lastnosti sistema Sn–Ni–Zn smo ovrednotili z uporabo splošnega modela raztopin in z drugimi geometrijskimi modeli. Ternarno talino (odvisnost presežne Gibbsove energije od temperature in kemijske sestave) smo opisali z uporabo dostopnih termodinamskih podatkov iz robnih binarnih sistemov (Ni–Sn, Sn–Zn in Sn–Ni). Preverili smo tudi veljavnost geometrijskih modelov. Izračune smo izvedli v širokem temperaturnem območju (1000−2000 K). Izračunane vrednosti smo primerjali s podatki iz literature. Rezultati tega ovrednotenja se dobro ujemajo s termodi-

Original scientific paper

namsko optimiranimi vrednostmi za sistem Sn–Ni–Zn, izračunanimi po metodi CALPHAD.

Key words: Sn–Ni–Zn system, liquid phase thermodynamics, general solution model, ternary interaction parameters
Ključne besede: sistem Sn–Ni–Zn, termodinamika talin, splošni model raztopin, ternarni interakcijski parametri

INTRODUCTION

The Sn–Ni–Zn system is interesting as a potential lead-free solder material because of the termination of lead-containing solders industrial application is envisaged, due to the high lead toxicity. That is why the development of lead-free solders is a current task. These materials are expected to be designed on the bases of systems including low-melting elements like tin alloyed with zinc or/and bismuth. On the other side, nickel metallization often appears as intrinsic part of the electronic devices. Thus, investigations on a number of related solder/nickel systems and the corresponding properties were reported in the literature[1, 2] but the thermodynamics of the system is still unknown.

The border-systems Ni–Sn[3–5] and Ni–Zn[6–10] are complex but they have been studied intensively. The binary system Sn–Zn presents a simple eutectic reaction.[11] These systems are included in the thermodynamic database developed by the European concerted action COST 531 and reliable thermodynamic optimizations are available for them.[12] Nevertheless, there is no data about the thermochemical properties of the ternary liquid phase required for further thermodynamic optimization of the system Sn–Ni–Zn. Thus, the task of the present study is to apply different ways to assess the thermochemical properties of the ternary melt Sn–Ni–Zn.

THEORETICAL FUNDAMENTALS OF THE ASSESSMENTS

The so called "geometric models" give the possibility to predict the thermodynamic properties of a ternary phase (in this case – liquid) using data belonging to the respective binary border systems. In this work, assessments were made by means of the most common classic geometric models of KOHLER,[13] MUGGIANU,[14] TOOP[15] and HILLERT[16] as well as by the newly-developed but prominent, general solution model (GSM) developed by CHOU.[17, 18]

HILLERT[16] classified the geometric models as symmetrical (e.g.[13, 14]) and asymmetrical (e.g.[15, 16]) while looking for a more universal approach to

ternary properties prediction. Such a universal approach was recently developed by CHOU[17, 18] and successfully employed in a variety of cases (e.g. ref. [19–22]). Nevertheless, a brief description of the techniques used shall be done below.

As usually, the molar excess Gibbs energy (ΔG^E/(J mol^{-1})) of the ternary liquid phase was chosen as a parameter which values had to be calculated by various models and compared. This quantity describes the contribution of the non-ideal mixing to the thermodynamic properties of a solution phase. The molar excess Gibbs energies values of all binary border-system (at a certain temperature and at specific compositions) are needed as starting points. These quantities were calculated by means of Thermocalc software package, using optimized parameters recently selected as result of the European concerted action for development of lead-free solders COST 531.[12]

In agreement with Redlich-Kister formalism, the composition dependence of the binary Gibbs molar excess energies (ΔG_{ij}^E) is given by the expression:

$$\Delta G_{ij}^E = X_i X_j (A_{ij}^0 + A_{ij}^1 (X_i - X_j) + A_{ij}^2 (X_i - X_j)^2 + ... + A_{ij}^n (X_i - X_j)^2) \quad (1)$$

Here, A^o_{ij}, A^1_{ij}, A^2_{ij} are adjustable temperature dependent parameters belonging to the binary system "*ij*"; X_i and X_j indicate the mole fractions of the corresponding constituents.

The Gibbs molar excess energy of a ternary phase (ΔG_{123}^E), consisting of elements 1, 2 and 3, is given by the expression:

$$\Delta G_{123}^E = X_1 X_2 \Delta G_{12}^E + X_2 X_3 \Delta G_{23}^E + X_3 X_1 \Delta G_{31}^E + \Delta G_{123}^E \quad (2)$$

where ΔG^E_{12}, ΔG^E_{23} and ΔG^E_{31} can be obtained as defined above (equation 1) and ΔG^E_{123} is the contribution of the ternary non-ideal mixing. In the simplest case of a regular ternary solution it may be assessed by means of Equation (3):

$$\Delta G_{123}^E = X_1 X_2 X_3 A_{123} \quad (3)$$

where A_{123} is a ternary interaction parameter that might be temperature and concentration dependent.

The most essential equations, associated to the geometrical models[13–16] are only shown below only, because a detailed presentation would be out of the scope of this work. Thus, in a general case, a ternary system with constituents 1, 2 and 3 is considered where X_1, X_2 and X_3 are the mole fractions of the respective components. The molar excess Gibbs energies of the ternary liq-

uid phase (at a specific composition, temperature and pressure,) are estimated by means of equations 4–7 according to the authors,[13–16] in the same order:

$$\Delta G^E_{123} = \Delta G^E_{12}(1-x_3)^2 + \Delta G^E_{23}(1-x_1)^2 + \Delta G^E_{31}(1-x_2)^2 \quad (4)$$

$$\Delta G^E_{123} = \frac{X_1 X_2}{(X_1+\frac{X_3}{2})(X_2+\frac{X_3}{2})}\Delta G^E_{12} + \frac{X_2 X_3}{(X_2+\frac{X_1}{2})(X_3+\frac{X_1}{2})}\Delta G^E_{13} + \quad (5)$$

$$\frac{X_3 X_1}{(X_3+\frac{X_2}{2})(X_1+\frac{X_2}{2})}\Delta G^E_{13}$$

$$\Delta G^E_{123} = \frac{X_2}{1-X_1}\Delta G^E_{12} + \frac{X_3}{1-X_1}\Delta G^E_{13} + (X_2+X_3)^2 \Delta G^E_{23} \quad (6)$$

$$\Delta G^E_{123} = \frac{X_2}{1-X_1}\Delta G^E_{12} + \frac{x_3}{1-x_1}\Delta G^E_{13} + \frac{x_2 x_3}{\nu_{23}\nu_{32}}\Delta G^E_{23} \quad (7)$$

In equations 4–7, the following symbols are represented: ΔG^E_{123} – Gibbs molar excess energy of the ternary liquid phase; ΔG^E_{ij} – the respective values of the two-component liquid phases, where the subscript indexes indicate the considered binary system. The symbols v_{23} and v_{32} in equation (7) denote the mole fractions of the constituents 2 and 3 in the binary system 2–3. The values $1 - X_1$ and $1 - X_3$ are numerically equal in such a case.

Equation (3) will be used for introduction to the General solution model (GSM) of CHOU[17, 18]:

$$\Delta G^E_{123} = X_1 X_2 X_3 f_{123} \quad (8)$$

Here f_{123} is the ternary interaction coefficient, related to the Redlich-Kister ternary interaction parameters A_{ijk} ($f_{123} = X_1 \cdot A^0_{123} + X_2 \cdot A^1_{123} + X_3 \cdot A^2_{123}$).

This parameter is assessed in the following way[17]:

$$f_{123} = (2\xi_{12}-1)\{A^2_{12}((2\xi_{12}-1)X_3 + 2(X_1 - X_2)) + A^1_{12}\} + (2\xi_{23}-1)$$
$$\{A^2_{23}((2\xi_{23}-1)X_1 + 2(X_2 - X_3)) + A^1_{23}\} + (2\xi_{31}-1)\{A^2_{31}((2\xi_{31}-1)X_2$$
$$+ 2(X_3 - X_1)) + A^1_{31}\} \quad (9)$$

Here ξ_{ij} are "similarity coefficients", that are defined by the quantity η_i called - "deviation sum of squares":

$$\xi_{ij} = \eta_i / (\eta_i + \eta_j) \quad (10)$$

According to this model (GSM) the values of η_i are explicit functions of ΔG^E_{ij}, and are easily calculated when the adjustable coefficients of the three binary end-systems are known.

Basic thermodynamic information on the constitutive subsystems, needed for the assessment, was taken from ref.[12] For the Ni–Sn liquid phase updated parameters were used.[24] Actually, the optimized Redlich-Kister parameters of each system (Table 1) are essentially needed. They are used for the calculation (equations 4–8) of the molar excess Gibbs energies of the binary border-systems liquid phases. The following sequence of components was adopted for the calculations: Ni – 1, Sn – 2 and Zn – 3.

Results and Discussion

Calculations of the coefficients f_{123} were done along three sections of the Ni–Sn–Zn system with molar Sn vs Zn ratios 1/3, 1/1 and 3/1 in the interval 1000–2000 K, at nickel molar fractions equal to 0, 0.1, 0.2, 0.3, 0.4, 0.5, 0.6, 0.7, 0.8, 0.9 and 1. In such a way a huge amount of information was obtained and used thereafter to derive the parameters A_{ijk}. For this purpose programming of Excel was used. The results are shown in Table 2.

Table 1. Optimized parameters (A^o_{ij}, A^1_{ij}, A^2_{ij}) for the liquid binary phases of the Ni–Sn[24], Ni–Zn[12] and Sn–Zn[12] systems used in the present work; T/K – temperature.

System, $i-j$	$A^o_{ij}(T)$ J/mol	$A^1_{ij}(T)$ J/mol	$A^2_{ij}(T)$ J/mol
Ni–Sn (1–2)	–106102.87 + 197.9089 · T –21.9959 · T · LN(T)	–29342.17 + 52.5528 · T –6.46094 · T · LN(T)	+1582.3
Ni–Zn (1–3)	–50721.64 +7.34178 · T	+8436.3 +1.97211 · T	–25136.08 +11.79211 · T
Sn–Zn (2–3)	+19314.64 – 75.89949 · T +8.751396 · T · LN(T)	–5696.28 +4.20198 · T	+1037.22 +0.98362 · T

Table 2. Ternary interaction parameters, A^v_{ijk}, for the Sn–Ni–Zn liquid phase obtained from the f_{123} coefficients. T/K – temperature.

System, ijk	$A^o_{ijk}(T)$ J/mol	$A^1_{ijk}(T)$ J/mol	$A^2_{ijk}(T)$ J/mol
Sn–Ni–Zn	–884.2 + 6.5534 · T	45415 – 18.16 · T	–28292.6 + 17.82 · T

As already mentioned the binary integral Gibbs excess energies ought to be obtained initially. This was done by the Thermocalc software package, calculating binary activity values (referred to the liquid phases of the pure elements) at the pertinent points.

The ternary integral molar Gibbs excess energies assessed by the geometrical methods are graphically compared to those obtained by Thermocalc, using the optimized adjustable parameters of the border-systems only (Table 1). Sections with constant molar ratios between two of the components are plotted.

Results from a section with constant molar Sn/Zn equal to 1/3, at 1800 K are plotted in Figure 1. As one can see the curves 2 and 6 from one side and 1, 4 and 5 from the other side are grouped together, while the CALPHAD-type calculated values (curve 3) are situated between both groups. Surely, one has to bear in mind that curve 3 contains values assessed by binary parameters only. The asymmetrical methods (curves 4 and 5) give practically equal ΔG^{E}_{123} values while the quantities obtained by symmetrical methods (curves 1 and 6) differ significantly between each other. It should be noted that curve 6 (Muggiani model) is situated below all other curves at both other Sn/Zn ratios (1/1 and 3/1).

Figure 2 represents ternary integral molar Gibbs excess energies assessed along a molar Ni/Zn ratio equal to 1/3, at 1800 K. In this case, the values assessed by symmetrical methods (curves 1 and 6) are quite similar and are accompanied by the CALPHAD-type calculated quanti-

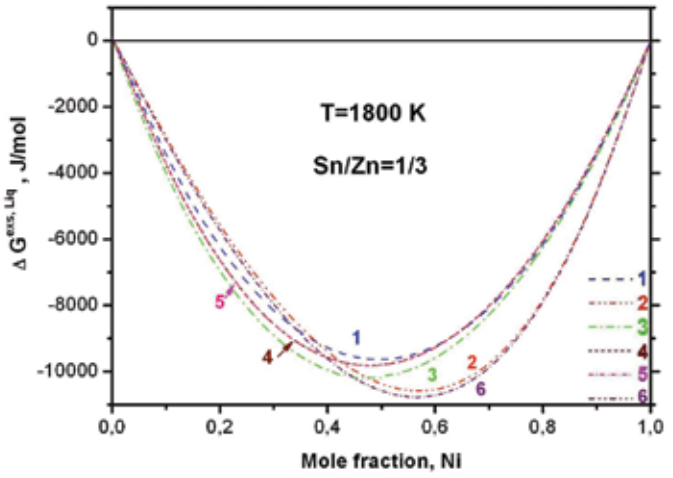

Figure 1. Molar Gibbs excess energies ($\Delta G^{ex, Liq,}$ J/mol) of the liquid phase, along a section with constant molar Sn/Zn ratio equal to 1/3, at 1800 K calculated in this work according to various techniques: 1 – up to KOHLER,[13] 2 – GSM,[34] 3 – CALPHAD (binary parameters only), 4 – TOOP,[15] 5 – HILLERT[16] and 6 – MUGGIANU.[14]

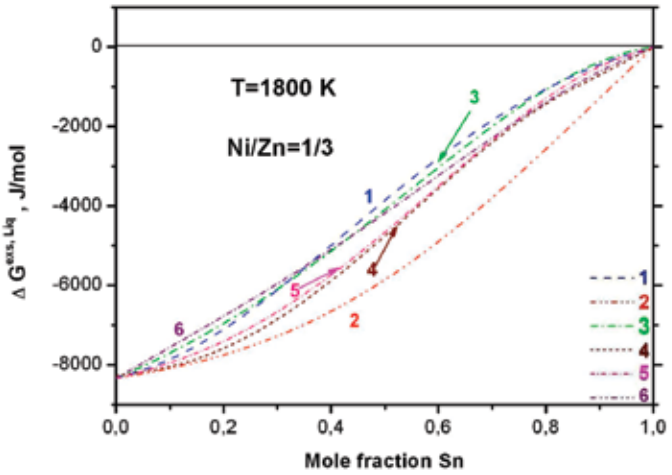

Figure 2. Molar Gibbs excess energies ($\Delta G^{ex, Liq}$, J/mol) of the liquid phase, along a section with constant molar Ni/Zn ratio equal to 1/3, at 1800 K calculated in this work according to various techniques: 1 – up to KOHLER,[13] 2 – GSM,[34] 3 – CALPHAD (binary parameters only), 4 – TOOP,[15] 5 – HILLERT[16] and 6 – MUGGIANU.[14]

ties (curve). The same is valid for the values calculated by both asymmetrical methods (curves 4 and 5). The GSM–assessed integral molar Gibbs excess energies (curve 2) deviate from all others. Similar disposition of the considered curves is observed at the sections along molar Ni/Zn ratios equal to 1/1 and 3/1.

It can be seen in Figure 3 (ΔG^{E}_{123} values along Sn/Ni molar ratio equal to 1/3, at 1800 K, are plotted) that the curves 1–3, from one side and 4–6, from the other side, are rather close to each another. Thus, the type of the method (symmetric or asymmetric) does not play a decisive role regarding the values of the calculated ΔG^{E}_{123}.

The ΔG^{E}_{123} values assessed in various ways along the sections with Sn/Ni molar ratios equal to 1/1 and 3/1 are roughly similar. The results for the ratio 3/1 are shown in Figure 4 in order to illustrate the shape of the curves.

In order to represent ΔG^{E}_{123} temperature dependence the values of the integral ternary molar Gibbs excess energies are plotted in Figures 5–7. The latter were calculated by GSM (by equations 9 and 10, using the parameters shown in Table 1) in the temperature range 1000–2000 K and along sections with Sn/Zn, Ni/Zn and Sn/Ni molar ratios equal to 1/1, respectively. Negative deviations from the Raoult's low are observed in general while in the regions rich of tin and zinc feeble positive ΔG^{E}_{123} are observed only.

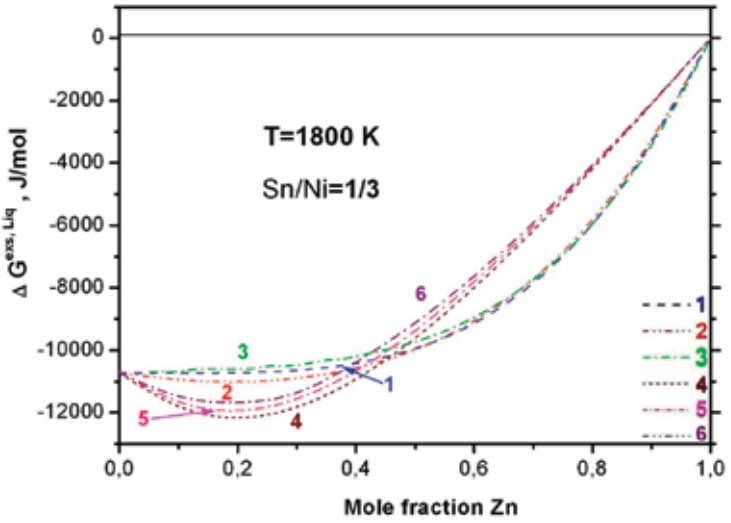

Figure 3. Molar Gibbs excess energies ($\Delta G^{ex, Liq}$, J/mol) of the liquid phase, along a section with constant molar Sn/Ni ratio equal to 1/3, at 1800 K calculated in this work according to various techniques: 1 – up to KOHLER,[13] 2 – GSM,[34] 3 – CALPHAD (binary parameters only), 4 – TOOP,[15] 5 – HILLERT[16] and 6 – MUGGIANU.[14]

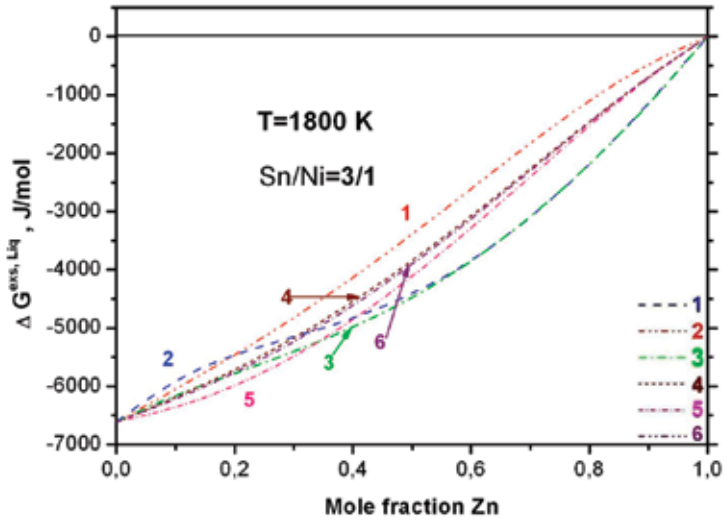

Figure 4. Molar Gibbs excess energies ($\Delta G^{ex, Liq}$, J/mol) of the liquid phase, along a section with constant molar Sn/Ni ratio equal to 3/1, at 1800 K calculated in this work according to various techniques: 1 – up to KOHLER,[13] 2 – GSM,[34] 3 – CALPHAD (binary parameters only), 4 – TOOP,[15] 5 – HILLERT[16] and 6 – MUGGIANU.[14]

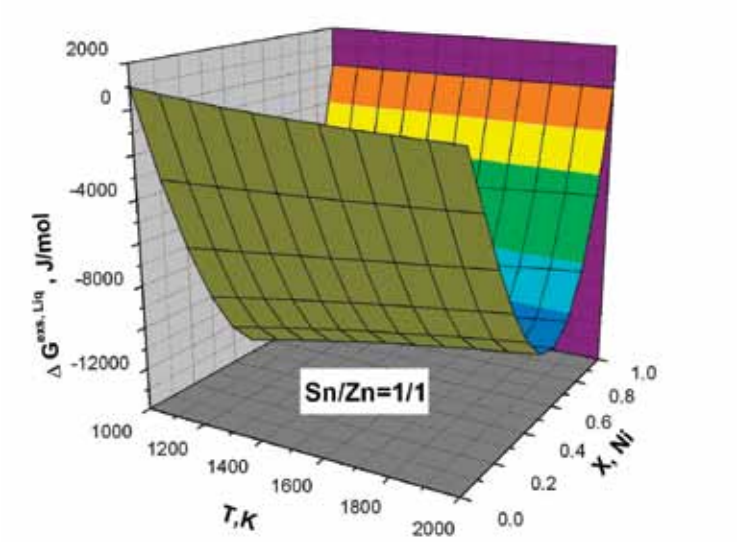

Figure 5. Calculated by GSM values of the integral ternary molar Gibbs excess energies in the temperature range 1000–2000 K. Section with Sn/Zn ratio equal to 1/1. $\Delta G^{ex, Liq}$, J/mol – molar Gibbs excess energy of the ternary liquid phase; x_{Ni} – nickel mole fraction; *T*/K – temperature.

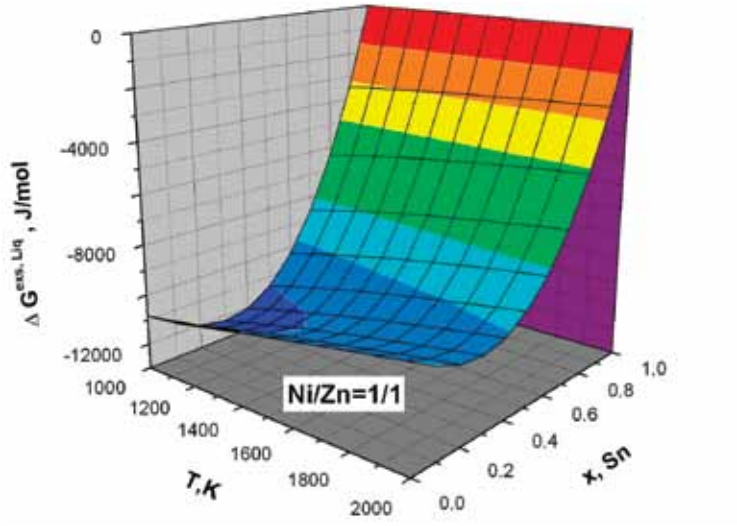

Figure 6. Calculated by GSM values of the integral ternary molar Gibbs excess energies in the temperature range 1000–2000 K. Section with Ni/Zn ratio equal to 1/1. $\Delta G^{ex, Liq}$, J/mol – molar Gibbs excess energy of the ternary liquid phase; x_{Sn} – tin mole fraction; *T*/K – temperature.

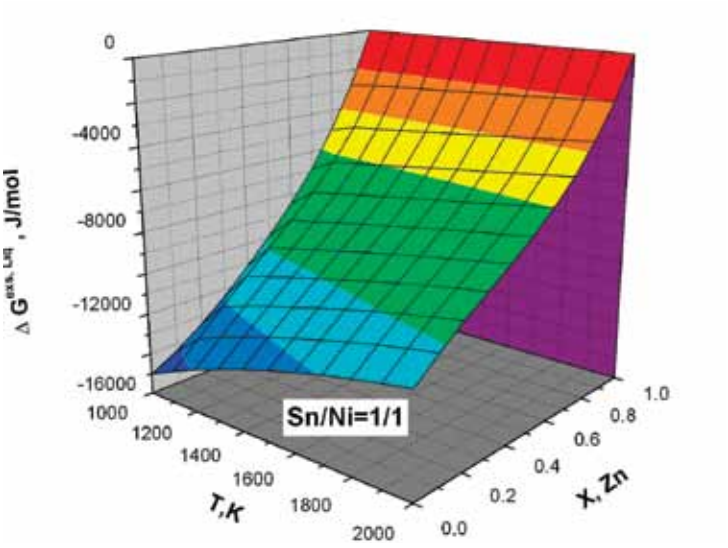

Figure 7. Calculated by GSM values of the integral ternary molar Gibbs excess energies in the temperature range 1000–2000 K. Section with Sn/Ni ratio equal to 1/1. $\Delta G^{ex, Liq}$, J/mol – molar Gibbs excess energy of the ternary liquid phase; x_{Zn} – zinc mole fraction; *T*/K – temperature.

CONCLUSIONS

Some thermodynamic properties of the Sn–Ni–Zn liquid phase were predicted using a general solution model developed by Chou, two symmetrical and two asymmetrical models. Redlich-Kister ternary interaction parameters of the liquid phase were assessed.

The values of the ternary liquid phase molar Gibbs excess energies assessed by geometric models were compared to those calculated by the CALPHAD method using binary optimized parameters only. Good mutual agreement was found indicating that the interaction parameters for the ternary system would have small values.

Acknowledgments

This work is related to the European concerted action COST MP 0602 and is financed by the University of Plovdiv (NPD) under contract No. RS09-HF-023.

REFERENCES

[1] KANG, S., RAI, R. S., PURUSHOTHAMAN, P. (1996): Interfacial reactions during soldering with lead-tin eutectic and lead (Pb)-free, tin-rich solders. *J. Electron. Mater.;* Vol. 25**,** pp. 1113–1120.

[2] ZHU, W., LIU, H., WANG, J., MA, G., JIN, Z. (2010): Interfacial reactions between Sn–Zn Alloys and Ni sub-

strates. *J. Electron. Mater.*; Vol. 39, pp. 209–214.

[3] Vassilev, G. P., Lilova, K. I., Gachon, J. C. (2006): Enthalpies of formation of Ni–Sn compounds. *Therm. Acta*; Vol. 447, No. 1, pp. 106–108.

[4] Vassilev, G. P., Lilova, K. I., Gachon, J. C. (2005): Calorimetric studies of the Ni–Sn system. *Proceedings of VIIIth Int. Workshop of Assoc. Phase Diagram and Thermod. Committee*, Košice, Slovakia, 19 November 2005, Ed. W. Zakulski, ISBN 83-921845-5-6, Published by, Ins. Met. and Mat. Sc., Polish Academy of Sciences, Krakow, Poland, pp. 27–34.

[5] Schmetterer, C., Flandorfer, H., Richter, K. W., Saeed, U., Kauffman, M., Roussel, P., Ipser, H. (2007): A New Investigation of the System Ni–Sn. *Intermetallics*; Vol. 15, No. 7, pp. 869–884.

[6] Budurov, S., Vassilev, N. Nentchev, N. (1974): The Nickel Side of the Phase Diagram Nickel–Zinc. *Z. Metallkunde*; Vol. 65, pp. 681–683.

[7] Budurov, S., Vassilev, G. P., Nentchev, N. (1973/74): The Nickel Side of the Nickel–Zinc Phase Diagram. *Annual of the Univeristy of Sofia, Faculty of Chemistry*; Vol. 68, pp. 171–177.

[8] Budurov, S., Vassilev, G. P. (1976): Kinetics of Eutectoide Decomposition of the Nickel–Zinc β-Phase. *Z. Metallkunde*; Vol. 67, pp. 776–779.

[9] Budurov, S., Vassilev G. P., Kuck, N. (1977): On the Kinetics of Intermetallic Phase Layers Growth in the Ni–Zn System. *Z. Metallkunde*; Vol. 68, pp. 226–230.

[10] Vassilev, G. P., Acebo, A. P., Tedenac, J. C. (2000): Thermodynamic optimization of the Ni–Zn system. *J. Phase Equilibria*; Vol. 21, No. 3, pp. 287–301.

[11] Massalski, T. (1996): Binary Alloy Phase Diagrams, CD-ROM, Ohio, USA, ASM International.

[12] Dinsdale, A., Watson, A., Kroupa, A., Vrestal, J., Zemanova, A., Vizdal, J. (2008): Atlas of Phase Diagrams for the Lead-Free Soldering, COST 531 (Lead-free Soders), Vol. 1, © COST office, 2008, ISBN 978-80-86292-28-1, Printed in the Czech Republic.

[13] Kohler, F. (1960): Zur Berechnung der thermodynamischen Daten eines ternären Systems aus den zugehörigen binären Systemen - Kurze Mitteilung. *Monatshefte fur Chemie*; Vol. 91, No. 4, pp. 738–740.

[14] Muggianu, Y. M., Gambino, M., Bros, J. P. (1975): Enthalpies de formation des alliages liquides bismuth-etain-gallium a 723 K. Choix d'une representation analytique des grandeurs d'exces integrales et partieles de mélange. *Journal de Chimie Physique*; Vol. 72, pp. 83–88.

[15] Toop, G. W. (1965): Predicting Ternary Activities Using Binary Data. *Transactions of the American Institute of Mining Engineers*; 233, pp. 850–855.

[16] HILERT, M. (1980): Empirical methods of predicting and representing thermodynamic properties of ternary solution phases. *CALPHAD*; Vol. 4, pp. 1–12.

[17] CHOU, K. C. (1995): A general solution model for predicting ternary thermodynamic properties. *CALPHAD*; Vol. 19, pp. 315–25.

[18] CHOU, K. C., LI, W. C., LI, F., HE, M. (1996): Formalism of new ternary model expressed in terms of binary regular-solution type parameters. *CALPHAD*; Vol. 20, pp. 395–405.

[19] LEE, S. K., KIM, S. J. (2001): Calculation of ternary mixing properties of melts and minerals from the bounding binaries. *CALPHAD*; Vol. 25, pp. 97–108.

[20] ŽIVKOVIĆ, D., KATAYAMA, I., YAMASHITA, H. MANASIJEVIĆ, D., ŽIVKOVIĆ, Z. (2006): Investigation of the thermodynamic model and ternary interaction parameter influence for Sn-Ag-Bi liquid alloys. *RMZ - Materials and Geoenvironment*; Vol. 53, pp. 155–161.

[21] MARJANOVIĆ, S., MANASIJEVIĆ, D., ŽIVKOVIĆ, D., GUSKOVIĆ, D., MINIĆ, D. (2009): Calculation of thermodynamic properties for ternary Ag–Cu–Sn system. *RMZ – Materials and Geoenvironment*; Vol. 56, pp. 30–37.

[22] ŽIVKOVIĆ, D., MANASIJEVIĆ, D., MIHAJLOVIĆ, I., ŽIVKOVIĆ, Z. (2006): Calculation of the thermodynamic properties of liquid Ag–In–Sb alloys. *J. Serb. Chem. Soc.*; Vol. 71, pp. 203–211.

[23] REDLICH, O., KISTER, A. (1948): Algebraic representation of the thermodynamic properties and the classification of solutions. *Indust. Eng. Chem.*; Vol. 40, pp. 345–348.

[24] ZEMANOVA, A., KROUPA, A.: In "Thermodynamic database of the action COST MP 0602"; http://cost-mp0602.epfl.ch.

Main damages on upper die in industrial hot forging

Glavne poškodbe na zgornjem orodju za vroče kovanje v industriji

Lejla Lavtar[1,*], Milan Terčelj[1], Matevž Fazarinc[1], Goran Kugler[1]

[1]University of Ljubljana, Faculty of Material Science and Engineering, Department of Materials and Metallurgy, Aškerčeva cesta 12, SI-1000 Ljubljana, Slovenia

*Corresponding author. E-mail: lavtar@steel.si

Received: July 8, 2010 **Accepted:** July 21, 2010

Abstract: An analysis of main damages on industrial hot-forging die, made of Dievar hot-working die steel is presented. Die was previously gas nitrided, sectioned and examined after its service life. The measurements of microhardness depth profiles and optical microscopy of nitrided layers were applied in analysis of wear, cracks and failures on the most loaded sections of tool. In order to prolong die service life some improvements were suggested.

Izvleček: V tem prispevku so prikazane glavne poškodbe na orodju za vroče kovanje, narejenem iz orodnega jekla Dievar. Orodje je bilo predhodno plinsko nitridirano ter preiskovano po izteku njegove trajnostne dobe. Za analizo poškodb, tj. obrabe, razpok, zlomov, na najbolj obremenjenih delih orodja, so bile uporabljene optična mikroskopija in meritve profila mikrotrdote. Za izboljšanje trajnostne dobe orodja so bile predlagane izboljšave.

Key words: hot forging, die, gas nitriding, damages
Kjučne besede: vroče kovanje, orodje, plinsko nitridiranje, poškodbe

Original scientific paper

INTRODUCTION

Hot-forging dies are during the process of hot forging subjected to a complex loading, i.e. to simultaneous thermal, mechanical, chemical and tribological loads. Various parts of hot-forging dies are subjected to mentioned loads that results in different types of damages, like erosive, abrasive and adhezive wear,[1–4] plastic deformation,[1, 8] thermal and mechanical cracking,[1, 7] gross cracking, etc.[1, 5, 6] Die life (service time) plays an important role in economy of hot forged products, thus goal of every technologist in practice is prolongation of die service life as much as possible on one hand and accurate prediction of die service time on the other hand.[1]

Damages and their propagation are also additionaly influenced by applied die steel, die shape, and applied technological processing parameters, i.e. schedule of forging sequences, way of manufacturing the die, operating forging parameters, used forging press, as well as forging stock properties, i.e. temperature, scaling, local adhesion between die and the workpiece, etc. Further, die steel should be produced in an appropriate way in order to achieve optimal microstructure, i.e. grain size as well as distribution, type, size and shape of carbides. Finally, manufacturing of die should be performed without negative influences on the die surface quality, and also shapes of die should be optimized with sequential forging steps in order to avoid areas of essentially higher loads in regard to other areas of die.[9,10]

In order to increase die service time, wear and fatigue resistance, the die surface is improved by coating, diffusion procesess like nitriding, etc.[11] During nitriding the die steels, two different types of microstructure are formed on the die surface, i.e. microstructure with "compound layer" on top of the surface and diffusion layer below, and in the second case diffusion layer alone. It is advisable for hot forging dies to produce nitrided microstructure without compound layer since it consists of brittle iron nitrides, i.e. ε phase (ε-$Fe_{2-3}N$), γ' phase (γ'-Fe_4N), or mixed phases ($\varepsilon+\gamma'$). At slightly higher contact pressures (about 20 MPa)[12, 13] compound layer usually spalls of the die surface at the very beginning of forging process and that usually essentially accelerates process of wear. In each application nitrided microstrucure as well as die design should correspond to actual loads that prevail on die in the selected forming process.

In order to elucidate doubtless relationships between occurrence of die damages, loads, properties of applied steel, die shape, etc. there are still not suffi-

cient data on failures of industrial dies, especially on dies that were previously nitrided, coated or duplex treated. Thus more data on die damage analysis from industrial practice are needed. Analysis of main damages that occurred on a gas nitrided industrial die for hot forging that has failed have been presented in this paper with aim to prolong its service life.

Experimental

Description of hot-forging die and shape of forged product

The main damages of die (Figure 1) with two impressions for penultimate forging operation and two impressions for the last forging operation were analysed after its service life. However, analysis was predominately focused on the impression used for the last forging operation since it gave final shape and dimensions of the product (see Figure 2). This shape was achieved in five sequential forging operations. Upper and lower parts of die had similar design of impressions. Essential difference between the upper and the lower die was height of mandrels. With regard to reference,[1] it could be supposed that the die surface temperature was in the range of 600–700 °C and contact pressure exceeded the value of 1000 MPa. Lubricant that was used was water suspension of graphite.

Die life is determined by surface quality of forged product as well as by its shape and dimensions. In our case customer had special demands for forged product in respect of the quality of impression surface, and the shape and dimensions at the base of mandrels. These areas were considered as critical areas of the hot-forging die (see Figure 1). The die with higher mandrels failed after 45 766 forging strokes due to change of shape of forged product in the depression around high mandrels.

Initial billet made of C35E steel for forging the steering mechanism had diameter of $\varnothing$ = 32 mm and weight of 930 g, and was heated to temperature interval of 1230–1280 °C. Geometry of forged product is adapted for steering mechanism in car that is a relatively simple 3D-geometry (Figure 2).

Die material, applied methods

Dievar, a high performance chromium-molybdenum-vanadium alloyed hot-working die steel (see Table 1), developed by Uddeholm, was used in manufacturing industrial die; steel is characterized by excellent toughness, ductility in all the directions, good tempering resistance and high-temperature strength, excellent hardenability, and good dimensional stability throughout the heat treatment procedure, as well as during coating operations. Consequently, this die steel has a very good resist-

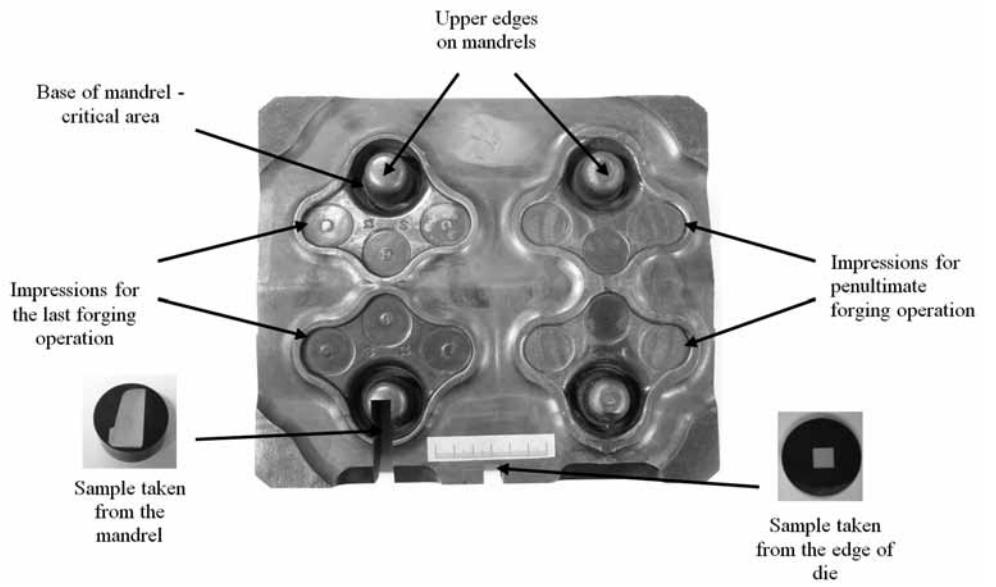

Figure 1. Upper die after 45 766 strokes; two impressions for penultimate forging operation and two impressions for the last forging operation with mandrels

Figure 2. Shape of steering mechanism after the last hot forging operation

ance to thermal fatigue, gross cracking, hot wear and plastic deformation. It is used for dies in die casting, hot forging, and hot extrusion.[14]

Die was gas nitrided and taken out of industrial process after its service time. Die was sectioned and examined with light microscopy (Olympus GX51) and by Vickers microhardness measurements (Leitz Miniload 2). Die surface was examinated using macro and micrograph techniques to reveal surface damages of nitrided layer. Additionally, metallographic examinations of samples taken from certain cross-sections were performed. Nital etchant for metallographic preparation of nitrided samples was used.

Table 1. Chemical composition of applied die steel (Dievar) in mass fractions, *w*/%

C	Si	Mn	Cr	Mo	V
0.37	0.26	0.5	5.0	2.36	0.55

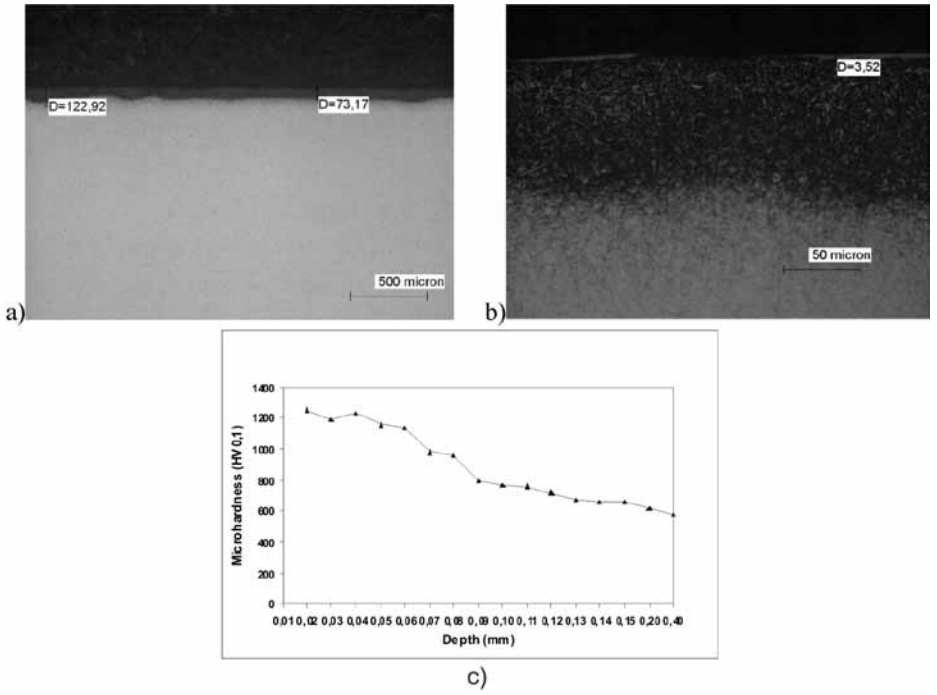

Figure 3. Microstructures and microhardness profile on cross-section of the die edge: nitrided diffusion layer with compound layer (a-b), microhardness profile (c)

Results and discussion

Initial nitrided microstructures

Diffusion layer can be well seen on cross-sections of the surface edge (Figure 3a). The depth of diffusion layer is not homogenous and it is thick from 73 μm to 122 μm (see Figure 3a). This nonhomogeneity could be atributed to unappropriate preparation of die surface before the nitriding process that resulted in different adsorption abilities of nitrogen into the die surface layer. Thickness of compound layer was in the range of about 0–3.5 μm (Figure 3b). Further, presence of nitrides was visible on grain boundaries. It was also remarked that microstructure was slightly overnitrided (nitrides on grain boundaries were in that area pependicular to diffusion front and parallel to die surface) that could result in premature spalling of die material from the die surface layer. Figure 3c gives microhardness profile; max. values were above $HV = 1200$.

Damages on die surface

The main damages of the die on macro level are shown in Figure 4. The relatively sharp edges of the upper die impression around mandrels show wear usually combined with plastic deformation and spalling (see Figures 4c, 4e, 4f). On these edges high contact pressures as well as large sliding lengths between deformed material and die surface took place. These conditions led to higher heating and consequently to higher tempering of the die surface layer that favoured wear, spalling of fragments of nitrided layer and plastic deformation. Spalling of relative large fragments is seen on the upper edge of mandrels (Figures 4c, 4e) for penultimate forging impressions. Mentioned spalling of fragments was, next to higher contact pressures that prevailed on these surfaces, also consequence of presence of nitrides on grain boundaries of the diffusion layer (see Figure 3b) that decreased toughness of die steel. But spalling on mandrels took place only on one mandrel (Figure 4e) while on the other one only emphasized wear was observed (Figure 4b). Further, also spalling on top of mandrel (see Figure 4i) was detected. This occurrence of spalling could be atributed to thermal fatigue in combination with high contact pressure. On impression radii shown in Figures 4g and 4d1 plastic deformation was not observed but only furrows as consequence of abrasion were visible. Namely contact pressures on this surfaces were relatively lower since radius of mandrel was greater. The base of mandrels previously indicated as critical areas in the hot-forging die (see Figure 1) is also critical for service life of dies and the quality of forged products. In these areas, due to pressure of forged material on both depression surfaces and consequently due to bending load on bottom of die depression, stress concentrations took place. These repeating mechanical loads resulted in formation of cracks at the base of mandrel (see Figure 4h) that caused surface, geometry and shape inadequacies of forged products. For comparison, such damage was not observed on similar area of die impression for penultimate forging sequence (see Figure 4d2). This indicated that the last impression was subjected to comparatively higher bending loads, and that required changes of impression design at the mentioned five sequential forging steps. In Figures 4a and 4f abrasion wear close to outer area of die impression as consequence of higher sliding length was observed. For further explanation and analysis of surface damages the cross-sectional microstructures especially of critical areas, i.e. on top, on upper and bottom edge as well as in the middle area of mandrel, will be presented.

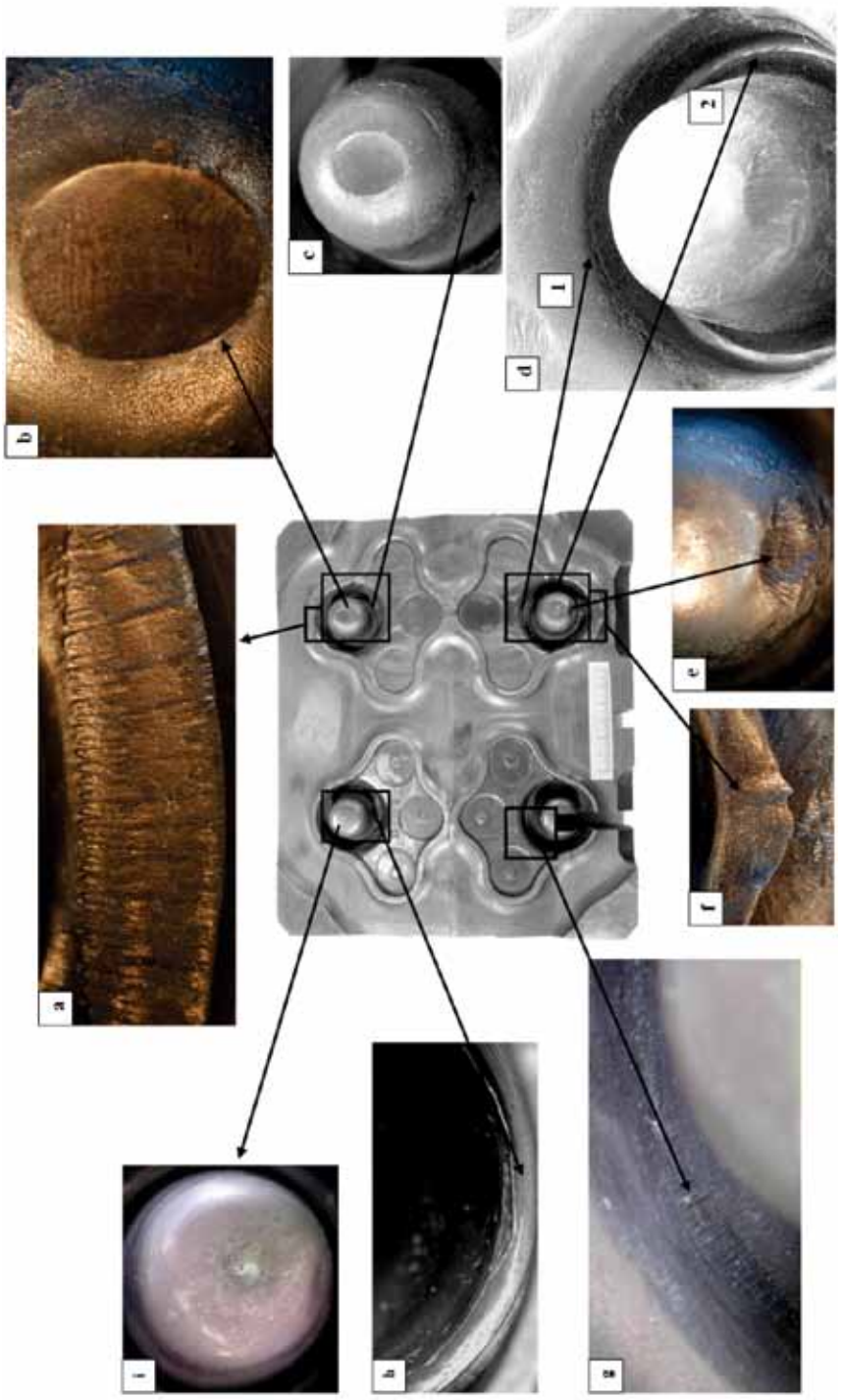

Figure 4. Damages of the die after 45 766 strokes; plastic deformation (a, f), mechanical deformation (b, c, d, e, g), spalling (d, e), cracks (d, h), wear (i).

Damages on mandrel cross-sections

Cross-sections of mandrel for the last forging operation revealed compound layer on the mandrel top (Figure 5) and in its middle area (Figure 7), while compound layer on the upper (Figure 6) and the bottom edge (Figure 8) was removed during the forging process; furthermore, formation of cracks in the diffusion layer was observed (see Figures 5 and 6). Removal of compound layer could be atributed to higher contact pressures and sliding lengths that preavailed in these areas and they led first to its cracking and then

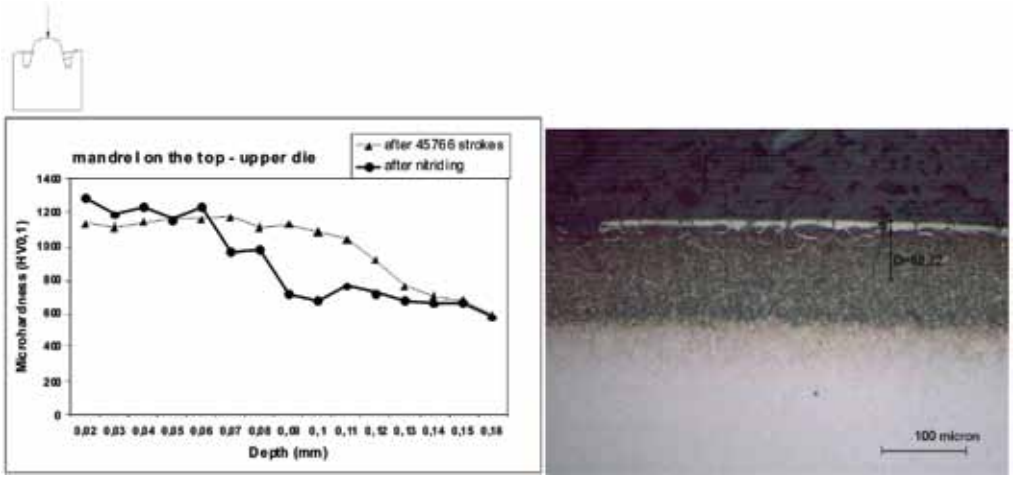

Figure 5. Hardness profile and cross-sectional microstructure on the top of mandrel

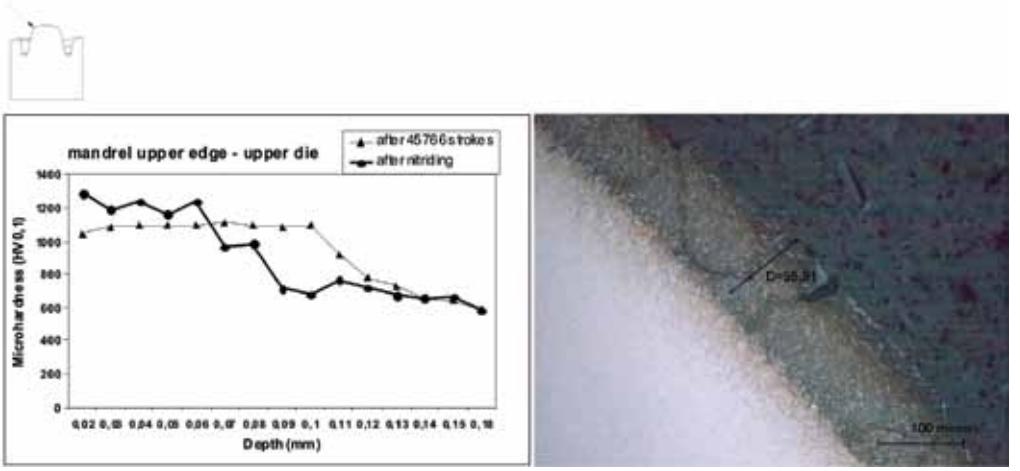

Figure 6. Hardness profile and cross-sectional microstructure on the upper edge of mandrel

to its spalling; compound layer is namely very brittle in comparison to the diffusion layer. Moreover, as mentioned above, nitrides were present on grain boundaries of nitrided microstructure that decreased toughness and accelerated spalling of fragments.

As already mentioned, cracks were also found in the diffusion layer on the upper edge having lengths of about 96 μm (Figure 6) and on the top of the mandrel with lengths of about 69 μm (Figure 5). Compound layer on the top of the mandrel also exhibited cracking as consequence

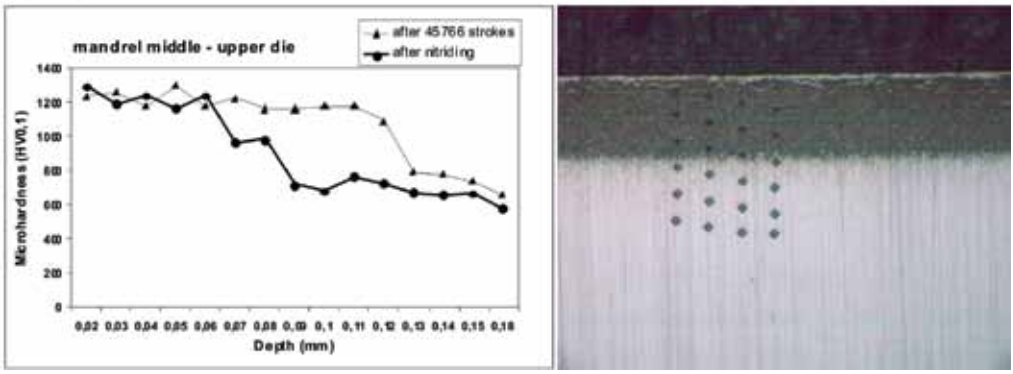

Figure 7. Hardness profile and cross-sectional microstructure in the middle part of mandrel

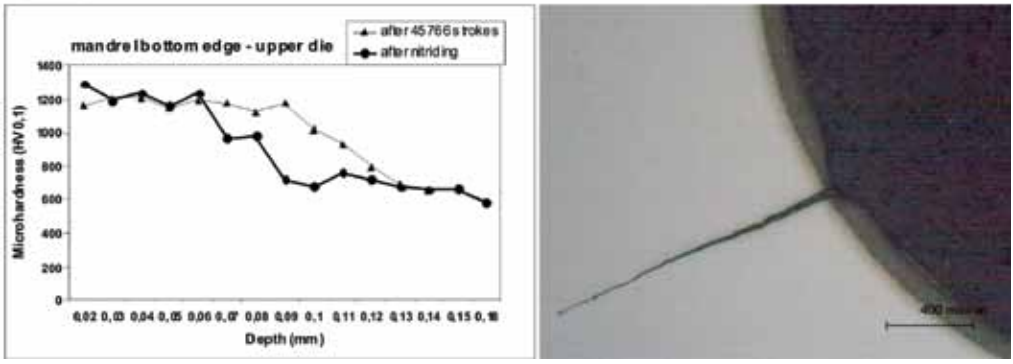

Figure 8. Hardness profile and cross-sectional microstructure on the bottom edge of mandrel.

of thermal fatigue and presence of higher contact pressures (compare Figure 5 with Figure 4i). Relative sliding between the die surface and the deformed material was reduced in these areas thus suface material was removed by spalling. Effective nitriding depths on all the cross-sections were in range of about 150–160 μm. Microhardness measurements showed the highest drop of hardness values from $HV_{0.1}$ = 1292 on the edge of die after the nitriding process, to $HV_{0.1}$ = 1044 (see Figure 6) on the upper edge of the high mandrel after die failure.

Furthermore, crack with length of about 1.5 mm at the base of mandrel was detected (Figure 8, compared with Figure 4h). In this figure also more intensive spalling of diffusion layer on the surface at the beginning of crack was observed. In fact, this surface damage limited die life since the surface quality and shape of forging did not fulfil demands of customer.

In Figures 5–8, increase of microhardness values was found at the depths of about 60 μm and less. This could be atributed to diffusion of nitrogen from the die surface layer into interior or eventual increase of carbon content since lubricant based on graphite was used for lubrication and cooling of die impressions.

CONCLUSIONS

In the presented work occurrence of damages of hot-forging die, made of Dievar, hot-working die steel that was used for hot forging of steering mechanism has been analyzed. Gas nitrided die was sectioned and examined after its service time, i.e. after 45 766 strokes using light microscopy and Vickers microhardness measurements. The essential conclusions are:

- Nitrided microstructure on cross-sections revealed presence of compound layer and nitrides on grain boundaries. Non-homogenous depth of diffusion layer that resulted in different adsorption abilities of nitrogen was observed and could be atributed to improper surface preparation prior to nitriding. In order to improve surface activation proper surface preparation prior to nitriding should be performed too.
- Proper selection of nitriding parameters is needed in order to avoid formation of nitrides on grain boundaries.
- Metallographical examination revealed that three main types of damages could be seen on die surfaces, i.e. cracks as consequence of mechanical and thermal fatigue, spalling of nitrided layer as consequence of thermal fatigue and mechanical loads, and furrows as consequence of abrasion.

- Mechanical fatique cracking occurred at the base of mandrels and it was decisive mechanism that was influencing die service life. Crack with length of about 1.5 mm was observed on the bottom edge of mandrel. This damage could be avoided by reducing the pressure of deformed material on die surface in the depression, i.e. by optimizing deformation sequences (steps) in forging.

References

[1] Hansen, P. H. (1990): Analysis of wear distribution in forging dies. Ph.D. Thesis, Pub. No. MM. 91.06, Technical University of Danmark.

[2] Rooks, B. W. (1974):The effect of die temperature on metal flow and die wear during high speed hot forging. *Proceedings of the 15th International MTDR Conference*, Birmingham, UK, Macmillan, London, 487–494.

[3] Singh, A. K., Rooks, B. W. & Tobias, S. A. (1973): Factors affecting die wear, Vol. 25, No. 2, 271–279.

[4] Silva, T. M. & Dean, T. A. (1974): Wear in drop forging dies. *Proceedings of the 15th International MTDR Conference*, Birmingham, UK, Macmillan, London, 479–486.

[5] Sharma, R. & Arrowsmith, D. J. (1982): The wear of forging in the first five forging blows. *Wear* 1981–1982, Vol. 74, 1–10.

[6] Siedel, R. & Luig, H. (1992): Friction and wear processes in hot die forging. *New Materials Processes Experiences for Dieing, Proceedings of the International European Conference on Dieing Materials*, Switzerland, 7.–9. September 1992, 467–480.

[7] Doege, E., Groche, P. & Bobke, Th. (1990): Application of adhesion theory to friction and wear processes in hot forging. *Proceedings of the 3rd International Conference on Technology on Plasticity*, Vol. 1, 27–32.

[8] Baar, C. (1993): Schmelzmetallurgische Massnahmen zur Standmengenerhöhung von Schmiedewerkzeugen. *Proceedings of the Seminar on Werkzeug- und Formenbau*, Univerität Hannover, September 1993, Hannover, 2/1–2/13.

[9] Schaefer, F. & Behrens, B. A. (2005): Prediction of wear in hot forging dies by means of finite-element-analysis. *Journal of Materials Processing Technology*; Vol. 167, 309–315.

[10] Ebara, R. & Kubota, K. (2008): Failure analysis of hot forging dies for automotive components. *Engineering Failure Analysis 2008*; Vol. 15, 881–893.

[11] Pye, D. (2003): Practical Nitriding and Ferritic Nitrocarburizing, ASM International, Materials Park, Ohio, 2003.

[12] Terčelj, M., Smolej, A., Fajfar, P. & Turk, R. (2007): Tribol. Int. 2007; Vol. 40, 374–384.

[13] Castro, G., Fernández-Vicente, A. & Cid, J. Wear (2007): 263, 1375–1385.[14]

Improvement of product accuracy and tool life at precise cold forming by suitable die prestressing

Izboljšanje natančnosti izdelka in vzdržljivosti orodja pri preciznem preoblikovanju v hladem z ustreznim prednapetjem matrice

Vid Krušič[1,*]

[1]Iskra Avtoelektrika, d. d., Polje 15, SI-5290 Šempeter pri Gorici, Slovenija

*Corresponding author. E-mail: vid.krusic@iskra-ae.com

Received: November 17, 2010 **Accepted:** December 3, 2010

Abstract: In the case of cold forming of an inner race of a homokinetic joint an analysis of die prestress influence on the product accuracy and tool life was made. Definition of optimum working interference of shrink fit for the die in combination with suitable stiffness of a shrink ring is important for production reliability of cold-formed elements. Smaller interference dimension with the rigid shrink ring enables lower elastic deformation of the die, which means higher accuracy of the products on one side, smaller specific plastic deformation on the critical tool part on the other side and consequently a reduced progress of damages. Stiffness of the shrink ring can be increased with higher elastic module material and/or combination of a ring composed of a cemented carbide core and a winded spring strip.

Povzetek: Na primeru hladnega iztiskavanja kroglaste glave homokinetičnega zgloba je podana analiza vpliva prednapetja matrice na natančnost izdelka in vzdržljivost orodja. Določitev optimalne nadmere krčnega naseda za matrico v kombinaciji z ustrezno togostjo krčnega obroča je pomembna za zanesljivost proizvodnje hladno preoblikovanih elementov. Manjša krčna mera naseda v kombinaciji s togim krčnim obročem zagotavlja manjšo elastično deformacijo matrice, kar pomeni večjo natančnost izdelkov in na drugi strani manjšo specifično plastično deformacijo na kritičnem delu orodja in tako počasnejšo rast poškodb. Togost krčnega obroča lahko poveča-

Original scientific paper

mo z večjim modulom elastičnosti materiala oziroma s kombinacijo obroča, sestavljenega iz jedra iz karbidne trdine in navitega vzmetnega traku.

Key words: cold forming, part accuracy, tool life, die prestressing
Ključne besede: hladno preoblikovanje, natančnost izdelka, vzdržljivost orodja, prednapetje matrice

INTRODUCTION

Cold massive forming of steels is an important technology in manufacturing of elements with demanding geometric forms and accurate dimensions. Fast development of automotive industry increases the requirements for manufacturing of elements with complex geometric forms and accurate dimensions. A product is understood as quality-made, when there are no inside or/and outside damages and when its dimension tolerances are as close to the centre of the tolerance area as possible. Attainment of accurate dimensions of a product and long tool life are two main requirements in the cold massive extrusion industry.

For a reliable manufacture of elements with the cold forming technology, a production process that ensures both quality manufacture of products and optimum tool life should be planned.[1] Figure 1 shows a forming system with input parameters of random and systematic deviation. The system response represents the desired function and/or in this case the product's quality and tool life within the desired and allowable scatter.

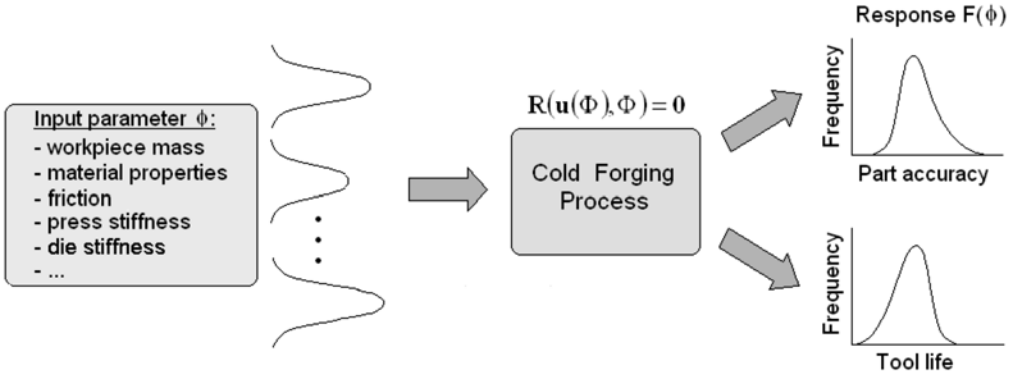

Figure 1. Scatter impact of input parameters of the forming system on the accuracy of products and tool life

A suitable die pre-stress and/or definition of the optimum shrink dimension is essential for long life of tools.[2] Dies for cold extrusion, which are heavily loaded, are prestressed with the help of the shrink rings. On the one side, it is necessary to ensure large enough prestress for as big as possible compensation of extreme loads of the forming process. as possible, However, one must be careful not to overload the tool too far in the plastic area by prestressing. Defining the appropriate tooling allowance requires good knowledge of the limit conditions that material can withstand without damages. The published text books propose more measures for evaluation of prestress together with cyclic tool loads. One of most often used criteria was defined by HÄNSEl;[3] it is based on the deformation energy

$$\Delta W^{t} = \Delta W^{e+} + \eta \, \Delta W^{p} \qquad (1)$$

where ΔW^{e+} represents specific deformation energy of the tensile stress and ΔW^{p} stands for specific energy of plastic deformations. In the equation above, η is a weight factor to the part of plastic deformations that cause damages in material. Graphic interpretation of this equation is shown in Figure 2, where tool life can be prolonged by reducing the influence of the specific deformation part of the tensile stress ΔW^{e+} and the specific part of plastic deformations ΔW^{p}. By the die pre-stress we can reduce loading of the tool $\Delta\sigma$ and decelerate damage development. Higher prestress makes the hysteresis loop move to the compression area. In this way the harmful effect ΔW^{e+} is reduced or even eliminated. The risk of damages can be reduced by an appropriate selection of materials for the shrink fit core. If we choose cemented carbide (prestressing E^{+})[4, 5] instead of steel, the system rigidity increases due to the higher elasticity module and deformation amplitudes $\Delta\varepsilon$ and consequently ΔW^{p} reduces accordingly. Lower deformation amplitudes of die are crucial for higher accuracy of products, as smaller deformation denotes smaller elastic deformation and in this way smaller elastic elongation of the die in the radial direction.

During the production process and under the conditions of mass production, the tools are loaded cyclically. The tool re-

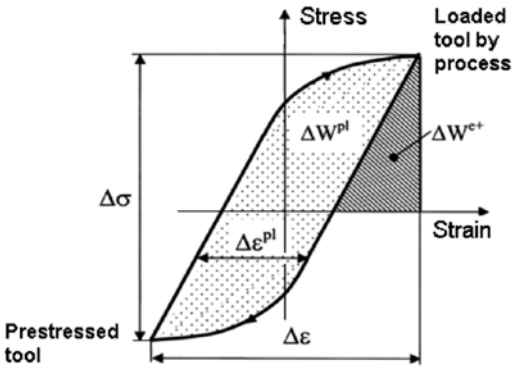

Figure 2. Effect of the specific deformation energy on the damage development

sponse on the critical spot is elasto-plastic and is defined by kinematic and isotropic hardening and damage development D

$$\dot{D} = \frac{\sigma_e^2 \left(\frac{2}{3}(1+\nu) + 3(1-2\nu)\left(\frac{\sigma_{kk}}{3\sigma_e} \right)^2 \right)}{2 \cdot S \cdot E(1-D)^2} \dot{p} \cdot \alpha(p) \quad (2)$$

where E stands for the elastic module, ν is a Poisson ratio, σ_e is an effective stress, σ_{kk} is a spherical stress tensor and $\alpha(p)$ a function, which defines beginning of the damage growth with reference to the size of comparative plastic deformation p. Detailed information regarding the constitutive model for damage D, suggested by Pedersen, is given in reference.[6]

The main objective of this research is to analyze the impact of the die prestressing on the accuracy of the product and tool life in cold extrusion of a inner race of the homokinetic joint (Figure 3). With suitable die prestressing the improvement of the product accuracy and tool service life is achieved, as well as the reliability of cold forming system.

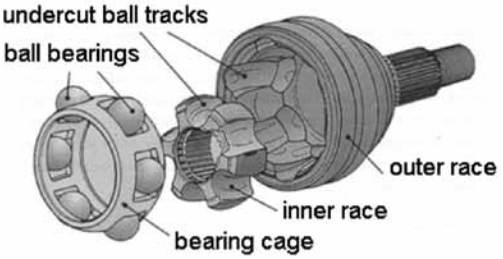

Figure 3. Homokinetic joint

ANALAYSIS OF THE RIGIDITY IMPACT ON THE ACCURACY OF THE INNER RACE

The forming process for manufacture of the inner race consists of three passages through the press (cf. Figure 4). At the first passage a preform (a) is made in the three-stage tooling. Heat treatment (process annealing) and surface treatment of the preform follows. As the lubricant carrier the preform contains phosphate and MoS_2. From the point of the tool life, the second passage is the most critical, as in operation (b) the required geometrical form of the preform is made and in operation (c) the product bottom is pierced. In the third passage, during the operation (d) calibration of the product is made to the specified dimensions of spheres diameter D_1 and D_2 and the product height. Hereinafter, the analysis will be given regarding the die rigidity impact on the accuracy of the inner race, namely for the last operation, where calibration of a pre-form is performed in order to achieve the final dimensions of the product (d) and impact of the die rigidity on the tool life for operation (b).

For the calibration of the inner race we used die with a conventional ring and die with a Strecon ring in order to analyze the die prestress on the product accuracy. Figure 4 shows the characteristic dimensions of spheres D_1 and D_2, of the inner race and the product height. Table 1 gives the values for dimensions

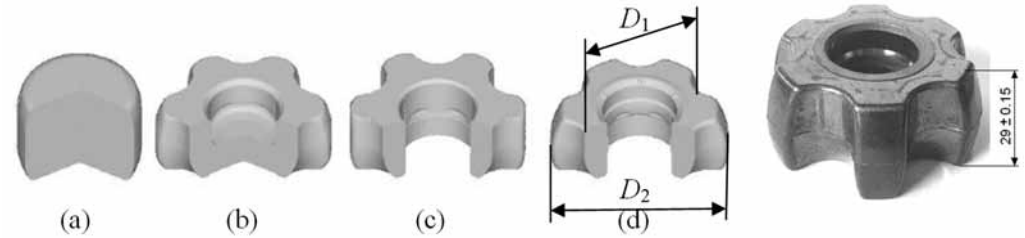

Figure 4. Sequence of forming operations in manufacture of the inner race and a product development

Table 1: Data for dimensions D_1 and D_2 for the die with the conventional and the Strecon shrink ring

Product (mm) (by drawing)	Die (mm) (by drawing)	Manufactured die (mm)	Cold forged product (mm)
D_1 70.9 + 0.15/–0.1	Clasic shrink ring		
	D_1 70.8–0.02	D_1 70.81–70.87	D_1 70.83–71.09
	D_2 50.8–0.02	D_2 50.79–50.87	D_2 50.83–51.14
D_2 50.9 ± 0.2	Strecon shrink ring		
	D_1 70.78–0.02	D_1 70.74–70.79	D_1 70.95–70.98
	D_2 50.78–0.02	D_2 50.74–50.79	D_2 50.98–50.99

D_1 and D_2 for the product by the drawing, constructional drawing of the die, the manufactured die and for the final product for the conventional and the Strecon shrink ring.

The Table 1 shows that the conventional shrink ring does not ensure manufacture of the inner race within the desired tolerances. With reference to the too high elastic elongation of both key dimensions of the die with the conventional ring, the objective is to manufacture a more rigid die. Instead of the conventional die composed of external steel ring with tooling interference 0.6 % , we used a shrink ring Strecon E^+ of cemented carbide and winded spring strip with tooling interference 0.4 % (cf. Figure 5). The die interference 0.4 % means that the outside die diameter is 0.4 % bigger than the inside core diameter of cemented carbide. The advantages of the Strecon ring are both that it enables higher extrusion pressures within the die working area and that its high rigidity substantially reduces the cyclic plastic deformations that are characteristic of a crack development on the working surfaces of tools in cold extrusion. The manufacturer of the new ring ensures

25 % smaller elongation of the inner race outside diameters. Due to the deviation of key diameter tolerances with the conventional die, we decided to reduce dimensions D_1 and D_2 on the die with the Strecon shrink ring by 0.02 mm, namely D_1 to 70.78 – 0.02 and D_2 to 78.0 – 0.02.

The main diameters of inner race in the upper and lower die with Strecon ring were made with lower tolerances. Tolerance comparison of dimensions D_1 and D_2 for the product by the drawing, the die and the calibrated product for the conventional and the Strecon ring is shown in Figure 6. Elastic ra-

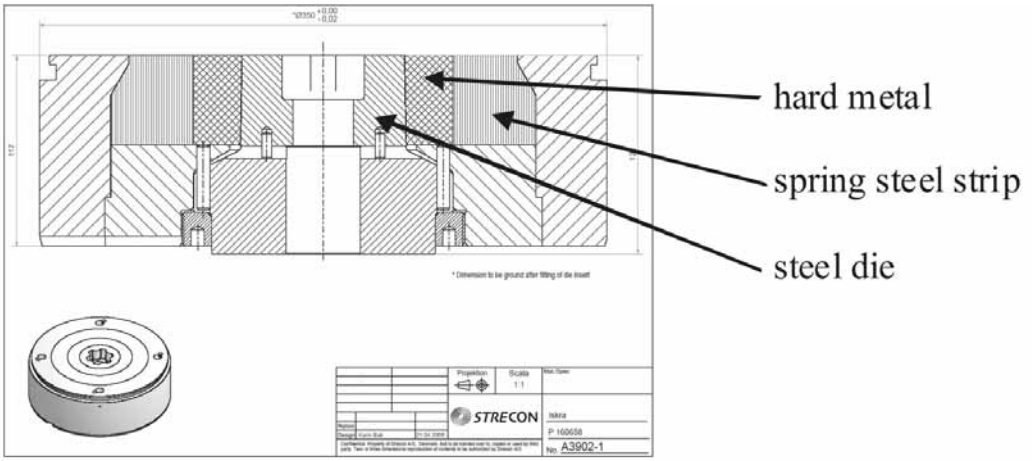

Figure 5. Lower die for inner race calibration

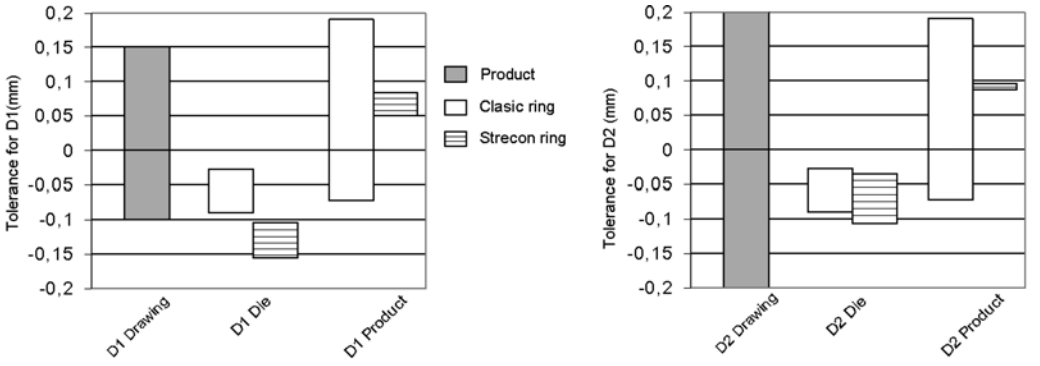

Figure 6. a) Tolerance scatter for dimension D_1 and (b) Tolerance Scatter for dimension D_2 of the spherical head for the conventional and Strecon shrink ring

dial elongation of the die with the Strecon shrink ring compared to the die with the conventional ring is lower for 20 %. Lower elastic elongation of the die is essential for higher accuracy of the product.

Furthermore, we were interested in the impact of a mass scatter of the product on the dimension D_1 of the inner race for the die with the conventional and the Strecon ring (cf. Figure 7). Strecon ring ensures smaller deviation for the dimension D_1 and in this way allows greater mass scatter of the formed piece. Suitable rigidity of the shrink ring is therefore essential to achieve desired dimensional accuracy of the products with the complex geometry.

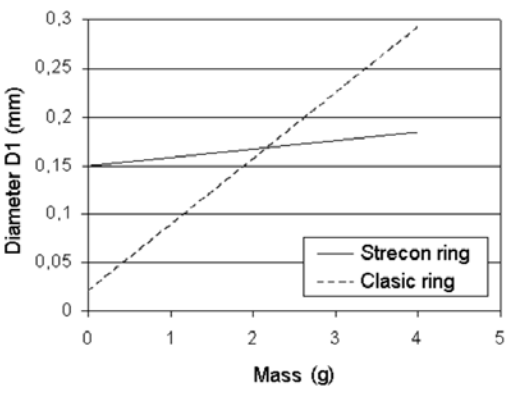

Figure 7. Impact of mass scatter on the accuracy of the diameter D_1 of the inner race with different die rigidities.

Analaysis of impact of die rigidity on tool life

In manucturing of the complex forms and accurate dimensions, tool life and/or good tool endurance is very important for reliability of the production. When producing such products, the main vital parts like dies, counter-punches and punches are loaded to the extreme limits of endurance, where even small deviations from the set values of the impact parameters can cause critical damage growth and too early destruction of tools. Great scatters regarding the tool life are characteristic of such production. Therefore, it is important that for a successful and reliable production we analyze, define and control those parameters that have an important influence on the tool life. It is known from practice and theory that key parameters with an impact on tool life are:

- optimum design, accurate definition of load and correct sizing of vital tool parts,
- selection of suitable materials and their optimum heat treatment and
- use of modern treatment procedures and protection of active tool parts against wear.

In the case of the preform extrusion (Figure 4, operation (b)) the impact of different die prestress on damage development was analysed. We analysed a die with a steel ring and 0.8 % tooling allowance and Strecon *E*+ prestress ring with 0.6 %

tooling allowance. The die was in both cases made from steel ASP 23 with hardness (60 + 1) HRc.

Figure 8 shows typical damage of the die working surface. For analysis of the tool life it is necessary to define the loads that are caused by the forming process on the tool surface. Active tool parts are loaded by stresses, which have been calculated by means of numerical analysis of the forming process. The tool was loaded cyclically as under conditions of mass production. The tool response on the critical spot is elasto-plastic and is defined by kinematic and isotropic hardening and damage development.[7] Increments of plastic deformations are in individual loading cycles relatively small. However, during the process of massive loads, these increases accumulate and cause macroscopic faults on the tool.

First we set the loads with a MKE analysis of the forming process. Based on the loads, tools were analysed by the help of

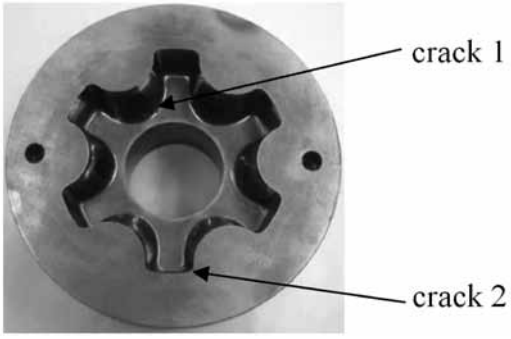

Figure 8. Occurrence of cracks on the lower die for cold forming of the inner race preform

MKE (Figure 9 (a)). For the numerical analysis the program Deform 3D V9.1 was used.[8] The results of the analysis show the most probable point of damage in the inside of the die (Figure 9 (b)). With the module for tool damage analysis, development of damages was analysed.[9]

Loads were copied to the die surface and we repeatedly performed cyclic loads. The response in the critical points of the die is elastoplastic and is described by the hysteresis loops, which results from kinematic and isotropic hardening of material at a concurrent damage development. Figure 10 shows impact of different tooling allowances on the position of the hysteresis loops in the stress deformation conditions at the cyclic load. Hysteresis loop *E*+ (0.6 %) is visibly narrower, therefore the specific part of plastic deformation is smaller and growth of damages slower. Slower damage growth in *E*+ ring compared to the steel ring is shown in Figure 11. A detailed insight into damage development within one cycle reveals that in the initial part of the cycle, when the tool is still in the elastic condition, damages do not grow. Towards the end of the forming operation, after the load of the tool increases so high that the stress in the critical points exceeds the yield stress, the damages in the tool increase intensively. When the stroke ends, ejection of the formed-piece follows and the tool is relieved of load. The first part of the load relieving is elastic; the second one is plastic due to the load in the opposite direction, caused by the prestressing of the shrink ring.

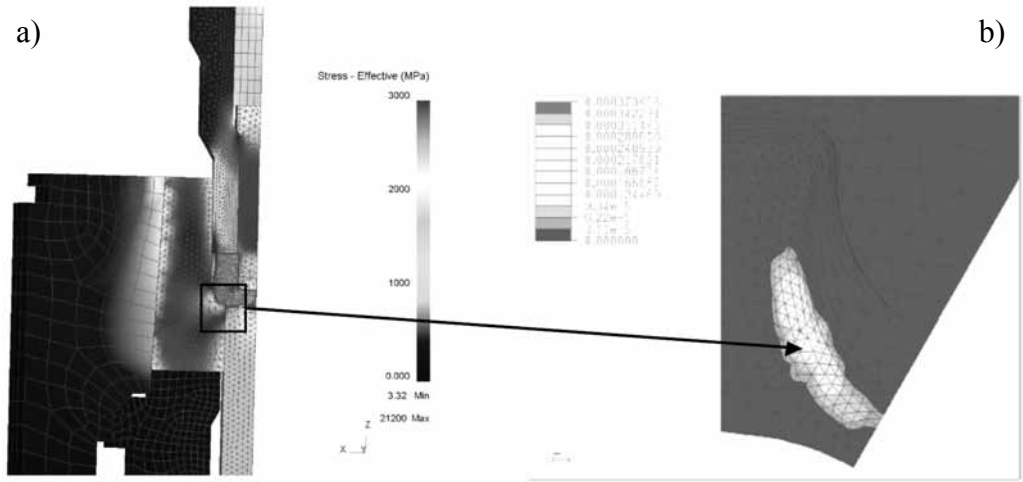

Figure 9. MKE-analysis of tools for operation – (a) and (b) damage on the tool

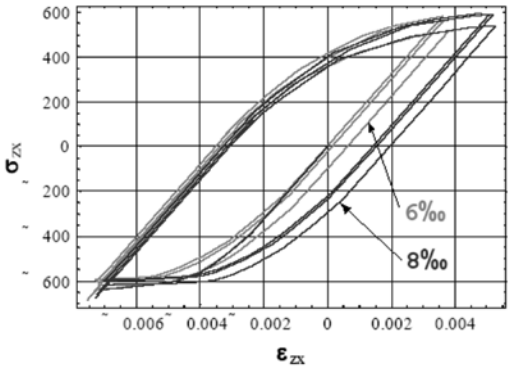

Figure 10. Hysteresis loop in cyclic loads of the die with steel ring and allowance 0.8 % and Strecon *E*+ ring and allowance 0.6 %

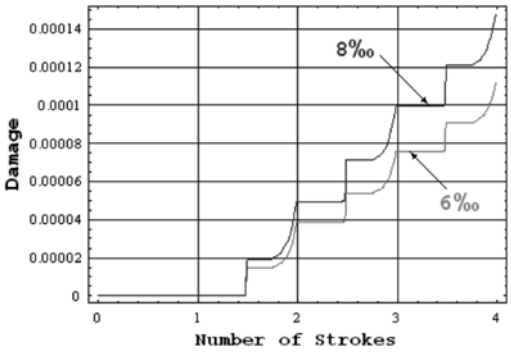

Figure 11. Damages depending on the number of loads for die with allowances 0.6 % and 0.8 %

For a reliable product manufacturing, adjustment of the preform mass to the maximum scatter of ± 0.5 % from the nominal value and the flow stress of ±8 % from the average value is required in addition to the suitable die rigidity. In this way with the Strecon ring we ensure the product height in tolerance of ±0,1 mm with the process centering index $C_{pk} > 1.67$ and endurance of the die on average for 38,000 pcs (operation b, Figure 4). Tool life in the last calibration operation is not as problematic. With optimum input parameters we can achieve over 70,000 pcs of manufactured inner races with one set of dies.

CONCLUSION

This article analyses impact of the die rigidity on dimensional accuracy of the inner race and on the tool life. Definition of the optimum die shrink fit is one of the key factors for reliable manufacture of products both from the point of view of product accuracy and the optimum tool life. Greater rigidity of the die shrink ring reduces cyclic plastic deformations on tool surface, which are typical for damage development. On the other side, greater rigidity of the shrink ring reduces radial elastic deformations of the die and in this way ensures stable dimensional accuracy of products. Greater die rigidity enables also compensation of greater mass scatters of input blanks. In short, die rigidity has a great impact on reliability and consequently on cost effectiveness of the production using precise cold forming.

REFERENCES

[1] KRUŠIČ, V. (2009): Reliabilty of system for precise cold metal forming. Ph. D. Thesis., University of Ljubljana, Faculty of Natural Sciences and Engineering, p. 140.

[2] RODIČ, T., GREŠOVNIK, I., HANSEL, M., MEIDERT, M. (1999): Optimal prestressing of cold forging dies. *Proceedings of the 6th International Conference on Technology of Plasticity Nuremberg*; pp. 253–258.

[3] HÄNSEL, M. (1993): Beitrag zur Simulation der Oberflächenermüdung von Umformwerkzugen. Ph. D. Thesis, LFT, Friderich-Alexander-Universitat Erlangen-Nuremberg.

[4] NIELSEN E. B., GROENBAEK J. (1995): Improved service life conditions for cold-forging die inserts through the use of high-stiffness strip-wound containers. *Proceedings of the 9th Cold Forging Congress*; Solihull, England, pp. 51–57.

[5] Strecon, Stripwound dies, Accessible on Internet: http://www.strecon.com

[6] PEDERSEN, T. O. (1998): Cyclic plasticity and low cycle fatigue in tool materials, Ph.D. Thesis. Technical University of Denmark, DCAMM, Report No. S 82, p. 122.

[7] KRUŠIČ, V., MAŠERA, S., PEPELNJAK, T., KUZMAN, K., RODIČ, T., PRISTOVŠEK, A. (2009): The Impact of the Forming System Parameters on Tool Service Life and Product Accuracy in Cold Forging. Int. J. of Microstructure and Materials Properties, Special Issue; *Industrial Tools and Materials Processing Technology*, Vol. 4, Nos. 5/6.

[8] SFTC, Scientific Forming Technologies Corporation, Deform 2/3D, Ver. 9.1. User Manual, Columbus, Ohio, 2009.

[9] RODIČ, T., KORELC, J., DUTKO, M., PRISTOVŠEK, A., KUNC, R., HÄNSEL, M. (2001): Cyclic plasticity and damage of cold forging tool for production of automotive shift fork. *Proceedings of the 3rd International Conference on Industrial Tools*; Rogaška Slatina, April, pp. 331–334.

Sequence stratigraphy study within a chronostratigraphic framework of 'Ningning field', Niger Delta

Sekvenčnostratigrafske raziskave "Področja Ninging" delte Nigra v kronostratigrafskem okviru

Oluwatosin John Rotimi[1, *]

[1]Petroleum Engineering Department, College of Science and Technology, Covenant University, Canaan Land, Km10 Idiroko road, P. M. B. 1023, Ota, Ogun State, Nigeria

*Corresponding author. E-mail: orotimi@covenantuniversity.com

Received: July 22, 2010 **Accepted:** November 5, 2010

Abstract: Sequence stratigraphy model developed for the Ningning field is based on the interpretation carried out on the different wells that penetrated the various subsurface lithologies. Basically three depositional sequences were delineated from the five wells studied. The Vail model used made out a third and forth order stratigraphic surfaces that all fall within the central swamp depobelt of the Basin. The five wells used show the presentation of the interpretation and the models. All the sequence tracts were appropriately represented starting from the Lowstand Transgressive and Highstand system tracts, except in well 005 where the Lowstand of the second sequence was missing. This is achieved by incorporating signature motifs from wireline logs coupled with biostratigraphy data and inferred paleobathymetry. This has revealed the field-wide reconstruction of a chronostratigraphically constrained biostratigraphy of subsurface lithological sequences with limited information.

Povzetek: Sekvenčno stratigrafski model polja Ningning temelji na interpretaciji različnih vrtin, ki sekajo različne kamnine pod površjem. Preiskava petih vrtin je omogočila prepoznati tri sedimentacijska zaporedja. Uporaba modela Vail je pokazala stratigrafske površine tretjega in četrtega reda, ki vse spadajo v osrednji močvirski sedimentacijski pas bazena. Interpretacijo in modele predstavljamo na podlagi petih uporabljenih vrtin. Ugotovili smo vsa sekvenčna zapo-

Original scientific paper

redja od začetnih plitvo transgresivnih do zaporedij z visoko vodo, razen v vrtini 005, kjer manjka plitvo stanje druge sekvence. Interpretacijo je omogočila povezava karotažnih zapisov z biostratigrafskimi podatki in s sklepanjem o nekdanjih globinah. Z maloštevilnimi podatki smo lahko podali širšo rekonstrukcijo kronostratigrafsko omejene biostratigrafije litoloških zaporedij pod površjem.

Key words: sequence, stratigraphy, depobelt, biostratigraphy, wireline-logs, lithologies
Ključne besede: sekvence (zaporedja), stratigrafija, pas sedimentov, biostratigrafija, karotaža, litologija

INTRODUCTION

A greater portion of the world's energy mix will come from hydrocarbon sources and its derivatives coming from the deeper portion of the various hydrocarbon habitats. It has therefore become imperative to apply newly emerging exploration and production tools and skills to adequately harness these resources. The petroliferous Niger Delta is one of the highest producing basins with more promising reserves yet to be discovered as exploration proceeds to the deeper water. Sequence stratigraphy is one of the twenty first century exploration and production tools that are used to unravel series of lithological and basinal intricacies bordering on sand packets, depositional sequences and paleoenvironmental analysis. Biostratigraphy is indispensable in the adequate delineation of chronostratigraphically significant surfaces in the subsurface formations encountered in hydrocarbon exploration. The study is aimed at subdividing the stratigraphic section within the study area into packages of sediments bounded by chronostratigraphically significant surfaces (condensed sections, their associated maximum flooding surfaces and sequence boundaries).

STUDY AREA AND REGIONAL GEOLOGY SETTING

The study area is a producing field located in the Niger Delta. The Niger Delta is situated in the Gulf of Guinea (Figure 1) and extends throughout the Niger Delta Province (KLETT et al., 1997). The Niger Delta is a large arcuate delta situated on the West Coast of Central Africa, between Lat 3^0 and 6^0 N and Long 5^0 and 8^0 E (REIJERS et al., 1997). The province contains known resources (cumulative production plus proved reserves) of 34.5 BBO and 93.8 TCFG (PETROCONSULT-

ANTS, 1996b). Currently, most of this petroleum is in fields that are onshore or on the continental shelf in waters less than 200 m deep. Exploration focus is presently shifting to the deeper waters in the Niger Delta with huge discoveries like Bonga and Agbami fields (with about 1BBO reserve) increasing the prospectivity of oil search in the riskier deeper waters despite the high cost of exploration and development at these water depths.

From the Eocene to the present, the delta has prograded southwestward, forming depobelts that represent the most active portion of the delta at each stage of its development (DOUST & OMATSOLA, 1990). These depobelts form one of the largest regressive deltas in the world with an area of some 300 000 km^2 (KULKE, 1995), sediment volume of 500 000 km^3 (HOSPERS, 1965), and a sediment thickness of over 10 km in the basin depocenter. The Niger Delta Province has been identified to be a prolific hydrocarbon habitat and is known to contain one identified petroleum system (EKWEOZOR & DAUKORU, 1984; KULKE, 1995) referred to as the Tertiary Niger Delta (Akata – Agbada) petroleum System. The sandstones and unconsolidated sands from which petroleum is produced in the Niger Delta have a geometry that has been grossly affected and controlled by the dominant growth fault configuration. The sand units are

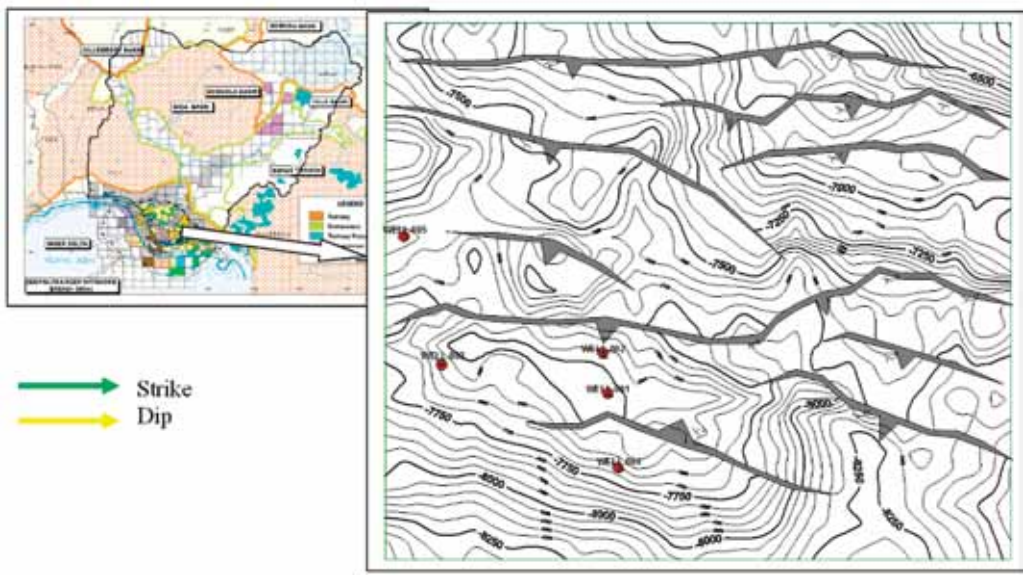

Figure 1. Niger Delta study location. Inset is field basemap with well positions and correlation directions.

seen to thicken in the downthrown portion towards the fault dip direction (ROTIMI et al., 2010, WEBER & DAUKORU, 1975).

MATERIALS AND METHODS

Wireline logs were used for the purpose of this study in conjunction with biostratigraphy data. The method employed in this study is that of lithofacies identifications coupled with sequence stratigraphic concepts. Parasequences were identified based on the principle described by (VAN WAGONER et al. 1990). Their boundaries were identified and separated from others by flooding surfaces which are often characterized by a cycle of sediment that either coarsens or fines upward. These changes in grain sizes are abrupt and very conspicuous and allow for correlation of the parasequence boundaries across the field thus being a valid tool for chronostratigraphy although care must be taken in choosing these surfaces.

Stacking pattern for parasequences sets were evaluated as fundamental building blocks of a sequence. The identified stacking patterns include progradational, retrogradational and aggradational stacking patterns (VAN WAGONER et al., 1990*)*. These patterns are dependent on the ratio of the rate of deposition to that of accommodation. A progradational stacking pattern of parasequences refers to the pattern in which facies at the top of each parasequence becomes progressively more distal i.e. basinward (POSAMANTIER & VAIL, 1988; WILGUS et al., 1998). A retrogradational parasequence set has successively younger parasequences deposited farther landward in a backstepping pattern. Overall, the rate of deposition is less than the rate of accommodation.

An aggradational parasequence set is one in which successively younger parasequences are deposited above one another with no significant lateral shifts. The rate of accommodation approximates the rate of deposition (i.e. $R_{accm} = R_d$).

Some other differentiating factors include lithological ratio interplay of material deposited (i.e. sandstone or mudstone), the environment of deposition (i.e. coastal/shallow marine to deep marine) and the ratio of the thicknesses of the different parasequences and parasequence sets. All the aforementioned points were used for the purpose of this study.

Chronostratigraphically Significant Surfaces

Sequence boundaries were identified based on the methodology described by VAN WAGONER et al., (1990). Sequence boundaries were identified by the most basinward shift in facies,

within a coarsening upward sequence (Emery & Myers, 1996). These are usually located between two maximum flooding surfaces. Typical lg pattern in neritic environment is an aggradational (massive) lg pattern that overlies an interbedded lg pattern. This boundary corresponds to the position of highest resistivity and lowest lithology lgs.

Below the sequence boundary is a trend of decreasing flooding surface as indicated by increasing flooding surface shale resistivity, while above the boundary is a trend of increasing flooding surface and decreasing flooding surface shale resistivity. Maximum flooding surface caps the transgressive system tracts which represents the most landward transgression of the shoreline.

In recognizing the various systems tract (lowstand, transgressive and highstand), procedure that involves first, locating the maximum flooding surfaces within major condensed sections on the well-lgs, followed by the location of the sequence boundary between the two maximum surfaces was adopted.

The Lowstand System Tract: This comprise of the basin floor fan, the slope fan and the prograding wedge complex all have their boundaries marked by maximum flooding surfaces (MFS) recognized as an extensive blanket of shale minor or major with fauna and floral diversities (Vail & Wornardt, 1992).

The Transgressive System Tracts**:** This is characterized by an overall upward fining and thinning (backstepping parasequence set) on lgs, although the individual parasequence tends to prograde. It is bounded below by a transgressive surface and above by a maximum flooding surface. The portion of the lg with lowest shale resistivity and which corresponds with the maximum deflection on the GR and/or the SP lg were selected as the maximum flooding surfaces. A condensed section is associated with the maximum flooding surface that marks the upper boundary of the transgressive system tracts as the parasequences backsteps landwards (Loutit et al., 1988). It is characterized by the greatest abundance and diversity of fauna within the sequence and starved of terrigenous materials.

The Highstand System Tracts**:** This is bounded below by a downlap surface of maximum flooding and above by a sequence boundary. The early highstand is characterized by aggradational parasequence set, while the late highstand is characterized by a set of prograding, coarsening upward and shallowing upward parasequences that terminate at the sequence boundary. Lg correlations in the highstand is difficult and lg patterns, commonly indicate interbedded sand and shale lithofacies, while

the reservoir continuity is fair (VAIL & WORNARDT, 1990).

Eustatic sea level charts derived from eustatic cycles of the Niger Delta and the coastal onlap have been correlated to derive the regional chronostratigraphy of the Niger Delta. This has aided the prediction, location and dating of sequences, their correlatable boundaries, and other chronostratigraphically important surfaces in the Niger Delta. The Niger Delta Cenozoic chronostratigraphic chart Figure 2, is a geological data table containing up to date information on the chronostratigraphy of the Niger Delta, its marker shales and maximum flooding surfaces, the Pollen (P-zone data) and Foraminifera zonation (F-zone data), the Niger Delta depobelts and its sequence stratigraphy (HAQ et al., 1988). The chart was used variously in the course of this study to determine amongst others, the ages of the maximum flooding surfaces and the sequence boundaries.

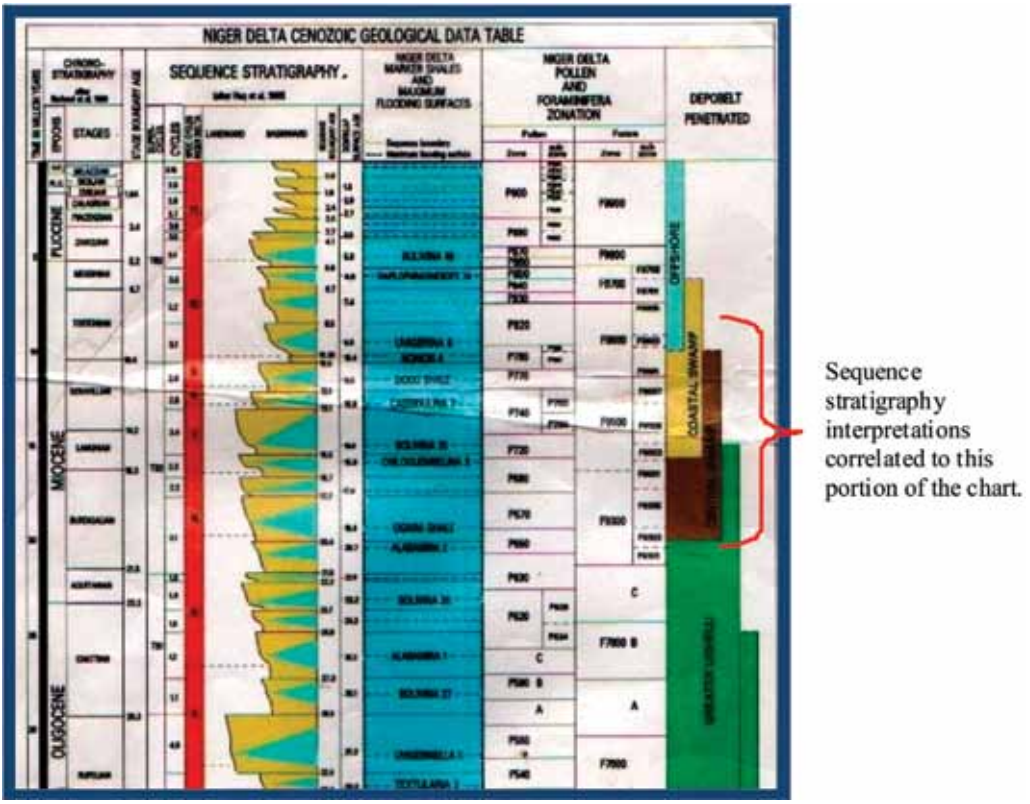

Figure 2. The Niger Delta Cenozoic Chronostratigraphic Chat (HAQ et al. 1988)

Well Correlation

Correlation of wells along strike and dip lines was made towards the development of a chronostratigraphic framework for the study area. The correlations made over the entire field starting from the control well 001. This was done to build a holistic sequence stratigraphic framework. The correlations were carried out along one strike and one dip line. This is limited based on the location and position of the wells as displayed on the base map and well positions relative to each other as seen on the basemap (Figure 1). Due to the localization of the wells, there is dire need to start correlation within this area and also in the vicinity of the identified chronostratigraphic surfaces e.g. the correlatable marker shales.

Results and interpretation

Sequence boundaries in the field were identified based on the interpretation of unconformity surface seen on the lgs assisted by the interpretation of stacking patterns, lg shapes and motifs. This is discovered to be the effect of basinal drift in the sediment/ horizon sets on and facies arrangement on the wells which was a major focus. The major Sequence Boundary recognized included 17.7 Ma, 14.8 Ma, 12.1 Ma, and 10.38 Ma. Unconformity surfaces marks the sequence boundaries while on the well lg the highest value on the Resistivity lg which corresponds to the lowest value on the SP lg indicates the sequence boundaries mapped. The formations mapped are predominantly of the prolific hydrocarbon bearing Agbada formation of the Niger Delta which is thick sequences of early to middle Miocene age. The discussion is presented below.

Discussion

SEQUENCE BOUNDARIES (SB)

17.7 Ma SB

This is the oldest sequence boundary identified in the study area. It was penetrated by Wells 001, 002 and 003 at depths of 2 951 m, 2 836 m, and 2 860 m respectively. This surface was not recognized on Well 005 due to the depth to which it was drilled and a projection was done to include Well 004 from the other array of wells, as it was situated at some distance basinward. The lg motif shows abrupt change from an upward deepening facies succession to an upward shallowing one. Paleobathymetric deduction and lg signatures shows that such horizons are devoid of pollens as there are indications of forams present (F-zone data). The depositional environment deduced from the lgs depicts a shelf environment (Figure 3).

14.8 Ma SB

This Sequence Boundary is well marked on all the lg signatures and was penetrated by all the wells in the field. The depth of occurrence varies with respect to the position of the wells on the block and relative to each other. The lg signature associated with this boundary is slightly featureless and in some part blocky. It is associated with a boundary of graded sandy shale sequence. This interpreted the pre-channel facies of the field as it resembles a basin floor fan complex but it can be said to be of the slope fan complex. Due to the non-uniform lg shape it could be inferred that the lithology must have been deposited in a high to moderate energy regime with limited time for sediment sorting and hence the intercalation of the beds and consequent aggradations (Figure 3).

12.1 Ma SB

The 12.1 Ma sequence boundary overlies the succession of lithologies penetrated by all the wells 001, 002, 003 and 005. A careful projection was also made to well 004 so as to gain proper chronostratigraphic correlation coverage of the field. This sequence boundary is well marked on all the wells as it occurs at different depth range, but as delineated in the field the boundary falls within the depth range of 1 762 m in Well 001 and 2 083 m in Well 005. The aggradational lg shape of the sand body sequence is typical of channel levee complex and at the proximal portion of the basin a prograding wedge complex (Figure 3). This near cylindrical lg shape shows slight left side deflection and a corresponding right side Resistivity lg signature. This is characteristic of a channel complex environment serving as a suitable clear demarcation for the overlying Lowstand system tract.

10.35 Ma SB

This marks the youngest sequence boundary penetrated in the study area as it marks the base of the Benin sand formation. It occurred in all the wells and also a projection done to incorporate the more proximal well 004. This marks the channel sequence of the distal pre Benin sequence deposited. This sequence has a blocky lg shape as much as depicted on the log motif and indicates a channel sand deposit marked abruptly by complex of slope wedge deposits. This is well correlated to the Niger Delta chronostratigraphic chart and accurately mapped (Figure 2).

Maximum Flooding Surfaces

Maximum flooding surface were delineated as points of occurrence of an extensive blanket of shale and starved of terrigenous material with biofacies diversity. The surfaces were picked on the well lgs as the top of a retrogradational complex. The lowest value on the Resistivity curve which corresponds to the highest value on the lithology curve depicts the point where the surface occurs.

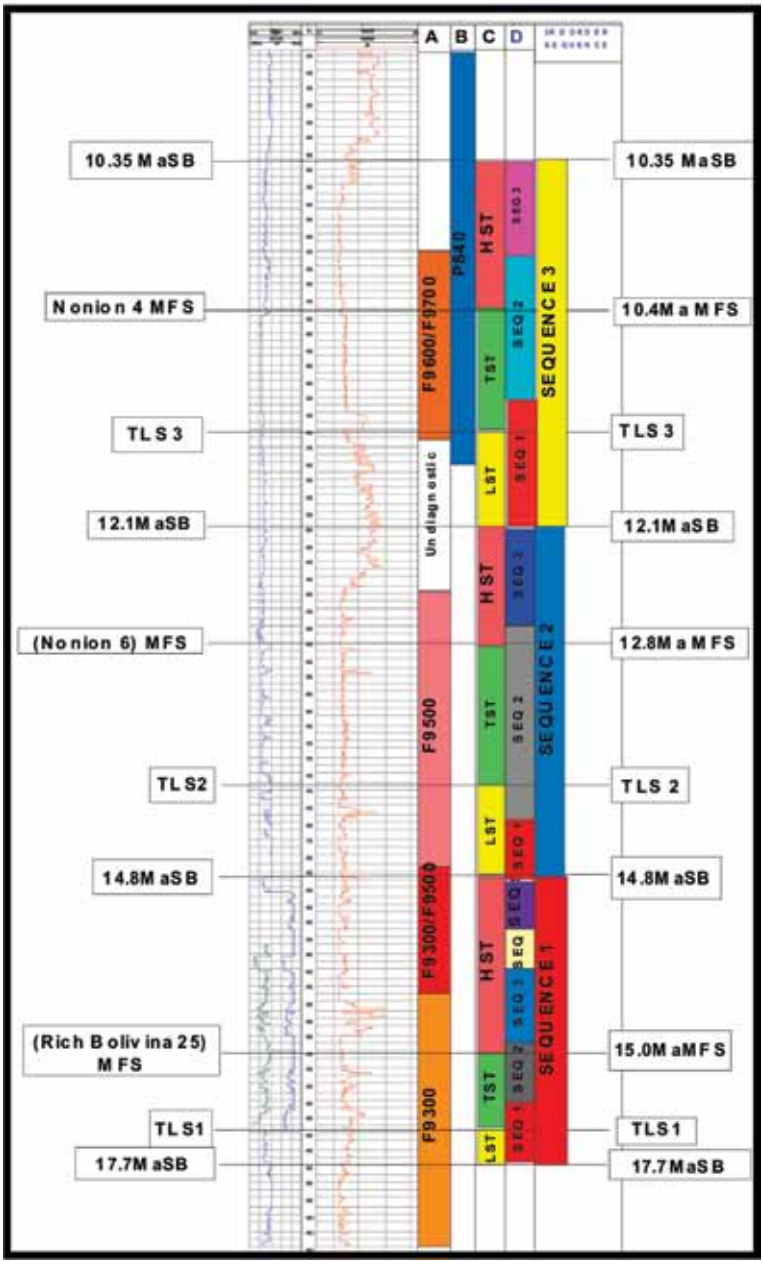

Figure 3. Well 1 showing sequences and stratigraphically significant surfaces

Identification of higher frequencies depositional sequences

In addition to the various 3rd order depositional sequences, system tracts and flooding surfaces identified, a number of higher order frequencies depositional sequences of the Forth order, were adequately identified and delineated in the wells studied (GOLDHAMMER et. al., 2000). Although most of the wells in the study area exhibited mainly 3rd order depositional sequences, these sequences were subsequently subdivided into higher order sequences denoted with numbers 1–3 and 1–6 as the case may be. This subdivision is done as a branching out of the major depositional cycle depicted by the major sequence boundaries of the depositional sequence and their associated flooding surfaces. This identified higher order sequences is interpreted as indications of the minor position at different times of the shoreline within the mega cycle which are therefore eustatic and represents the major depositional sequences.

THIRD (3RD) ORDER DEPOSITIONAL SEQUENCE STRATIGRAPHIC INTERPRETATION OF WELLS

Well 001

Sequence 1

This sequence starts at depth 2 951 m and ends at 2 743 m. The lowstand system tract begins this sequence bounded below by the 17.7 Ma sequence boundary. The sand package above the boundary is described as a prograding complex showing a fining upward pattern capped by a minor condensed section associated with abundance and diversity peak that terminates at the maximum shale point (i.e. top of lowstand - TLS 1). This is overlain by the transgressive system tract (TST) that covers a depth of 144m above the TLS 1 and consists of an overall retrograding parasequence stacking pattern capped by the 15.0 Ma *Rich Bolivina 25* maximum flooding surface (Figure 3).

The highstand system tract rest on the TST and covers the depth range of 2 743 m to 2 416 m. It starts with an aggradation parasequence stacking pattern and subsequently starts to prograde upward. It is truncated at the top by the 14.8 Ma sequence boundary.

Sequence 2

This sequence starts with an almost uniform shape, non graded sand body of about 160 m that forms the base unit of the lowstand system tract (Figure 3). The near blocky signature signifies a sandy lithology showing a slightly fining upward trend indicating a well developed channel sand body of a slope fan complex and terminates at the to of lowstand (TLS) 2.

The transgressive system tract extends from a depth of 2 256 m to 1 984 m.

This portion of the subsurface is found to exhibit individual Parasequence pattern prograding and showing a motif similar to that of an incised valley fill. The TST is capped by the 12.8 Ma – *Nonion 6* MFS associated with a major condensed section.

This sequence is terminated by the highstand system tract which starts at depth 1984 m showing some initial aggradational stacking pattern and later progrades to be terminated at the distal portion by the 12.1 Ma sequence boundary (Figure 3).

Sequence 3

Resting upon the 12.1 Ma sequence boundary is the uppermost sequence encountered in this well. It is characterized by back stepping signature o the lithology lg although it shows spurious effect on the saturation. Such can be interpreted to be a channel facies deposited under turbulent energy this with no time for consolidation or sorting. The Nonion4 MFS appears at 1364 m to caps the top of the transgressive system tract appearing in the middle of the LST and HST. The pattern that starts this sequence grades into a more uniform and characteristically blocky unit of rock typical of a time of recession in energy of the medium. At 1 070 m the 10.35 Ma sequence boundary caps this section to terminate the observed third order sequences for this well.

Well 002

Sequence 1

The Lowstand system tract begins this sequence at depth 2 836 m and ends at 2 735 m. The whole sequence covers a total depth of 466.6 m (1531 ft) and bounded at the base by the 17.7 Ma sequence boundary (Figure 4). The sediment package constituting this system tract shows a rounded lg signature typical of an aggradational Prograding complex. The Transgressive system tract overlies the LST and covers a depth of 231 m above it. The laterally extensive shale blanket which distinguishes it from the major condensed section is of the shelf environment, it consists of a series of fining upward retrograding parasequence pattern capped by the 15.0 Ma *Bolivia 25* maximum flooding surface (Figure 4). The highstand systems tract caps sequence 1 as it sits on the TST at depth of 2 504 m to 2 370 m just below sequence 2. This system tract shows bulky aggradational parasequence pattern as it progrades upward to be capped by the 14.8 Ma sequence boundary.

Sequence 2

Sequence 2 starts with a crescent shaped lg pattern which grades into a Prograding complex and body with no grading pattern observed. This basal unit of the Lowstand system tract starts from depth of 2 370 m to 1 923 m. It is bounded below by the channel sand body which marks the base of this se-

quence boundary of 17.7 Ma. Parasequence set motifs exemplified by some minor abundance and diversity peaks mark the top of this system tract (Figure 4). The Transgressive system tract covers a total depth of 166m as it exhibits a slightly aggradational parasequence set typical of a shelf environment terminated at the top by the major condensed section embedded in the 12.8 Ma maximum flooding surface.

The highstand systems tract found directly overlying sequence 2 starts from the top of the TST at depth 1 923 m to 1 818 m showing some initial crescent-shaped retrogradational stacking pattern fining upward indicating that of a channel complex. This system tract terminates at the 12.1 Ma sequence boundary.

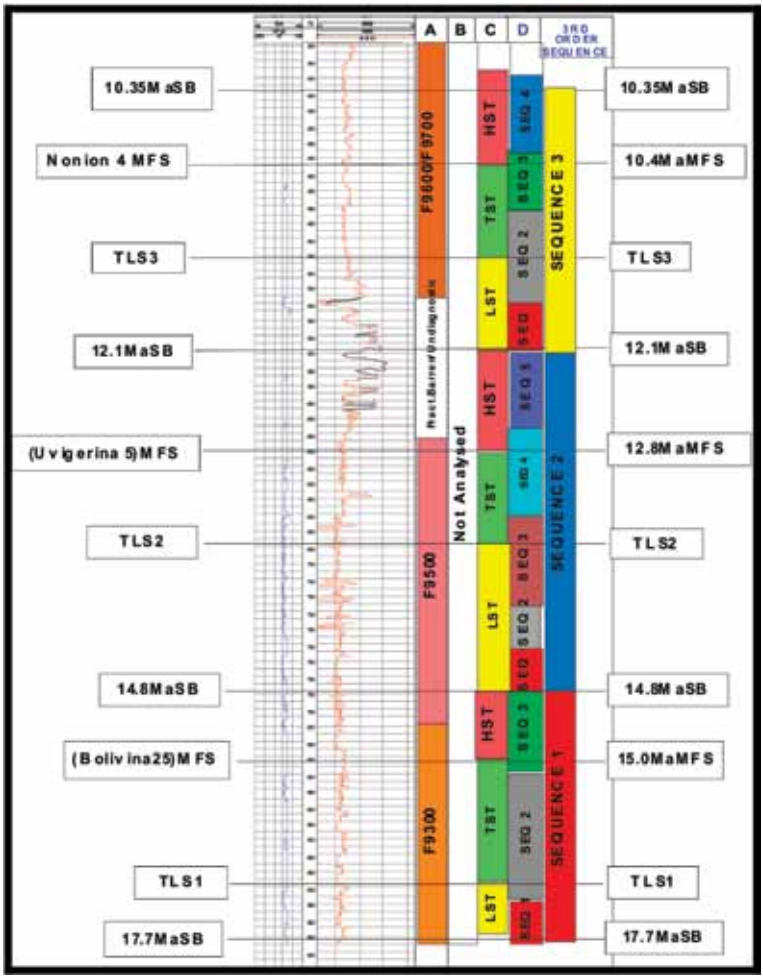

Figure 4. Well 2 showing sequences and stratigraphically significant surfaces

Sequence 3

Sequence 3 episode of deposition extends from 1 736 m (lower sequence boundary) to 1 242 m (upper sequence boundary). The lowstand system tract starts this sequence with the slope fan complex covering about 494 m and overlain by the transgressive systems tract deposit. A laterally extensive marine shale which serves as the maximum flooding surface at 1 382 m is observed to cap this deposit as it is marked by the 10.4 *Nonion 4* MFS at 1382 m. The highstand system tract terminates this sequence at 1 242 m and covers 140 m (Figure 4).

Well 003

Sequence 1

This sequence starts with the lowstand sequence tract at the depth of 2 859 m to 2 329 m. The whole sequence is about 530 m and has a combination of Prograding and slightly aggrading parasequence stacking pattern. The lowstand systems tract has a sand package which shows a fining upward sequence and then interfingering of some minor shale lithology which marks the top of the lowstand systems tract (Figure 5). The transgressive system track overlies this and covers the depth of about 164 m showing a series of upward aggradational pattern typical of the shelf environment. A blanket of extensive marine shale is seen to be truncating the TST with the embedded condensed section. highstand system tract caps this deposit at 2 329 m and marked by the 14.8 Ma sequence boundary.

Sequence 2

The upper and lower sequence boundary occurs at depth 1 709 m and 2 329 m respectively, enveloping the whole system tracts of this depositional episode. The prograding complex and the slope fan deposits mark the lowstand system tract which covers a depth of 184 m within the interval of 2 329 m and 2 145 m. The transgressive system tract with its characteristic fining upward pattern rests on the transgressive surface (i.e. top of the lowstand system tract TLS 2), and truncated by the shale blanket of the maximum flooding surface at 1 909 m marked by the 12.8 Ma *Cassidulina7* MFS (Figure 5). This depositional sequence has the highstand system tract deposit as the cap which starts from 1 909 m to terminate at 1 709 m which is the topmost sequence boundary.

Sequence 3

Sequence 3 episode of deposition started with the lowstand system tract having a slope fan complex as a typical signature at 1 709 m to 1 574 m, and was immediately followed by the transgressive system tract deposits of about 140 m. The maximum flooding surface marked by the 10.4 Ma *Nonion 4* MFS truncates it at 1 434 m as it is subsequently overlain by the highstand system tract. This system tract represented by the aggrading to prograding

lg pattern terminates the studied depositional episode of this well. The lower and upper sequence boundaries of the highstand systems tract occur at 1 434 m to 122 m respectively.

Well 004

Sequence 1

Sequence 1 episode of deposition commenced with the lowstand system tract

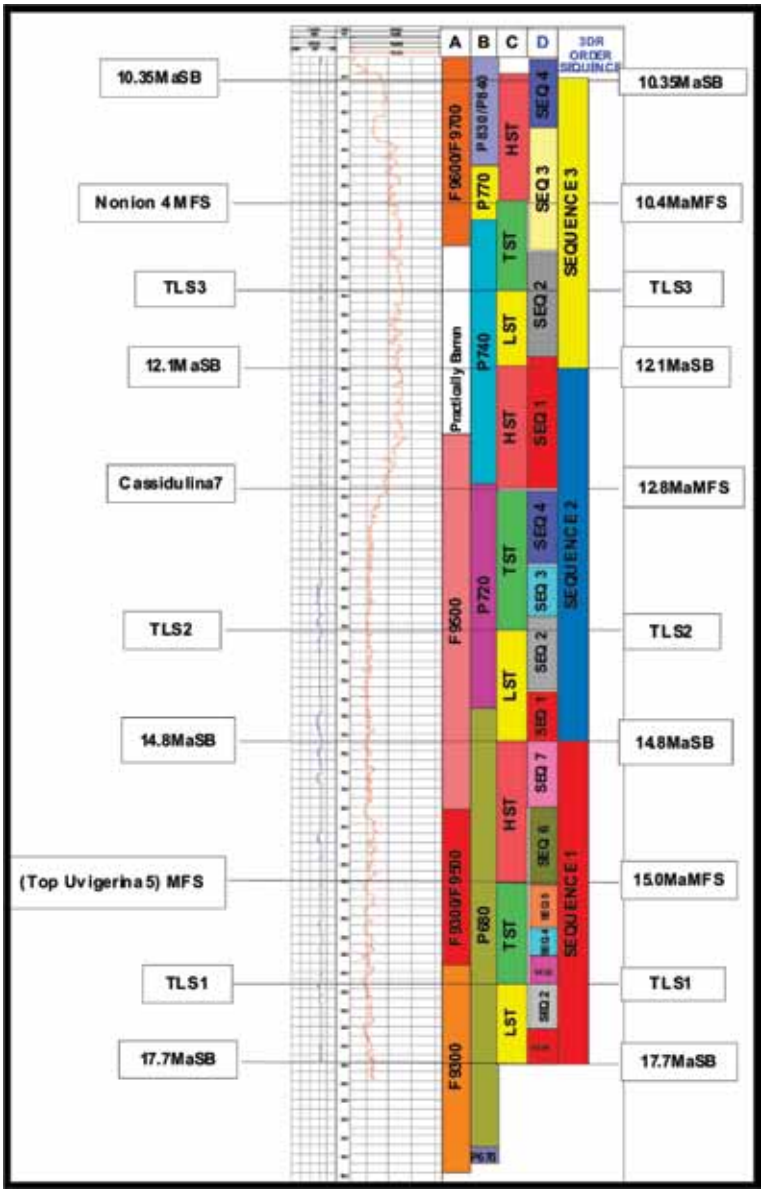

Figure 5. Well 3 with sequences and stratigraphically significant surfaces

which range from 3 459 m to 3 133 m. A short interval of transgressive system tract overlies this prograding slope fan deposit of the lowstand systems tract deposit. Maximum flooding surface marked by 15.0 Ma *Rich Bolivina 25* MFS occurs at 2 940 m to cap the retrogradational pattern of the transgressive systems tract that terminates at the same point. Overlying it unconform-

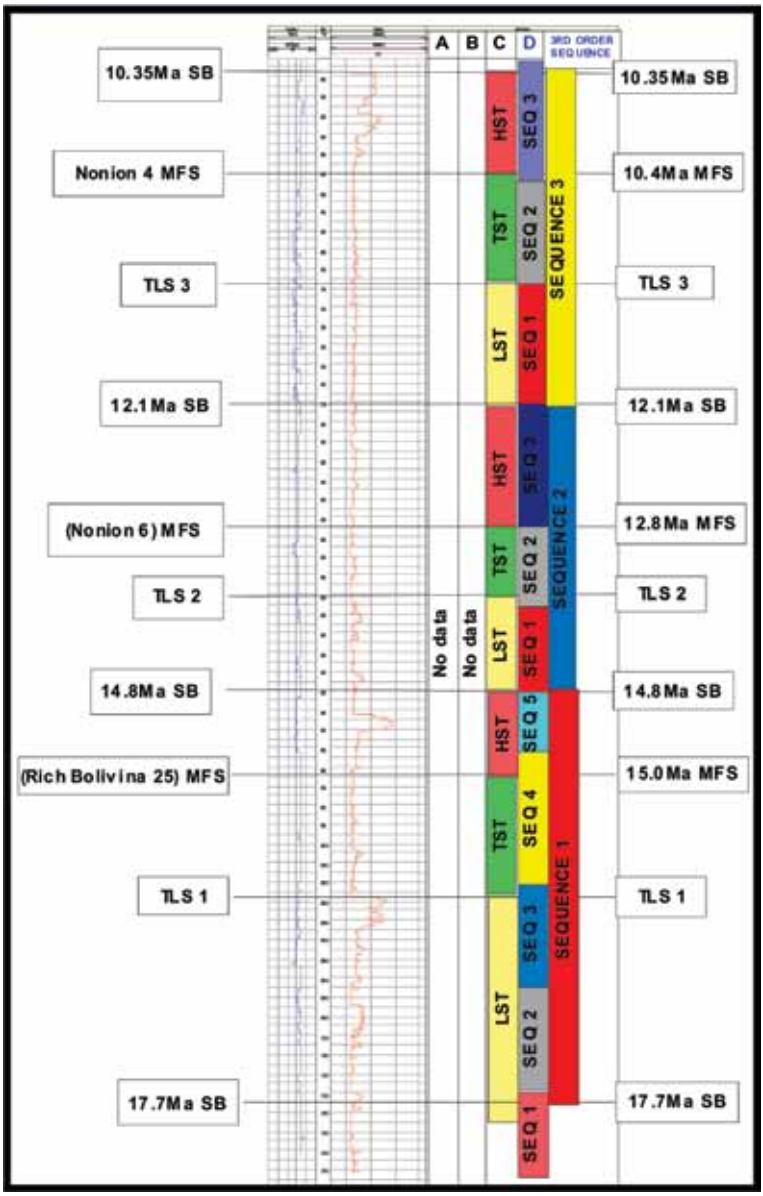

Figure 6. Well 4 with sequences and stratigraphically significant surfaces

ably is the highstand systems tract deposit covering about 133 m and bounded at the upper part at 2 807 m by the 14.8 Ma sequence boundary (Figure 6).

Sequence 2

Sequence 2 observed in well 004 in the study area is bounded at the base and top by sequence boundaries at depths 2 807 m and 2 352 m respectively covering 153 m. it starts with a lowstand systems tract covering 152 m, overlain by a Transgressive Systems Tract that is truncated by a maximum flooding surface marked by the 12.8 Ma *Nonion 6* MFS at 2 540 m. Capping this sequence is the Highstand Systems Tract extending from the top of the maximum flooding surface to a depth of 2 352 m marking the top of the sequence.

Sequence 3

Sequence 3 of Well 004 in this field of study has a thickness ranging from 2 352 m at the lower boundary to 1 821 m at the apex of the sequence. The Lowstand Systems Tract lies on the lower sequence boundary covering 196 m as it terminates at the occurrence of an extensive shaly bed initiating the start of the transgressive systems tract seen to overlay the lowstand system tract. The 10.4 Ma *Nonion 4* maximum flooding surface caps this transgressive system tract at 1 981 m. The Highstand Systems Tract covers the top of this sequence and terminates at 1 821 m, a total of 160 m has been observed for it (Figure 6).

Well 005

Sequence1

The lower sequence boundary of this Sequence 1 occurs at 3 030 m. The top of the lowstand systems tract occurs at 2 841 m with prograding complex pattern as it is overlain by the transgressive systems tract. The maximum flooding surface with lowest shale resistivity value and high value on the SP lg occurs at depth of 2 769 m (Figure 7).

This is in turn overlain by the blocky sand of the highstand systems tract initiated by the slightly coarsening upward pattern immediately above the marker surface. The upper sequence boundary occurs at 2 498 m.

Sequence 2

This sequence lies on the lower sequence boundary at 2 498 m, and the depositional episode commenced with the deposition of transgressive systems tract unconformably on the lower boundary, culminating in the transgressive peak at the maximum flooding surface at a depth of 2 324 m. The highstand systems tract extends from the top of the maximum flooding surface to terminate at 2 083 m, at the position which marks the top of the sequence boundary (Figure 7).

Sequence 3

This depositional sequence covers a total depth of 672 m as it commenced with a lower sequence boundary at 2 083 m. This

sequence is initiated by the lowstand system tract as it is marked by a characteristic lg motif typical of coarsening upward backstepping aggradational stacking pattern. This system tract is overlain by the shaly formation of the transgressive system tract. This transgressive system tract initiated at 1 896 m was caped by the maximum flooding surface depicted by the *Nonion 4* marker at 1 699 m. The highstand system tract tops the set of sequences interpreted in this well as it covers a total depth of 287 m and terminates at 1412 m which marks the upper boundary.

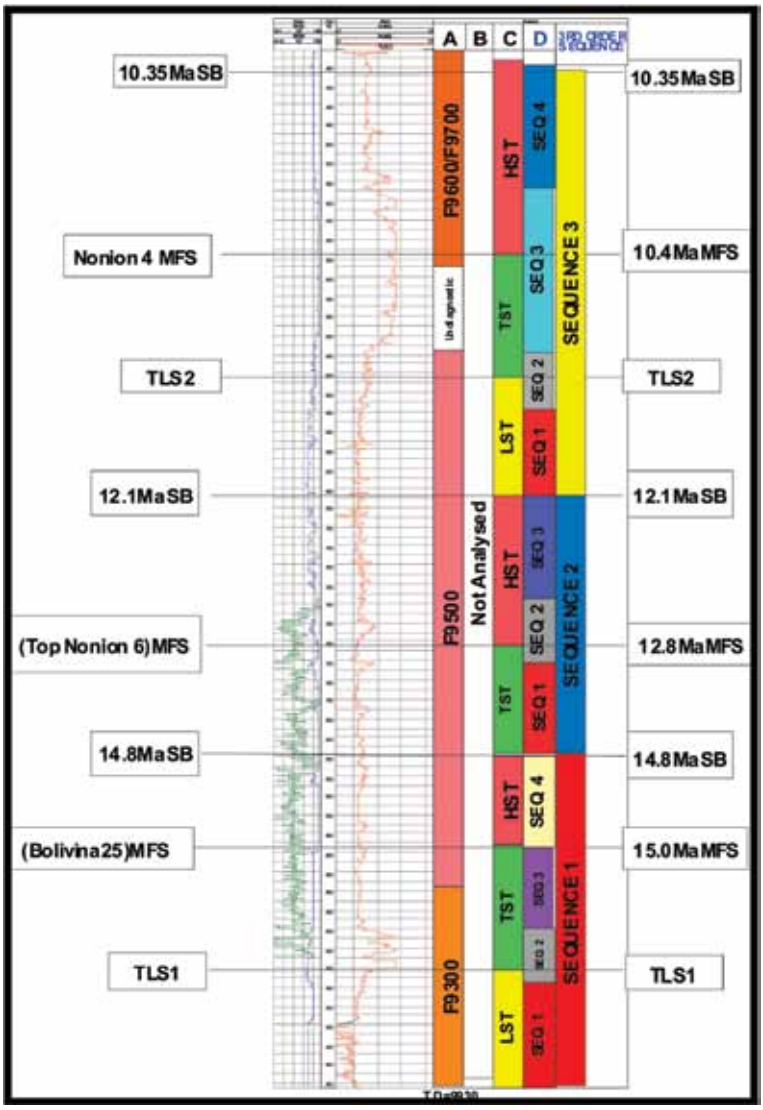

Figure 7. Well 5 with sequences and stratigraphically significant surfaces

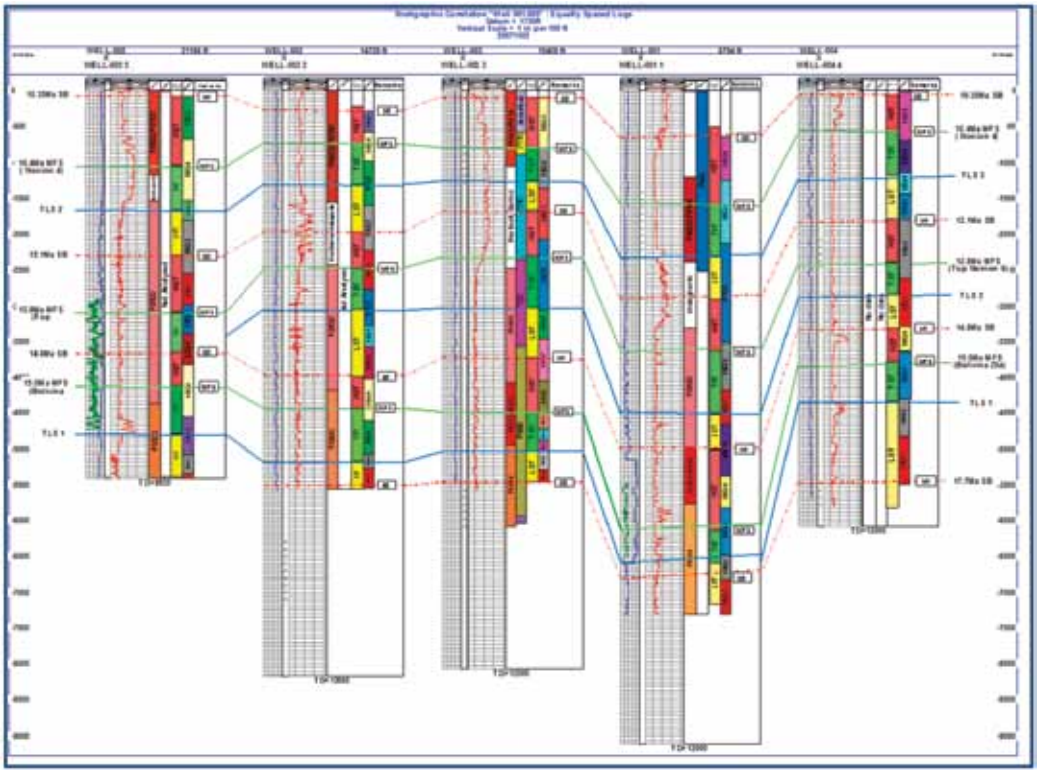

Figure 8. Stratigraphic correlation showing all 5 wells in the field of study

WELL CORRELATION

Strike line Correlation

This is carried out along the fault blocks in a bid to understand the relationships between well tops and stratigraphic surfaces in the studied wells, and in building a depositional model to know what the basin architecture looks like. This assisted in the determination of the lateral extent, continuity and homogeneity of the reservoir units and some marker shales, and also for accurate age dating of the subsurface strata of interest penetrated in the field. Figure 8 shows the lithofacies correlation and the crosscutting effect of fault on it at the subsurface. Figures 8 and 9 show the strike line and dip line correlation respectively carried out along fault blocks in the site of the wells as shown on the map (Figure1). This strike section cuts across wells 002 and 003, and the correlation shows normal delta progradation, continuity of lithofacies with thickening and thinning effect of some sequences. It is inferred in agreement with OZUMBA (2005), the late Miocene sequences

are thicker than the middle Miocene sequences. Furthermore, sandy lithologies with shale interfingering identified are of middle Miocene which is comparable with other facies of the same age in the Agbada Formation. The sequence stratigraphic correlation shows that the sequences and surfaces identified were present and then confirms the continuity of the lithologies and horizons mapped (Figure 8)

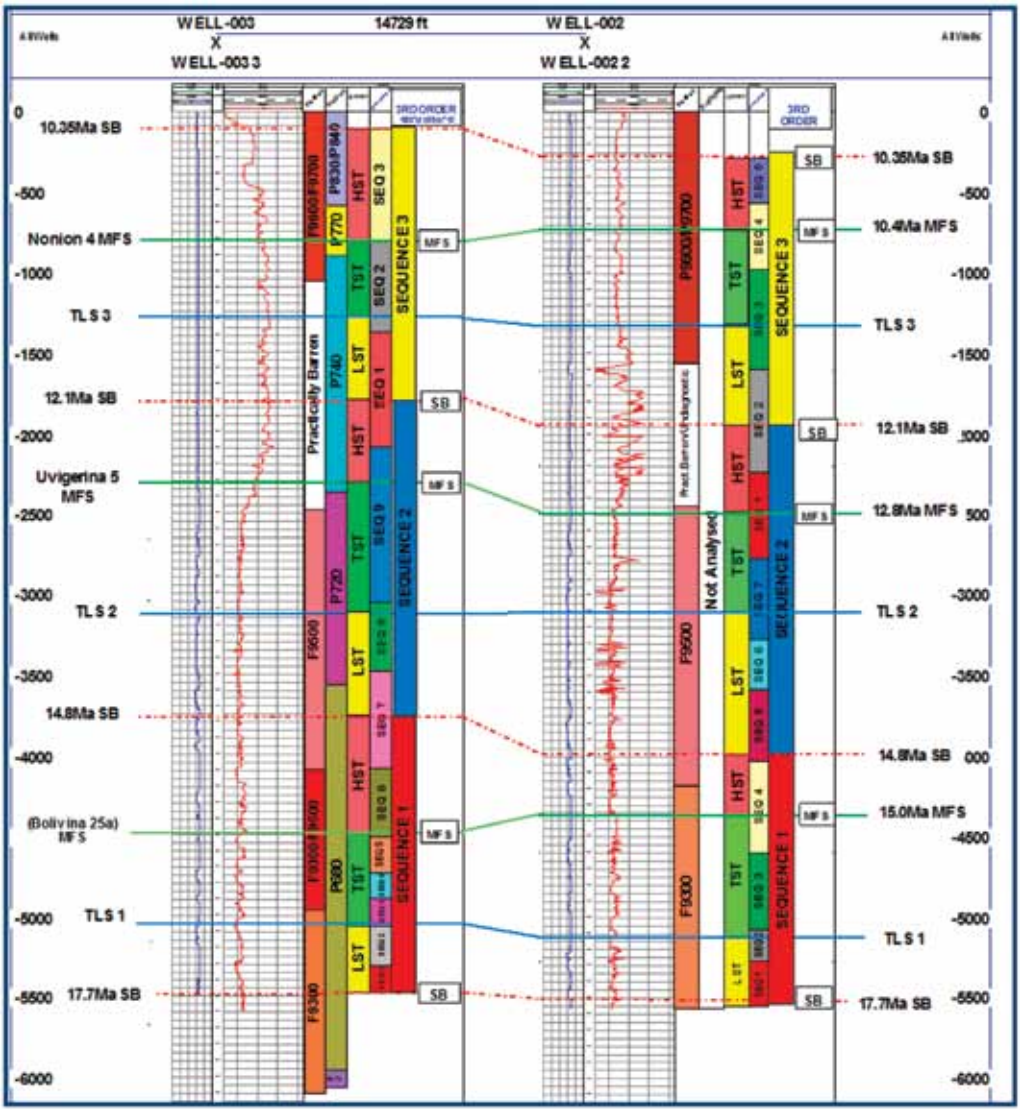

Figure 9. Strike line stratigraphic correlation of wells 002 and 003

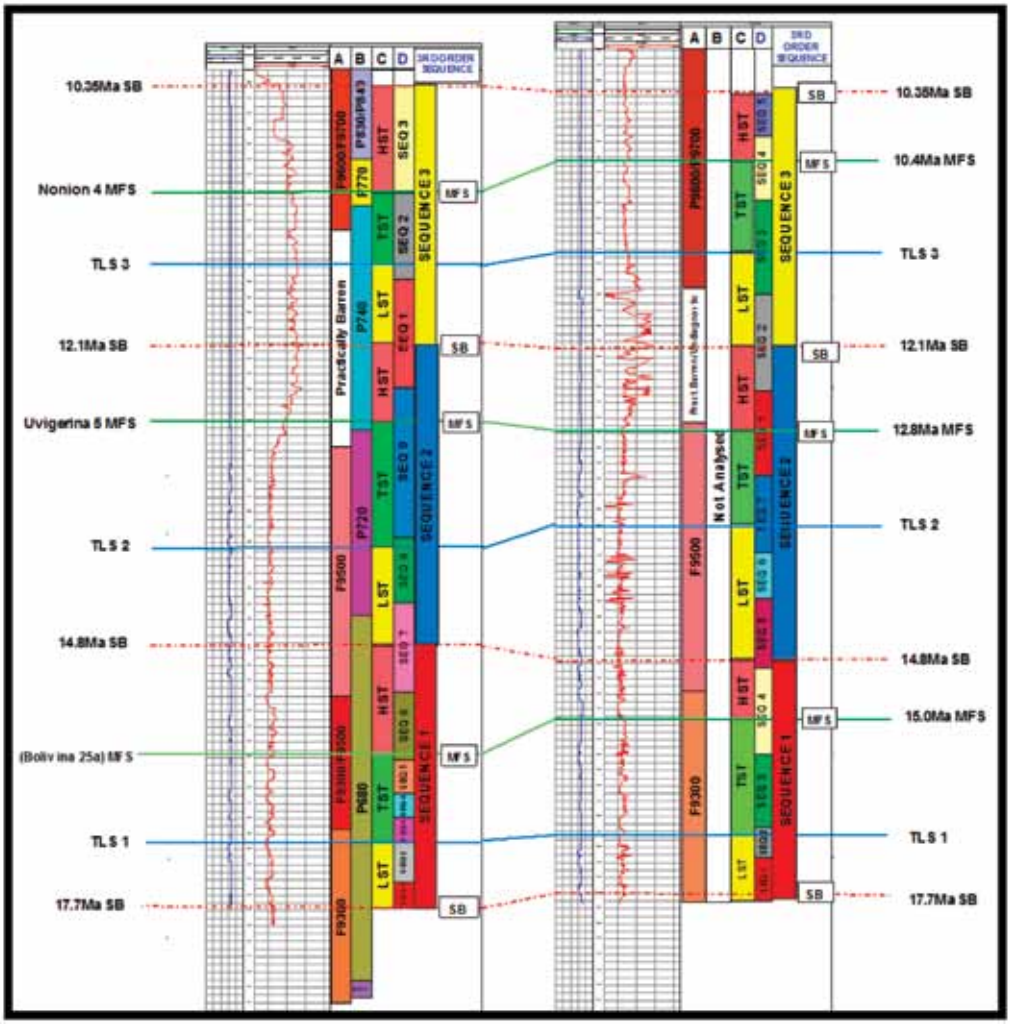

Figure 10. Structural cross-section showing features of wells 002 and 003

Dip line correlation

Dip line correlation was made across different fault blocks from the northern end to the southern end in the distal portion of the field of study. This was necessary in a way to determine the effects of structural elements like faults, and anticlinal closures on the connectivity and continuity of the reservoir sand bodies as they cut across different fault blocks. Essentially the dominant migration pathway of hydrocarbon which was along fault planes and also the trapping mechanism of hydrocarbon in the field were appreciated as much insight was gained into this. Basinal progradation was seen more clearly here as the thickening and thinning of the litholo-

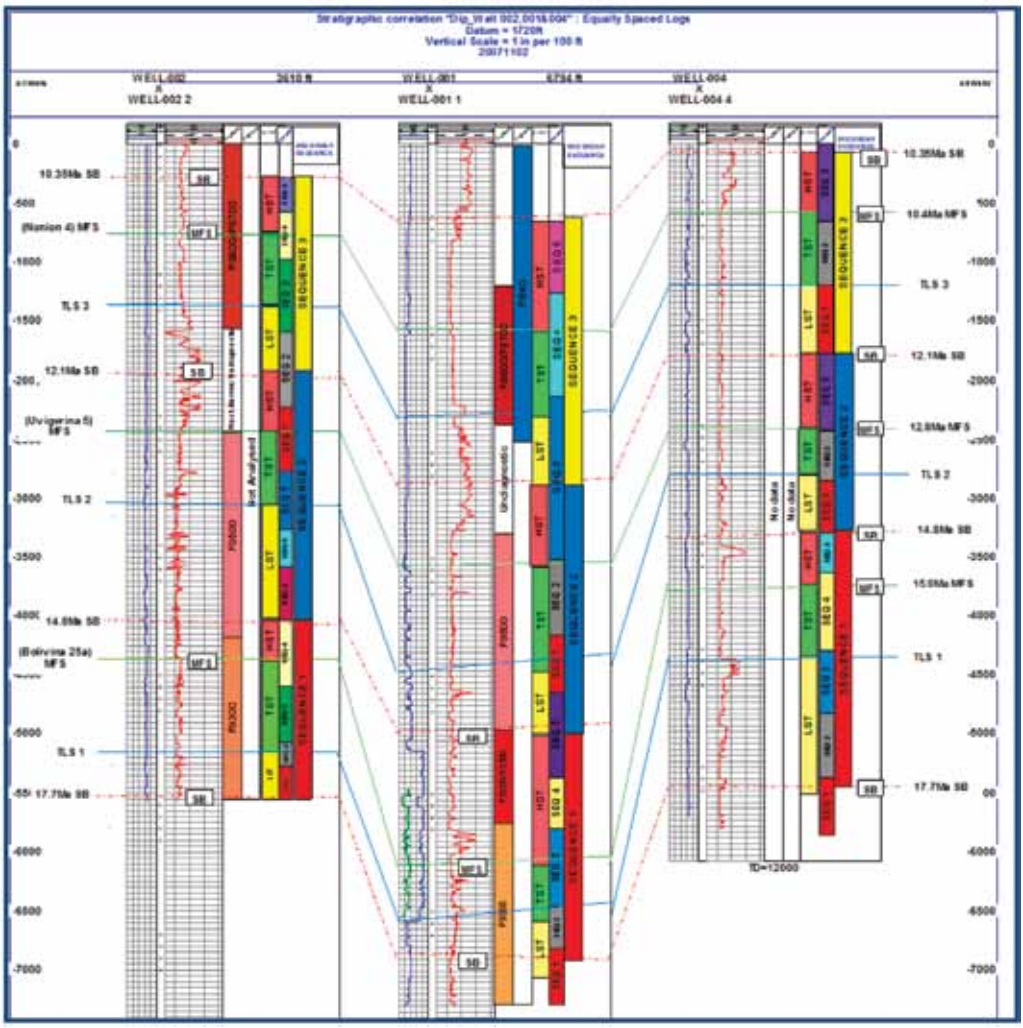

Figure 11. Dip line stratigraphic correlation of wells 002, 001 and 004.

gies was obvious (Figures 11 and 12). The wells 002, 001 and 004 used exhibited the effect of structural instability. The up and down pattern signifies the presence of this lithological units on separate portions of a growth fault structure with some sort of roll-over anticline typical of the Basin. The reservoir horizon mapped which shows some alternation of lithologies is that of the Agbada Formation.

The horizon shows continuity and connectivity, though the shaliness of the beds is slightly high. It could be inferred from the sequence stratigraphic correlation of the chronostratigraphic significant surface that the LST and the

TST hosts the reservoir units mapped in the Agbada Formation on the downthrown side in the hanging wall of the synsedimentary faults (AINSWORTH, 2005). They are seen to increase and show maturity in thickness downslope as the basin progrades in the proximal direction and hence the high probability of having enormous accumulation of commercially exploitable hydrocarbon in the deeper portion and offshore depobelt of the basin beyond the field of study (Figure 13).

CONCLUSIONS

In the light of the various approaches of investigations and detailed analyses discussed earlier in the methodology, a series of 3rd and 4th order stratigraphic surfaces were identified. The study area has a sequence stratigraphy within a chronostratigraphic framework that is composed of four sequence boundaries varying from 17.7 Ma to 10.35 Ma and three intervening maximum flooding surfaces between 15.0 Ma and

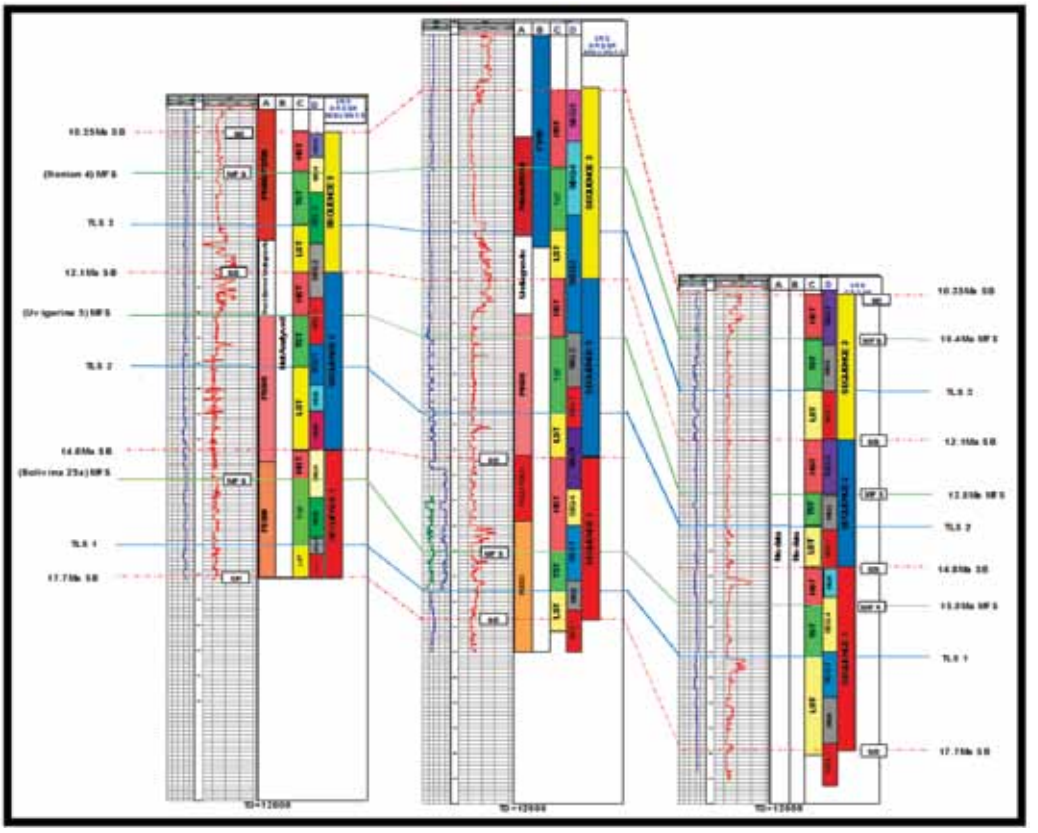

Figure 12. Dip line structural cross-section correlation of wells 002, 001 and 004

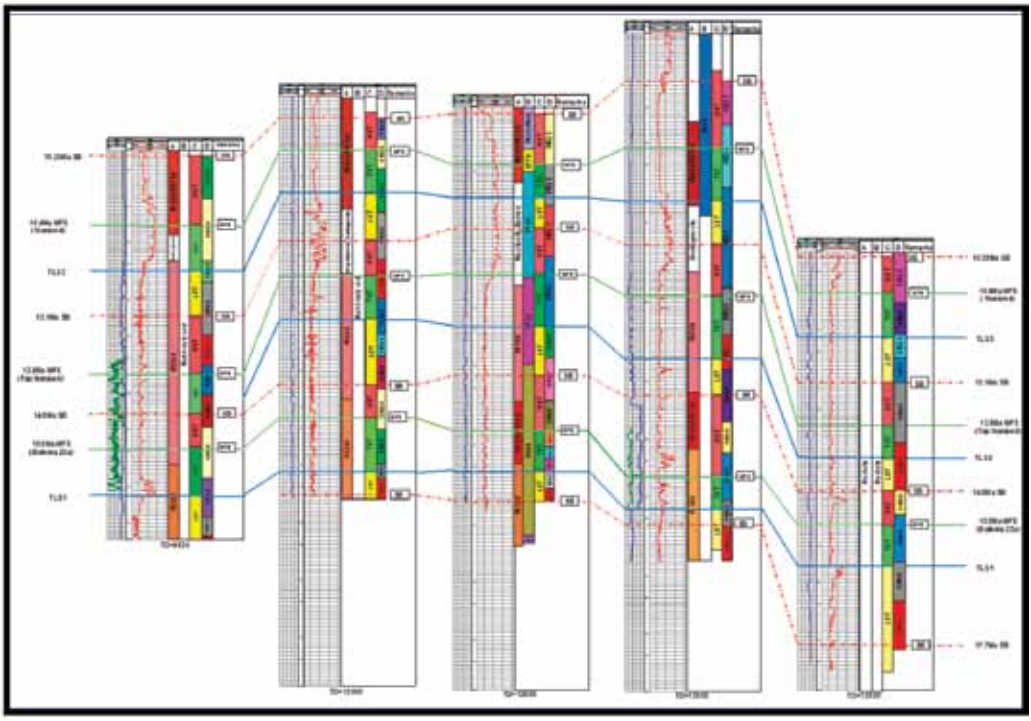

Figure 13. Structural cross-section correlation of all the wells in the field

10.4 Ma. These surfaces were all associated with the strata of early to middle Miocene age and corresponding to pollen zones P830-P670 and foram zones F9300- F9600 and foram sub zones F9301-F9605. The recognized maximum flooding surfaces were tied to the Niger delta chronostratigraphic chart and all was found to fall within the Central Swamp Depobelt.

Acknowledgements

The author is grateful to the Shell Petroleum Development Company (SPDC) for providing the data used for this study and the effort of Dr. Orodu O. D., is also appreciated for prove reading the manuscript.

References

Ainsworth, R. B. (2005): Sequence stratigraphic-based analysis of reservoir connectivity: influence of depositional architecture – a case study of a marginal marine depositional setting. *Petroleum Geoscience*; EAGE/ Geological Society, London; Vol. 11 2005, pp. 257–276.

Doust, H., Omatsola, M. E. (1990): Niger Delta, In: J. D. Edwards, P. A Santogrossi (eds.), Divergent/passive

margin basins, *American Association of Petroleum Geologists*; pp. 239–248.

EKWEOZOR, C. M., DAUKORU, E. M. (1984): Petroleum source-bed evaluation of Tertiary Niger Delta; discussion and reply*, AAPG Bulletin*; Vol. 68, pp.387–394.

EMERY, D. & MYERS, K. (1996): *Sequence Stratigraphy*. Blackwell Science Ltd., London, UK. 297.

GOLDHAMMER, R. K., DEV WICKENS, H., BOURMA, A. H. & WACH, G. (2000): Sequence stratigraphic architecture of the late Permian Tanquan submarine fan complex, Karoo Basin South Africa, in A. H. Bourma and C. G. Stone, ed., fine grained Turbidite systems, *AAPG Memoir 72/SEPM special Publ.*; Vol. 68, p.165–172.

HOSPERS, J. (1965): Gravity field and structure of the Niger Delta, Nigeria, West Africa. *Geological Society of American Bulletin*; Vol. 76, p. 407–422.

HAQ, B. U., HARDENBOL, J. & VAIL, P. R. (1988): Mesozoic and Cenozoic chronostratigraphy and eustatic cycles. In: Sea-level –an integrated approach, Wilgus, C. K., Hasting, B. S., Kendall, C. G. St., Posamentia, H., Ross, C. A. and Van Wagoner (eds.). *Jour. Soc. Econs. Paleotol. Mineral. Spec. Pub.*; Vol. 42, p. 47–70.

KULKE, H. (1995): Nigeria, In: Kulke, H., ed., Regional Petroleum Geology of the World: Part II, Africa, America, Australia and Antarctica: Berlin, Gebruder, Bontraeger, p. 143–172.

KLETT, T. R., AHLBRANDT, T. S., SCHMOKER, J. W. & DOLTON, J. L. (1997): Ranking of the world's oil and gas provinces by known petroleum volumes: U.S. *Geological Survey*, Open-file Report, 97–463, CD-ROM.

LOUTIT, T. S., HARDENBOL, J., VAIL, P. R., BAUM, G. R. (1988): Condensed section: the key to age dating and correlation of continental margin sequences. In: Seal level changes: an integrated approach (Eds Wilgus, C. K., Hasting, B. S., Kendall, C. G. St., Posamentia, H., Ross, C. A. and Van Wagoner, J.), *Soc. Econs. Paleotol. Mineral. Spec. Publi.*; Vol. 42, pp. 3–17.

OZUMBA, M. B., OMENE, D. A. & OTOGBILE, C. (2005): The Opuma channel area 3D prospectivity review, impact of high-resolution sequence stratigraphy, *NAPE Bulletin*; Vol. 18, No. 1, p. 1–10.

PETROCONSULTANTS (1996): Petroleum exploration and production database: Houston, Texas, Petroconsultants, Inc.

POSAMENTIER, H. W & VAIL, P. R. (1988): Eustatic control on clastic deposition, conceptual framework. In: Seal level changes: an integrated approach (Eds., Wilgus, C. K., Hasting, B. S., Kendall, C. G. St., Posamentia, H., Ross, C. A. and Van Wagoner, J., *Soc. Econs. Paleotol. Mineral. Spec. Publi.*; Vol. 42, pp. 125–154.

REIJERS, T. J. A., PETTERS, S. W. & NWAJIDE, C. S. (1997): The Niger Delta ba-

sin. In: Selley, R. C. (Ed), African basins, Amsterdam, *Elsivier science, sedimentary basins of the world*; Vol. 3, p. 151–172.

Rotimi, O. J., Ameloko, A. A., Adeoye, O. T. (2010): Application of 3-D Structural Interpretation and Seismic attribute Analysis to Hydrocarbon Prospecting over X – Field, Niger – Delta. *International Journal of Basic & Applied Sciences*, IJBAS/IJENS, 10(4) 105104 – 8383, ISSN: 2077–1223.

Vail, P. R. & Wornardt, W. W. (1990): Well log seismic Sequence stratigraphy: An integrated tool for the 90's: gulf coast section of Society of Economic Paleontologist and Mining Foundation, Eleventh Annual Research program and extended abstract, pp. 379–388.

Vail, P. R. & Wornardt JR, W. W. (1992): Well log-seismic sequence stratigraphy, course notes presented on behalf of Global Geotechnical & Mosunmolu limited, November 26–28th 1992, Lagos, Nigeria, 490 pp.

Van Wagoner, J. C., Mitchum, R. M., Campion, K. M. & Rahmanian, V. D. (1990): Siliciclastic sequence stratigraphy in well logs, cores and outcrops: concept for high-resolution correlation of time and facies, AAPG methods in exploration series, No. 7, 55 pp.

Weber, K. J. & Daukoru, E. M. (1975): Petroleum geology of the Niger Delta: Proceedings of the 9th World Petroleum Congress, Vol. 2, Geology: London, Applied Science Publishers, Ltd., p. 210–221.

Wilgus, C. K., Hasting, B. S., Ross, C. A., Posamentier, H. W., Van Wagoner, J. & Kendall, C. G. ST. C. (1998). Sea level changes, an integrated approach, *SEPM special publication*; Vol. 42, 407 pp.

Radon potential of a fly ash pile - a criterion for its use as a building lot

Radonski potencial odlagališča elektrofiltrskega pepela kot merilo za njegovo uporabo kot gradbeno zemljišče

Janja Vaupotič[1,*], Asta Gregorič[1], Krzysztof Kozak[2], Jadwiga Mazur[2], Elzbieta Kochowska[2] & Dominik Grządziel[2]

[1]Jožef Stefan Institute, Department of Environmental Sciences, Radon Center, SI-1000 Ljubljana, Slovenia
[2]Laboratory of Radiometric Expertise, Henryk Niewodniczański Institute of Nuclear Physics, Polish Academy of Sciences, 31-342 Kraków, Poland

*Corresponding author. E-mail: janja.vaupotic@ijs.si

Received: August 3, 2010 **Accepted:** October 2, 2010

Abstract: Radioactivity survey on a fly ash pile was carried out. Concentration of radon (^{222}Rn) in fly ash at a depth of 1 m was in the range of 0.3–46.9 kBq m^{-3}, with arithmetic mean of (23.8 ± 0.2) kBq m^{-3}. Radon exhalation rate was about 24 mBq m^2 s^{-1} on the part of the pile covered with grass, and about 37 mBq m^2 s^{-1} on the part with trees and bushes. Gamma dose rate was about 168 nSv h^{-1} and ash permeability around 3.9 × 10^{-13} m^2 on both parts.

Izvleček: Na odlagališču elektrofiltrskega pepela smo izvedli raziskavo radioaktivnosti. Na globini 1 m smo v elektrofiltrskem pepelu izmerili koncentracije radona (^{222}Rn) 0,3–46,9 kBq m^{-3} s povprečjem (23,8 ± 0,2) kBq m^{-3}. Na s travo poraščenem delu odlagališča smo izmerili hitrost ekshalacije radona okrog 24 mBq m^2 s^{-1}, na delu, kjer odlagališče preraščajo drevesa in grmičevje, pa okrog 37 mBq m^2 s^{-1}. Hitrost doze sevanja gama smo izmerili okrog 168 nSv h^{-1}, prepustnost pepela pa okrog 3,9 × 10^{-13} m^2 na obeh predelih.

Key words: radon, concentration, exhalation rate, gamma dose rate, fly ash
Ključne besede: radon, koncentracija, hitrost ekshalacije, hitrost doze sevanja gama, elektrofiltrski pepel

Original scientific paper

INTRODUCTION

Radon (^{222}Rn) is a radioactive noble gas (α radioactive transformation, half-life, $t_{1/2}$ = 3.82 d) originating from radioactive transformation of radium (^{226}Ra) in the natural radioactive chain of uranium (^{238}U) (NAZAROFF & NERO, 1988). Only a small fraction of radon atoms emanate from the solid and enter the space between mineral grains, from where they migrate through the medium, by both diffusion and advection, and eventually exhale into the atmosphere (ETIOPE & MARTINELLI, 2002). Radon is always accompanied by its short-lived products (^{218}Po, ^{214}Pb, ^{214}Bi and ^{214}Po) formed by its radioactive transformation and appearing in air as nano aerosols. Together, radon and radon short-lived products contribute more than half to the effective dose a member of the general public receives on the world average from all natural radioactive sources (UNSCEAR, 2000) and are a major cause of lung cancer, second only to cigarette smoking (DARBY et al., 2005). Keeping low radon levels in dwellings and at workplaces is therefore a serious social concern and a great scientific challenge.

Radon enters the indoor air mostly from the ground on which a building is standing. Other radon sources, such as outdoor air, building material, burning natural gas and using water, are usually minor if not negligible. It is therefore important where and how the building is constructed. Particularly important is the quality of the basic floor slab and parts of the walls contacting the ground. Obviously, the higher the uranium content in the ground, and, consequently, radon concentration in soil gas, the higher quality is needed to keep radon level in indoor air acceptably low. In this sense, radon concentration in soil gas together with soil permeability, as a measure of radon potential (WIEGAND, 2001; NEZNAL & ŠMARDa, 1996), should be considered when constructing a new, or remodelling an old building. In Germany, KEMSKI et al. (2001) have proposed the following ranking of radon risk with respect to radon concentration in soil: low at <10 kBq m^{-3}, medium at 10–100 kBq m^{-3}, increased at 100–500 kBq m^{-3}, and high radon risk at >500 kBq m^{-3}. In Sweden, the ranking is slightly different: low at <10 kBq m^{-3}, normal at 10–50 kBq m^{-3} and high at >50 kBq m^{-3} (EC, 2005). A classification of soil with respect to radon potential in Slovenia has not been accepted.

Radon potential varies markedly from soil to soil. It is reasonable to expect that it will be higher in the technologically enhanced naturally occurring radioactive material (TENORM). Such are wastes and by-products of technological processes

in which some members in the uranium radioactive chain are concentrated and hence their contents elevated. An example is burning coal in a thermal power plant. As in any material, also in coal, there is certain, though low, level of ^{226}Ra which, after burning, grows concentrated in the fly ash. A question emerges what is the radon potential of a layer of fly ash and thus which radon risk is expected when using this layer as a building lot.

In Slovenia, there are several fly ash disposal sites of various sizes. For this study, a small fly ash pile of well defined geometry was chosen. In addition to radon concentration in fly ash also radon exhalation rate from fly ash, permeability of fly ash and gamma dose rate were measured, and the site was classified according to radon risk. These have been the first such measurements in Slovenia, aimed only at showing as an example how radon potential for this kind of sites may be dealt with.

Materials and methods

Site description

To the site selected as an example for this study, the fly ash of a thermal power plant burning lignite had been disposed of for years. At present it is a 5–7 m thick layer of an approximate 150 m × 200 m surface area.

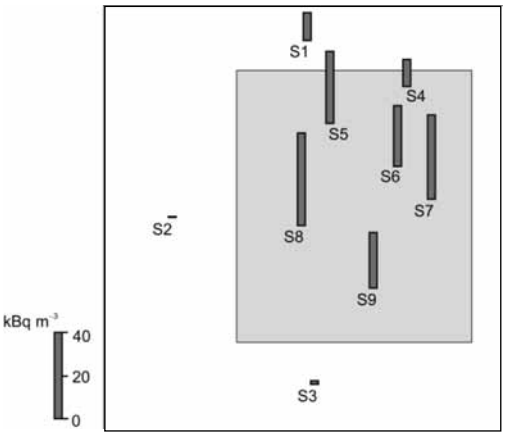

Figure 1. A schematic outline of the fly ash pile: the part covered by grass only is shadowed; measurement points are indicated, with vertical bars representing radon concentration in ash-gas.

A gamma spectrometric analysis of an averaged dry ash sample had shown the following concentrations of radionuclides (Bq kg^{-1}): ^{238}U: 200 ± 26, ^{232}Th: 37 ± 8, ^{226}Ra: 237 ± 8, ^{210}Pb: 102 ± 14, ^{40}K: 410 ± 23. For comparison, the following ranges were found in the terra rossa soil in various points in the karstic area: ^{238}U: 52–70, ^{226}Ra: 53–74, ^{40}K: 320–450, (Vaupotič et al., 2007a). A small part of the pile is a glade covered with grass only, while the rest, with dense bushes and trees (Figure 1). Complete measurements of all the parameters were carried out only in the former part because the movement of the equipment (except of scintillation cells) to the latter was practically impossible.

Radon in fly ash

To measure radon concentration (C_{Rn}/(Bq m^{-3})) in the ash-gas (gas contained in the bulk of fly ash) an AlphaGuard radon monitor and alpha scintillation cells were used. Because the cells showed similar values and are, in addition, more simple to move and use, only at two points in the part covered with grass the AlphaGuard monitor was used and the cells everywhere else.

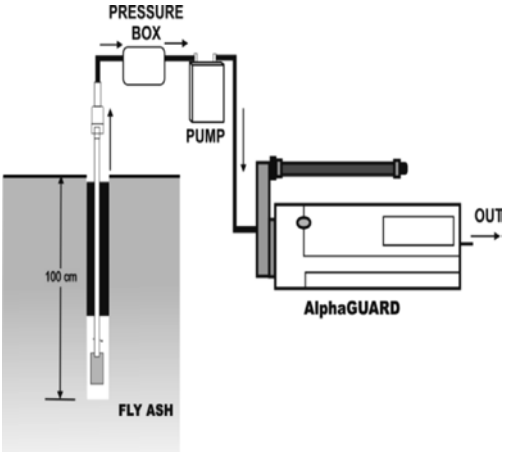

Figure 2. Schematic set-up for measuring radon concentration in ash-gas.

1. AlphaGuard

The measurement set-up to analyse radon concentration in soil gas consisted of an AlphaGuard PQ 2000 PRO (AG) radon monitor, a soil-gas probe and an AlphaPump (AP) (Genitron, Germany) (Figure 2). A borehole of 7 cm diameter was hand-drilled into the fly ash to a depth of 100 cm. The soil-gas probe was inserted to the bottom and the rubber ring around it inflated to isolate the bottom part of the borehole from the outdoor air. Soil gas was then pumped from the bottom through the AG ionization chamber at a flow rate of 0.3 dm^3 min^{-1}. The temporary radon (^{222}Rn) concentration was registered in one-minute intervals over approximately a 20-minute period. After initial growth, the concentration became stabilised. The average of the last few stabilised values was taken as the radon concentration in soil gas. At this low flow rate, contribution of thoron (^{220}Rn, half-life 55 s) was negligible (ŽUNIĆ et al., 2006).

2. Alpha scintillation cells

For this experiment, the Spanish 0.3 dm^3 alpha scintillation cells were used (QUINDOS-PONCELA et al., 2003). After the measurement with the AlphaGuard had been finished, a cell was connected to the soil-gas probe and pump, and ash-gas was flushed through the cell at a flow rate of 1 dm^3 min^{-1} for 3 minutes, necessary to exchange the air in the cell by the ash-gas sample. In a time longer than three hours, when the secular equilibrium between radon and its short-lived products had been reached, gross alpha activity of ^{222}Rn, ^{218}Po in ^{214}Po was measured in an PRM 145 α-counter (AMES, Ljubljana) (Figure 3). Cell efficiencies are from 0.000218 s^{-1} Bq^{-1} m^3 to 0.000428 s^{-1} Bq^{-1} m^3 and their background from 0.1 min^{-1} to 0.5 min^{-1}, thus assuring a lower limit of detection from 50 Bq m^{-3} to 110 Bq m^{-3} at counting times of 15 min.

Figure 3. Alpha counter with a scintillation cell.

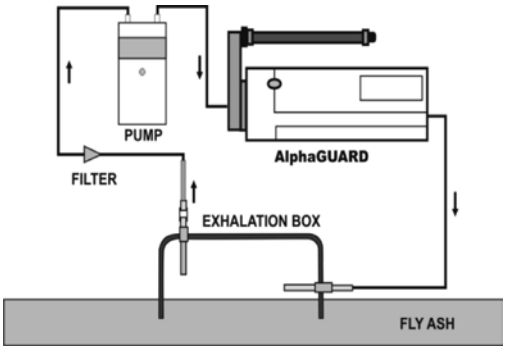

Figure 4. Schematic set-up for measuring radon exhalation rate from fly ash.

Radon exhalation from fly ash

The radon exhalation rate E_{Rn}/(Bq m^{-2} s^{-1}) from soil was measured using the Exhalation Box (EB, dimensions 0.7 m × 0.7 m × 0.2 m) and the same AG monitor and AP pump as in the previous section (Figure 4). The air was circulated in the closed circuit for about 90 min and the concentration of radon accumulated in EB was recorded every 10 min. The exhalation rate was calculated using the formula:

$$E_{Rn} = B \times \frac{V}{F} \quad (1)$$

in which: B – slope of the straight line fixed to the increasing radon concentration points in the EB, V/m^3 – volume of the EB, F/m^2 – surface area covered by EB (Žunić et al., 2006).

Fly ash permeability

The system to measure fly ash permeability k_{ash}/m^2 at 1 m depth consisted of a Multisensor Unit D/D device (Genitron, Germany) and the same AG monitor, AP pump and soil-gas probe as for measuring radon concentration (Figure 5). Ash-gas was sucked from soil by soil-gas probe and pumped through the AG and Multisensor. The pressure difference (ΔP) between ash and open air, and flow rate of ash-gas (Q) were measured by the Multisensor D/D. The fly ash permeability was calculated using a modified equation of Fick's law of diffusion (Janik, 2005):

$$k_{ash} = \mu \frac{Q}{W \times \Delta P} \quad (2)$$

in which: k_{ash}/m^2 – permeability of fly ash, μ – dynamic viscosity of air (Pa s), W/m – shape parameter of the soil-gas probe, Q/(m^3 min^{-1}) – gas flow rate and ΔP/Pa – pressure difference measured (Žunić et al., 2006).

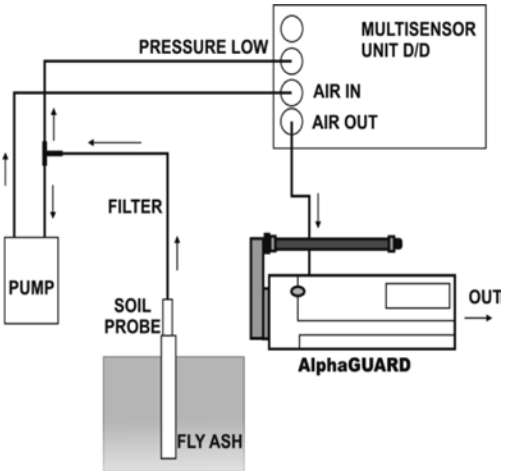

Figure 5. Schematic set-up for measuring fly ash permeability.

Gamma dose rate

Gamma dose rate $\dot{H}_\gamma$/(nSv h^{-1}) was measured in outdoor air at the height of 1 m above the ground using a Gamma-Tracer TM Wide Type E probe (Genitron, Germany). The values of gamma dose rate were registered in 5-min intervals. The average value of 12–15 records was taken as a final result.

RESULTS AND DISCUSSION

Figure 6 shows the initial increase in readings when measuring radon concentration in the ash-gas with the AlphaGuard monitor. A time of about 20 min was needed to reach the correct, saturated value, taken as the results for C_{Rn}. Accumulation of radon under the exhalation box during exhalation rate measurements is presented in Figure 7. The initial slope of the curve was used to calculate E_{Rn} (in this case (10 ± 1.2) Bq m^{-3} min^{-1}).

Values of radon concentration in ash-gas are given in Table 1, together with radon exhalation rate, fly ash permeability and gamma dose rate. Based on good agreement between radon concentrations obtained with both devices in boreholes 1 and 6 (less than 15 % difference) we decided to use the AlphaGuard monitor only at two points easily accessible for the equipment, and scintillation cells everywhere else. Except at points 2 and 3, concentrations were in the range from about 10 kBq m^{-3} to about 45 kBq m^{-3}, with an average of (23.8 ± 0.2) kBq m^{-3}. This is similar as in gravel deposits and lake sediments (38.1 kBq m^{-3} and 20.3 kBq m^{-3}, respectively) but lower than at carbonates (50.4 kBq m^{-3}) in Slovenia (VAUPOTIČ et al., 2007b; VAUPOTIČ et al., 2008), although ^{226}Ra concentration in fly ash is about four times higher, and therefore higher radon concentration would be expected, than in an ordinary soil (VAUPOTIČ et al., 2007a). The lowest two values (points 2 and 3) belong to boreholes at the very edge of the pile where the ash layer was thinner. Differences in values among points (except 2 and 3) are normal, as it is well known that even at a homogeneous distribution of ^{226}Ra, radon levels may differ markedly from borehole to borehole because of micro fractures in the ground (DURRANI

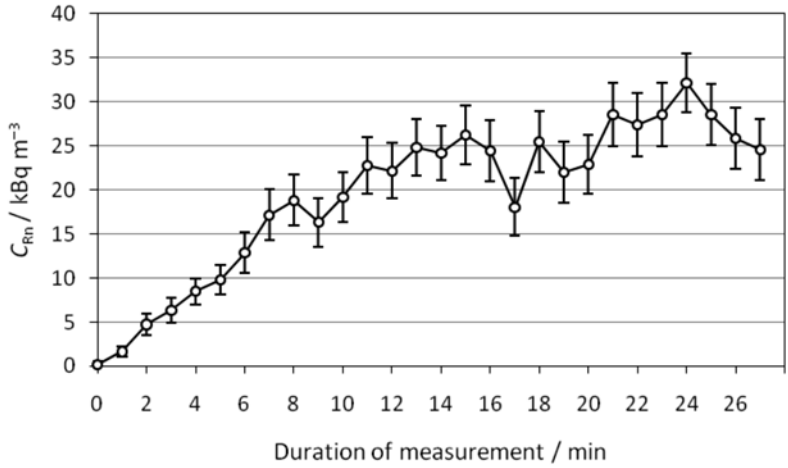

Figure 6. Initial increase in readings (S6) when measuring radon concentration in the ash-gas with the AlphaGuard monitor.

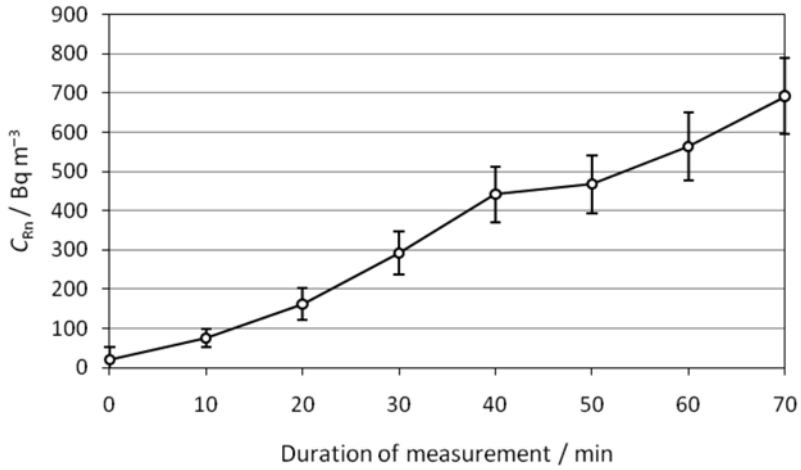

Figure 7. Accumulation of radon under the exhalation box during exhalation rate measurements (S1).

& Badr, 1995; Baixeras et al., 1996; Kemski et al., 2001; Winkler et al., 2001; Iakovleva & Ryzhakova, 2003; Vaupotič et al., 2007a). Point 4 is at the same level as other points but only 1 m or so away from the steep edge of the pile. We may speculate that atmospheric air may penetrate horizontally into the borehole, diluting the ash-gas and thus reducing radon concentration. Such a situation has not been observed at point 7 where radon concentration was second the highest. Although the radon exhalation rate is similar as

somewhere else in Slovenia (VAUPOTIČ et al., 2010; VAUPOTIČ et al., 2007b) it is higher at point 1 (36.9 mBq m^{-2} s^{-1}) than at point 8 on glade (24.2 mBq m^{-2} s^{-1}), most probably because the roots of trees and bushes here break up the bulk structure of the pile and thus enhance radon diffusion (MOLDRUP et al., 2000). Also the permeability of fly ash does not differ from that measured at other places (VAUPOTIČ et al., 2010; VAUPOTIČ et al., 2007b). It is practically the same at point 1 and 6, thus pointing out that higher exhalation rate at point 1 is due to enhanced diffusion (MOLDRUP et al., 2000) and not higher advection in the ash.

Gama dose rate of 168 nSv h^{-1} is about 50 % higher than over a nearby ground and about 15 % (27 nSv h^{-1}) lower than over the Pohorje granite (195 nSv h^{-1}) (BRAJNIK et al., 1992).

With respect to radon concentration in ash-gas (never exceeding 50 Bq m^{-3}), this fly ash pile may be considered as a building lot with a normal radon risk according to the Swedish (EC, 2005) and a medium radon risk according to the German (KEMSKI et al., 2001) classification. This classification is conservative, because the measurements were carried out in summer after a long period of dry weather when radon concentration is higher than it would be in wet condition (HOSODA et al., 2007; PAPACHRISTODOULOU et al., 2007).

CONCLUSIONS

Concentration of radon in ash-gas was in the range of 0.3–46.9 kBq m^{-3}, with arithmetic mean of (23.8 ± 0.2) kBq m^{-3}, and radon exhalation rate about 24 mBq m^2 s^{-1} on the part of the pile cov-

Table 1. Radon concentration (C_{Rn}), obtained with alpha scintillation cells and AlphaGuard monitor, radon exhalation rate (E_{Rn}), permeability of fly ash (k_{ash}) and gamma dose rate ($\dot{H}_{\gamma}$) on the fly ash pile.

Meas. point	C_{Rn}/(kBq m^{-3}) Scintillation cell	C_{Rn}/(kBq m^{-3}) AlphaGuard	E_{Rn}/(mBq m^{-2} s^{-1})	k_{ash}/m^2	$\dot{H}_{\gamma}$/(nSv h^{-1})
S1	13.6 ± 0.3	15.5 ± 2.9	36.9 ± 4.9	3.7×10^{-13}	166
S2	0.3 ± 0.05				
S3	1.2 ± 0.08				
S4	13.0 ± 0.4				
S5	37.0 ± 0.6				
S6	30.8 ± 0.6	26.5 ± 3.3		4.0×10^{-13}	169
S7	42.8 ± 0.6				
S8	46.9 ± 0.7		24.2 ± 2.5		
S9	28.9 ± 0.5				

ered with grass, and about 37 mBq m^2 s^{-1} on part with trees and bushes. According to the German classification the pile may be considered as a building lot with medium radon risk, and according to the Swedish, normal radon risk.

Acknowledgements

This work was financially supported by the Slovenian Research Agency within the project "Physico - chemical processes involved in formation of radioactive nano aerosols" (contract number J1-0745).

References

Baixeras, C., Bacmeister, G. U., Climent, H., Albarracin, D., Enge, W., Freyer, K., Treutler, H. C., Jonsson, G., Ghose, R., Monnin, M. M., Font, L., Devantier, R., Seidel, J. L., Sciocchetti, G. & Cotellessa, G. (1996): Report on the first phase activity of an EU project concerning coordinated radon measurements in five European countries. *Environ. Int.;* Vol. 22, pp. S687–S697.

Brajnik, D., Miklavžič, U. & Tomšič, J. (1992): Map of natural radioactivity in Slovenia and its correlation to the emanation of radon. *Radiat. Prot. Dosim.;* Vol. 45, pp. 273–276.

Darby, S., Hill, D., Auvinen, A., Barrios-Dios, J. M., Baysson, H., Bochicchio, F., Deo, H., Falk, R., Forastiere, F., Hakama, M., Heid, I., Kreienbrock, L., Kreuzer, M., Lagarde, F., Makelainen, I., Muirhead, C., Oberaigner, W., Pershagen, G., Ruano-Ravina, A., Ruosteenoja, E., Rosario, A. S., Tirmarche, M., Tomasek, L., Whitley, E., Wichmann, H. E. & Doll, R. (2005): Radon in homes and risk of lung cancer: collaborative analysis of individual data from 13 European case-control studies. *Br. Med. J.;* Vol. 330**,** No. 7485, pp. 223–226.

Durrani, S. A. & Badr, I. (1995): Geostatistically controlled field-study of radon levels and the analysis of their spatial variation. *Radiat. Meas.;* Vol. 25**,** No. 1–4, pp. 565–572.

EC (2005): An overview of radon surveys in Europe, European Commission.

Etiope, G. & Martinelli, G. (2002): Migration of carrier and trace gases in the geosphere: an overview. *Phys. Earth. Planet. In.;* Vol. 129**,** No. 3–4, pp. 185–204.

Hosoda, M., Shim, M., Sugino, M., Furukawa, M. & Fukushi, M. (2007): Effect of soil moisture content on radon and thoron exhalation. *J. Nucl. Sci. Technol.;* Vol. 44**,** No. 4, pp. 664–672.

Iakovleva, V. S. & Ryzhakova, N. K. (2003): Spatial and temporal variations of radon concentration in soil air. *Radiat. Meas.;* Vol. 36**,** No. 1–6, pp. 385–388.

Janik, M. (2005): Radon transport model and its verification by measurements in houses. 1966/AP, IFJ PAN, Krakow.

Kemski, J., Siehl, A., Stegemann, R. & Valdivia-Manchego, M. (2001): Mapping the geogenic radon potential in

Germany. *The Science of The Total Environment;* Vol. 272**,** No. 1–3, pp. 217–230.

Moldrup, P., Olesen, T., Gamst, J., Schjonning, P., Yamaguchi, T. & Rolston, D. E. (2000): Predicting the gas diffusion coefficient in repacked soil: Water-induced linear reduction model. *Soil Sci. Soc. Am. J.;* Vol. 64**,** No. 5, pp. 1588–1594.

Nazaroff, W. W. & Nero, A. V. (1988): *Radon and its decay products in indoor air*. New York: John Wiley & Sons.

Neznal, M. & Šmarda, J. (1996): Assessment of radon potential of soils - A five-year experience. *Environ. Int.;* Vol. 22, pp. S819–S828.

Papachristodoulou, C., Ioannides, K. & Spathis, S. (2007): The effect of moisture content on radon diffusion through soil: Assessment in laboratory and field experiments. *Health Phys.;* Vol. 92**,** No. 3, pp. 257–264.

Quindos-Poncela, L. S., Fernandez, P. L., Sainz, C., Arteche, J., Arozamena, J. G. & George, A. C. (2003): An improved scintillation cell for radon measurements. *Nuclear Instruments & Methods in Physics Research Section a-Accelerators Spectrometers Detectors and Associated Equipment;* Vol. 512**,** No. 3, pp. 606–609.

UNSCEAR (2000): Sources and effects of Ionizing radiation. UNSCEAR 2000 Report to the General assembly, with Scientific Annexes. Vol. 1.

Vaupotič, J., Barišić, D., Kobal, I. & Lulić, S. (2007a): Radioactivity and radon potential of the terra rossa soil. *Radiat. Meas.;* Vol. 42**,** No. 2, pp. 290–297.

Vaupotič, J., Gregorič, A., Kobal, I., Žvab, P., Kozak, K., Mazur, J., Kochowska, E. & Grządziel, D. (2010): Radon concentration in soil gas and radon exhalation rate at the Ravne Fault in NW Slovenia. *Nat. Hazards Earth Syst. Sci.;* Vol. 10**,** No. 4, pp. 895–899.

Vaupotič, J., Žvab, P., Gregorič, A., Kobal, I., Kocman, D., Kotnik, J. & Križman, M. (2008): Radon mapping in Slovenia based on its levels in soil gas. In: *33rd International Geological Congress;,* 6–14 August 2008, Oslo, Norway, Abstracts.

Vaupotič, J., Žvab, P., Gregorič, A., Kobal, I., Kocman, D., Kozak, K. & Mazur, J. (2007b): Soil gas radon potential on radon prone areas. Report–9694, Jožef Stefan Institute, Ljubljana.

Wiegand, J. (2001): A guideline for the evaluation of the soil radon potential based on geogenic and anthropogenic parameters. *Environ. Geol.;* Vol. 40**,** No. 8, pp. 949–963.

Winkler, R., Ruckerbauer, F. & Bunzl, K. (2001): Radon concentration in soil gas: a comparison of the variability resulting from different methods, spatial heterogeneity and seasonal fluctuations. *Sci. Total Environ.;* Vol. 272**,** No. 1–3, pp. 273–282.

Žunić, Z. S., Kobal, I., Vaupotič, J., Kozak, K., Mazur, J., Birovljev, A., Janik, M., Čeliković, I., Ujić, P., Demajo, A., Krstić, G., Jakupi, B., Quarto, M. & Bochicchio, F. (2006): High natural radiation exposure in radon spa areas: a detailed field investigation in Niška Banja (Balkan region). *J. Environ. Radioactiv.;* Vol. 89**,** No. 3, pp. 249–260.

Assessment of heavy metal contamination in paddy soils from Kočani Field (Republic of Macedonia): part I

Ocena onesnaženja s težkimi kovinami v tleh riževih polj iz Kočanskega polja (Republika Makedonija): 1. del

Nastja Rogan Šmuc[1,] *

[1]University of Ljubljana, Faculty of Natural Sciences and Engineering, Department of Geology, Aškerčeva cesta 12, SI-1000 Ljubljana, Slovenia

*Corresponding author. E-mail: nastja.rogan@guest.arnes.si

Received: October 6, 2010 **Accepted:** November 15, 2010

Abstract: The research focuses on the assessment of heavy metals contamination in paddy soils from Kočani Field (Republic of Macedonia). Very high concentrations of Ag, As, Cd, Cu, Mo, Ni, Pb, Sb and Zn were found in the paddy soils samples from the vicinity of the Zletovska River (western part of Kočani Field). This river drains the untreated effluents from the Pb-Zn mine in Zletovo-Kratovo region and it is used for irrigation of the surrounding paddy fields. Heavy metal contamination of Kočani paddy soils was evaluated by using contamination factor and contamination degree, which confirmed a very high heavy metal contamination status for Kočani paddy soils, especially around Zletovska River area. Taking into account the results of this research the area around the Zletovska River is considered as the most anthropogenically impacted part of Kočani Field.

Izvleček: V tej študiji smo ocenili in opredelili onesnaženje s težkimi kovinami v tleh riževih polj Kočanskega polja (Republika Makedonija). Zelo visoke koncentracije Ag, As, Cd, Cu, Mo, Ni, Pb, Sb in Zn smo ugotovili v vzorcih tal iz bližine reke Zletovske (zahodni del Kočanskega polja). Reka Zletovska odvaja neprečiščene odplake in odpadke z območja rudnika Pb-Zn Zletovo, kmetje pa jo uporabljajo za namakanje riževih polj. Visoke vrednosti težkih kovin v tleh riževih polj območja Kočanskega polja smo potrdili tudi z izračunom faktorja onesnaževanja in stopnje onesnaževanja. Na podlagi zelo

Original scientific paper

visokih koncentracij težkih kovin v vzorcih tal riževih polj smo ugotovili, da je območje okoli reke Zletovske resna ekološka grožnja bližnjim ekosistemom.

Key words: assessment of contamination, heavy metals, paddy soil, Kočani Field, Republic of Macedonia
Ključne besede: ocena onesnaženja, težke kovine, tla riževih polj, Kočansko polje, Republika Makedonija

INTRODUCTION

Soil is a specific component of the biosphere because it is not only treated as geochemical sink for contaminants, but also as a natural buffer system controlling the transport of chemical elements and substances into the atmosphere, hydrosphere and biota. It has always been important to humans and their health, especially as a resource that can be used for shelter and food production (KABATA-PENDIAS & PENDIAS, 2001). Unfortunately, heavy metal contamination of soils has become a widespread global problem over the past two decades and represents a long-term risk to ecosystem health and quality (KABATA-PENDIAS & PENDIAS, 2001).

Base-metal mining activities together with milling and grinding operations, concentrating ore and the disposal of tailings, acid mine and mill wastewater provide important sources of heavy metals entering into the environment (ADRIANO, 1986). Consequently, very high concentrations of heavy metals can be found in and around abandoned and active mines, which can affect nearby agricultural soils, food crops, riverine water and stream sediments (ADRIANO, 1986; JUNG, 2001; JUNG & THORNTON, 1997; KORRE et al., 2002; LEE et al., 2001; LIU et al., 2005; LU & ZHANG, 2005; SIMMONS et al., 2005; WITTE et al., 2004, WONG et al., 2002; YANG et al., 2004).

Numerous studies worldwide have investigated the heavy metal concentrations in soils (KABATA-PENDIAS & PENDIAS, 2001). Although mining is one of the most important industries in the Republic of Macedonia, studies about heavy metal concentrations in soils originating from historical or current base-metal mining activities are scarce, especially in the area of Kočani region (DOLENEC et al., 2007; ROGAN et al., 2009; ROGAN et al., 2010).

In this context, the major aims of the presented study are:

- to detect the total heavy metal concentrations and distribution in pad-

dy soil samples from Kočani Field and compare these results with permissible levels of heavy metals in arable soils;

- to assess the soil contamination by environmental indexes, contamination factor (HAKANSON, 1980; LOSKA et al., 2004) and degree of contamination (HAKANSON, 1980) and;
- to evaluate the overall environmental risk of the soil system in the Kočani Field area.

MATERIALS AND METHODS

Study area

Kočani Field is located in eastern Macedonia, about 32 km from the city of Štip and 115 km from the capital city Skopje. With an average length of 35 km and width of 5 km, Kočani Field lies in the valley of the Bregalnica River between the Osogovo Mountains in the north and Plačkovica Mountains in the south (Figure 1).

Figure 1. Study area, Kočani Field

The broader region is well known as an agricultural and mining province, with significant thermal activity. The municipality of the Kočani area comprises 28 settlements with 38,092 inhabitants.

The Bregalnica River, together with its tributaries, represents the principal drainage system in the investigated area and is, therefore, an important water supply for the irrigation of the surrounding paddy fields. The main tributaries of the Bregalnica River are the Kamenica River in the northeastern part of the study area and the Zletovska River in the western side of Kočani Field (Figure 1). The Zletovska River originally drained the central part of the Zletovo-Kratovo volcanic complex as well as the untreated mine effluents from the Pb-Zn Zletovo mine and its ore processing facilities. Both rivers are used by local farmers for the irrigation of the nearby paddy fields. The Kočanska and Orizarska Rivers are two small tributaries of the Bregalnica River (Figure 1) that drain the southern part of the Osogovo Mountains, as well as the untreated municipal wastes and domestic sewage of the cities of Kočani and Orizari. The riverine water of the Kočanska and Orizarska Rivers is also used for the irrigation of the paddy fields located in the northeastern part of Kočani Field.

The paddy soil of Kočani Field was estimated to originate from the composite material of the sediment derived from igneous, metamorphic and sedimentary rocks located in the wider area of Kočani. The sediment material was transported by the Bregalnica River and its tributaries and deposited in the Kočani depression (DOLENEC et al., 2007). The soil mineralogy and elemental composition are closely related to the acidic and intermediate rocks of the Kočani region (DOLENEC et al., 2007).

Zletovo-Kratovo ore district

The Zletovo-Kratovo Pb-Zn ore district is situated 5 km northwest of the Zletovo village and about 7 km from the city of Probistip (Figure 1). It is located in the central part of the Zletovo-Kratovo volcanic complex. The mineral association comprises galena (principal ore mineral) and sphalerite, with subordinate pyrite, lesser amounts of siderite and chalcopyrite and occasionally pyrrhotine, marcasite and magnetite. Minor occurrences of U-mineralisation have also been discovered (pitchblende). The Zletovo mine has an annual capacity of 350,000 tons of Pb-Zn concentrate (8 % Pb and Zn) and significant concentrations of Ag, Bi, Cd and Cu. Ore is concentrated at the flotation processes at Probistip, and tailings material is stored in two impoundments in the adjacent valleys (ALDERTON et al., 2005).

Paddy soil sampling and analysis

The sampling of the paddy soils was carried out in autumn 2005. The sampling locations are shown in Figure 2. Paddy soil samples were assembled at 38 locations from seven profiles across Kočani Field (Sections I–VII).

Near surface paddy soils (0–20 cm in depth) were collected because it is impossible to distinguish the A, B and C horizons in the agricultural soil. The paddy soils were sampled using a plastic spade to avoid any heavy metal contamination. Each paddy soil sample comprised a composite of five subsamples taken within a (1 × 1) m^2.

The paddy soil samples were air dried at 25 °C for one week and sieved through a 2 mm polyethylene sieve to remove plant debris, pebbles and stones. Afterwards they were ground in a mechanical agate grinder into a fine powder for subsequent physicochemical parameters and geochemical analysis.

All paddy soil samples were analysed for heavy metal concentrations in a certified commercial Canadian laboratory (Acme Analytical Laboratories, Vancouver, B. C., Canada) by extraction for 1 h with 2-2-2-HCl-HNO_3-H_2O at 95 °C with ICP-MS.

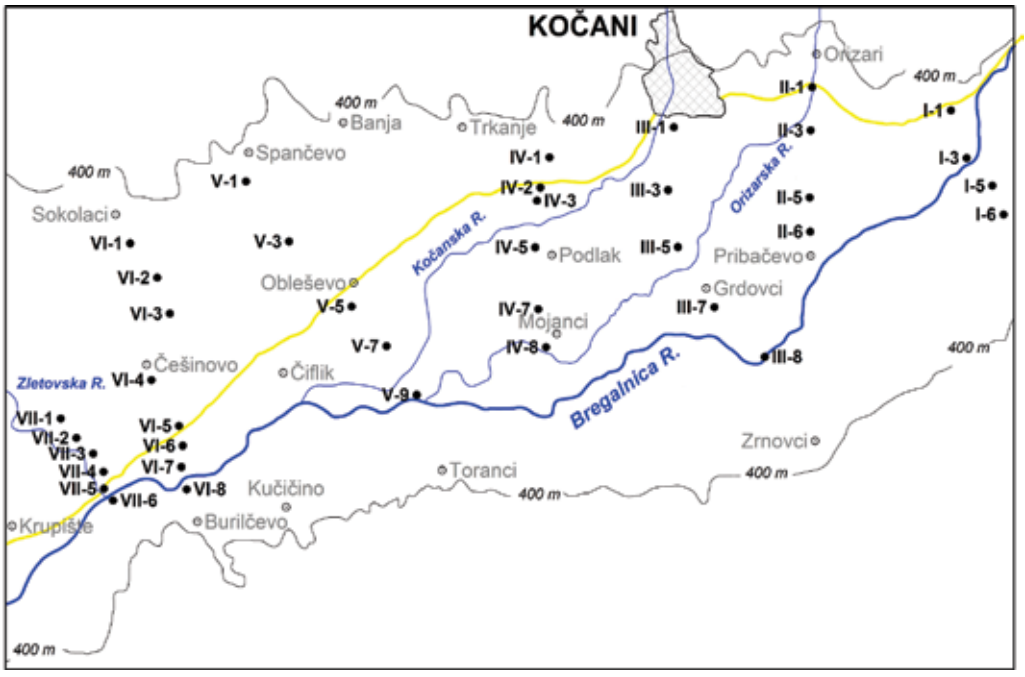

Figure 2. Paddy soil sampling locations map

The accuracy and precision of the paddy soil analysis were assessed using an international reference material such as Canadian Certified Reference Material Project (CCRMP) SO-1 (soil) and United States Geological Survey (USGS) G-1 (granite). The analytical precision and accuracy were better than ±5 % for the investigated elements. This was indicated by the results of the duplicate measurements in 10 soil samples as well as duplicate measurements of the G-1 and SO-1 standards.

RESULTS AND DISCUSSION

Heavy metal concentration in the paddy soil

Table 1 shows the concentrations of Ag, As, Cd, Cu, Mo, Ni, Pb, Sb and Zn determined in the paddy soil samples from Kočani Field together with the assumed permissible level (1st limiting level) of heavy metals adopted by the National Environmental Protection Agency of Slovenia (URADNI LIST RS, 1996), typical heavy metal contents of comparable soils around the world (BOWEN, 1979) and the maximum allowable concentrations (MAC) of trace elements in agricultural soil proposed by the GERMAN FEDERAL MINISTRY OF ENVIRONMENT (1992). The permissible level of heavy metals and the MAC of trace metals signify the values above which toxicity is considered possible.
Table 2 displays the descriptive statistical parameters (mean, median, range and standard deviation (SD)).

The Ag, Mo, Ni, Sb concentrations defined in the paddy soil samples from Kočani Field were corresponding to the average worldwide values for Ag (WEDEPOHL, 1974) and Sb (BOWEN, 1979) and did not exceed the limit values for Mo and Ni reported by the Environmental Protection Agency of Slovenia (Table 1).

Very high concentrations of As, Cd, Cu, Pb and Zn (Table 1) were found in the paddy soils samples from Section VII. The determined values significantly exceeded the typical As content within comparable soils around the world (BOWEN, 1979), as well as the limit values for As, Cd, Cu, Pb and Zn suggested by the environmental protection agencies of Slovenia and Germany (Table 1).

To compare the distribution of each heavy metal in the paddy soil samples between Sections I–VII, whisker plots were employed (Figure 3). All soil samples in Sections I–VI had similar levels of median values, suggesting that their intersection differences were not substantial, whereas significant variations existed only between Section VII and the other sections. The only exception and consequently difference was is the distribution of the Ni values in the paddy soil samples.

Table 1. Total heavy metal concentrations in the paddy soil of Kočani Field: (1) typical contents of Ag, As, Cd, Cu, Mo, Ni, Sb, Pb and Zn in comparable soils around the world; (2) limits for elemental concentrations in soil (Environmental Protection Agency of Slovenia (Uradni list RS, 1996); (3) maximum allowable concentrations (MAC) of trace elements in agricultural soils proposed by the German Federal Ministry of the Environment (1992).

Element (μg/g)	Ag	As	Cd	Cu	Mo	Ni	Pb	Sb	Zn
Location									
I-1	0.7	3.4	0.1	14.9	0.5	15.6	19.1	0.2	53
I-3	0.2	18.7	0.5	40.3	1	31.1	81.3	0.6	162
I-5	0.1	5.6	0.2	32	0.5	29.7	18.8	0.2	85
I-6	0.7	5.1	0.1	25.9	0.5	25.7	13.1	0.2	70
II-1	0.1	6.1	0.2	26.7	0.5	29.4	26.6	0.2	93
II-3	0.1	5	0.1	29.1	0.4	28.2	21	0.2	81
II-5	0.1	5.3	0.2	24.9	0.5	22	20.8	0.3	80
II-6	0.1	11.8	0.3	25.7	0.6	20.8	32.1	0.8	100
III-1	0.1	6.1	0.2	27.2	0.6	27.5	18.1	0.2	89
III-3	0.1	3.1	0.4	32.6	0.3	25.4	20.4	0.2	95
III-5	0.1	8.3	0.2	32.7	0.5	36.8	23.9	0.2	102
III-7	0.7	8.2	0.2	16.8	0.3	13.9	22.1	0.4	64
III-8	0.7	4.2	0.1	21.8	0.5	20.8	10.5	0.1	64
IV-1	0.1	3.8	0.1	28.5	0.7	21.7	13.9	0.2	74
IV-2	0.7	3.5	0.2	17.1	0.6	17.3	17.9	0.2	68
IV-3	0.7	4.3	0.3	23.4	0.5	24.1	19.1	0.2	102
IV-5	0.1	6.3	0.2	25.7	0.6	25.5	15.4	0.2	94
IV-7	0.1	8.1	0.2	26.2	0.7	26.1	17	0.2	83
IV-8	0.1	5.9	0.2	28.9	0.6	28.6	18.1	0.2	96
V-1	0.1	10	0.2	19	0.7	9.1	30.8	0.3	85
V-3	0.1	7.8	0.2	20	0.6	9.5	26.9	0.2	73
V-5	0.1	6.5	0.2	25	0.6	22.8	22.1	0.2	98
V-7	0.1	6.4	0.2	22.8	0.4	17.2	17.8	0.3	67
V-9	0.1	4.5	0.2	20.8	0.3	16.7	19.2	0.3	69
VI-1	0.1	5	0.2	21.4	0.3	17.1	24.1	0.3	71
VI-2	0.1	6.8	0.3	24.5	0.6	9.9	39.4	0.2	76
VI-3	0.1	10.1	0.3	34.1	0.6	22.3	35.4	0.3	86
VI-4	0.1	9.9	0.3	28.6	0.5	25.2	41.4	0.4	105
VI-5	0.1	10.5	0.3	25	0.5	21.7	39.6	0.4	94
VI-6	0.1	11.5	0.3	28.3	0.6	22	45.1	0.5	107
VI-7	0.7	7.7	0.1	19.3	0.5	16.4	20	0.4	66
VI-8	0.7	6.2	0.2	29.5	0.5	30.5	16.3	0.2	72
VII-1	0.9	22.2	2.7	48.8	1.3	10.9	411.9	1.8	531
VII-2	2	42	5.6	99.4	1.8	15.4	892.4	2.5	1134
VII-3	1.4	35.1	4.5	89.4	1.4	15.5	726.7	2	893
VII-4	2.1	47.6	6.4	80.1	1.8	11.9	983.1	3	1245
VII-5	1.6	39.6	5	68.3	1.6	14.1	745.1	2.2	928
VII-6	0.6	20.7	2	47.1	0.9	19.8	295.7	1	384
1	0.1-8	6	0.35	30	/	/	35	1	90
2	/	20	1	60	10	50	85	/	200
3	/	/	1.5	60	/	/	100	/	200

Table 2. Descriptive basic statistic parameters for heavy metals in the paddy soils of Kočani Field

Elements (μg/g)	Ag	As	Cd	Cu	Mo	Ni	Sb	Pb	Zn
Mean	0.306	11.4	0.9	33	0.682	21.0	0.57	128	206
Median	0.100	6.7	0.2	26	0.600	21.7	0.25	22	88
Minimum	0.066	3.1	0.1	15	0.300	9.1	0.10	11	53
Maximum	2.100	47.6	6.4	99	1.800	36.8	3.00	983	1245
S.D.	0.541	11.3	1.7	20	0.389	6.8	0.72	260	310

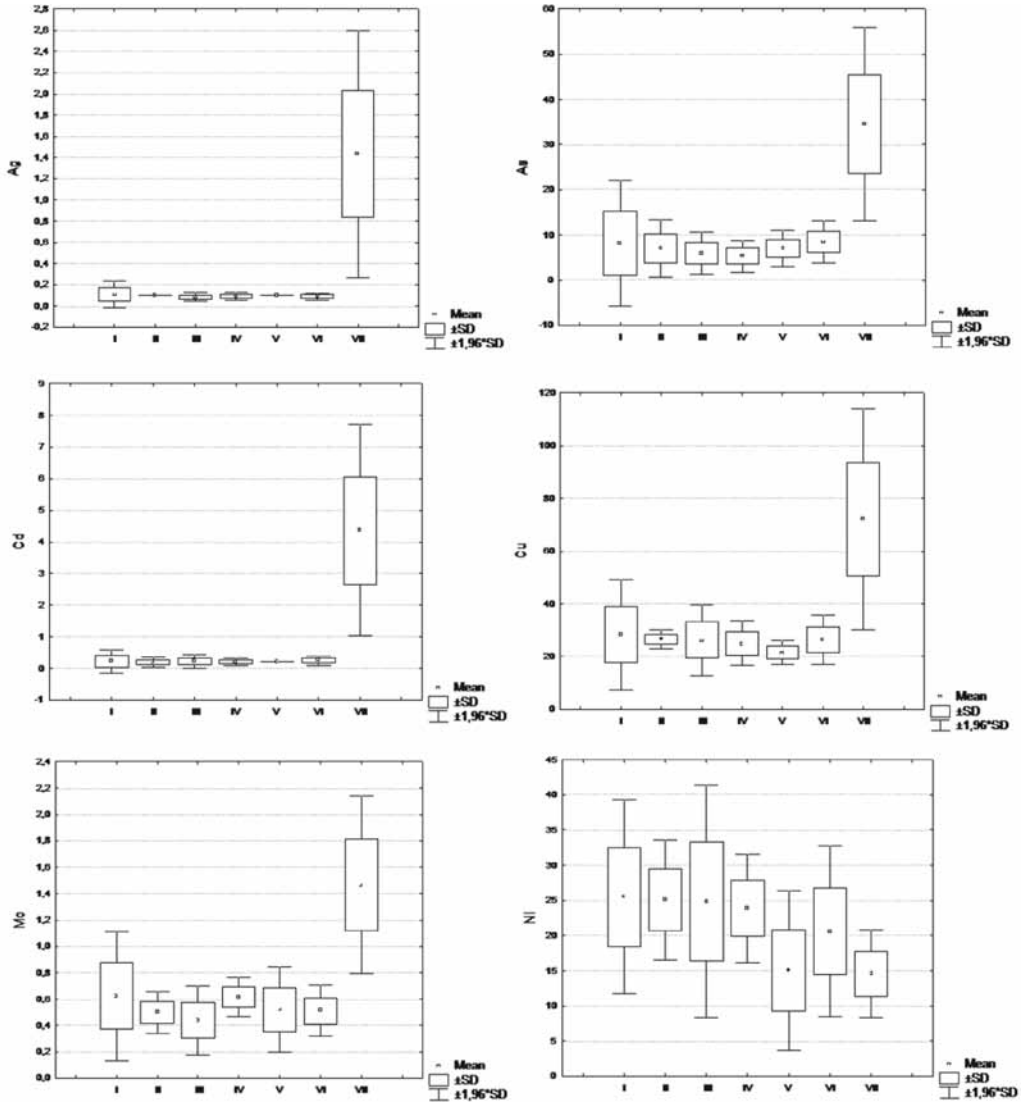

Figure 3. Whisker plots of Ag, As, Cd, Cu, Mo, Ni, Pb, Sb and Zn for ddy soil samples.

Contamination factor (c_f^i) and contamination degree (C_{deg})

According to contamination factor (c_f^i) values (mean), the paddy soils from the Kočani Field were classified as slightly (low) contaminated with Mo, moderately contaminated with Cu and Ni, considerably contaminated with Ag, Pb, Sb and Zn and very highly contaminated with Cd and As (Figure 4). The highest Ag, As, Cd, Pb, Sb and Zn c_f^i values (very high contamination factor) and the highest Cu and Mo c_f^i values (moderate contamination factor) were found in the paddy soil samples from Section VII (close to Zletovska River area). The highest Ni c_f^i values (moderate contamination factor) were determined in Section I. The calculated c_f^i values entirely confirmed the I_{geo} results.

The complete assessment of the paddy soil contamination was evaluated by degree of contamination (C_{deg}). The C_{deg} (mean) of the studied soils samples was 36.2 (Table 3), which signified very high contamination. Cd and As represented the largest contamination degree factors with 23 % and 20 %, respectively. Ag and Pb both contributed 16 %, Sb 9 % and Zn 8 %. Cu, Ni and Mo negligibly influenced the soil contamination with 4 %, 3 % and 1 %, respectively.

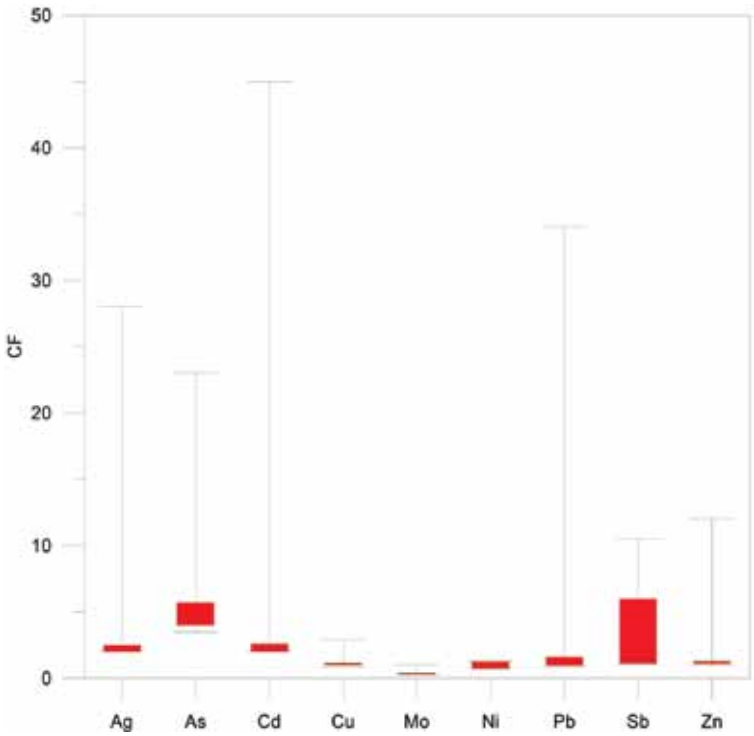

Figure 4. Contamination factor (c_f^i) values for the paddy soils from the Kočani Field

Table 3. Contamination factors and degrees for heavy metals in the paddy soils.

Metal	Range	Average
Ag	2.0–28.0	5.8
As	3.5–23.0	7.3
Cd	2.0–45.0	8.3
Cu	0.9–2.9	1.3
Mo	0.3–1.0	0.4
Ni	0.7–1.3	1.1
Pb	0.9–34.0	5.9
Sb	1.0–10.5	3.4
Zn	0.9–12.0	2.7
Degree of contamination	12.2–157.7	36.2

The paddy soil samples from Section VII, located in the vicinity of the Zletovska River and Zletovo-Kratovo ore district, received a comparatively higher input of anthropogenically derived heavy metals than other parts of the Kočani area. The As, Cd, Cu, Pb and Zn concentrations determined in the paddy soils from Section VII significantly exceeded maximum permissible levels. The distinction between heavy metal contents in Section VII and the other sections was also confirmed by statistical analysis. The pollution in Section VII is undoubtedly related to the irrigation of the paddy fields with the riverine water from the Zletovska River, which drains acidic mine waters and untreated mining waste effluents from the Zletovo-Kratovo mine (ALDERTON et al., 2005).

Elevated concentrations of As, Cd, Cu, Pb and Zn were observed in other paddy soil sections (especially Sections V and VI). This elevation originates from the discharges of the untreated municipal and domestic waste from the city of Kočani and the village of Orizari into the riverine systems of the Kočanska and Orizarska Rivers, which are both used for irrigation purposes. The increased concentrations of the investigated heavy metals could also be explained by the agricultural application of various fertilisers and pesticides, urban and traffic sources and atmospheric deposition.

Although the concentrations of Ag, Mo, Ni and Sb were below the mentioned threshold values, their enrichment in the paddy soil samples near the Zletovska River was also noticeable. This situation confirms the higher input of heavy metals in the area around the Zletovska River.

The high anthropogenic impact on the paddy soils in Section VII was as well

demonstrated by the calculation of the following environmental indexes: contamination factor and degree of contamination. The elevation of the heavy metals present in the paddy soil samples from the other parts of Kočani Field was similarly verified with the results of the environmental indexes. From an environmental point of view, it is evident that the paddy soil samples from Section VII represent a serious risk to the surrounding ecosystems (Dolenec et al., 2007; Rogan et al., 2009, Rogan et al., 2010).

Conclusions

As, Cd, Cu, Pb and Zn concentrations determined in the paddy soils from Section VII significantly exceeded the permissible maximum levels. Although the concentrations of Ag, Mo, Ni and Sb were below the mentioned threshold values, their enrichment in the paddy soil samples near the Zletovska River was noticeable, consequently confirming the higher input of heavy metals in the area around the Zletovska River.

The high anthropogenic impact on the paddy soils in Section VII was demonstrated by the calculation of the contamination factor and degree of contamination. The elevation of the heavy metals present in the paddy soil samples from other parts of Kočani Field was similarly verified with the results of the environmental indexes.

According to the results of the heavy metal concentrations present in the paddy soil the area around the Zletovska River is considered as the most anthropogenically impacted part of Kočani Field. The highly elevated concentrations of the analysed heavy metals were undoubtedly related to past and present mining activities, especially in the Zletovo-Kratovo ore district.

Acknowledgements

The research was financially supported by the Slovenian Research Agency (ARRS), contract number 1000-05-310229.

References

Adriano, D. C. (1986): *Trace Elements in the Terrestrial Environment (1st ed.)*. New York: Springer-Verlag.

Alderton, D. H. M., Serafimovski, T., Mullen, B., Fairall, K., James, S. (2005): The chemistry of waters associated with Metal Mining in Macedonia. *Mine water and the Environment*; Vol. 24, p. 139–149.

Bowen, H. J. M. (1979): *Environmental Chemistry of the Elements* (1st ed.). New York: Academic Press.

Dolenec, T., Serafimovski, T., Tasev, G., Dobnikar, M., Dolenec, M., Rogan, N. (2007): Major and trace elements in paddy soil contaminated by Pb–Zn mining: a case study of Kočani Field, Macedonia.

Environmental Geochemistry and Health; Vol. 29, p. 21–32.

GERMAN FEDERAL MINISTRY OF THE ENVIRONMENT (1992): Novelle zur Verordnung über das Aufringen von Klärschlamm (Bundesgesetzblatt).

HAKANSON, L. (1980): An ecological risk index for aquatic pollution control: a sedimentological approach. *Water Resources*; Vol. 14, p. 975–1001.

JUNG, M. C. (2001): Heavy metal contamination of soils and waters in and around the Imcheon Au-Ag mine, Korea. *Applied Geochemistry*; Vol. 16, p. 1369–1375.

JUNG, M. C. & THORNTON, I. (1997): Environmental contamination and seasonal variation of metals in soils, plants and waters in the paddy fields around a Pb-Zn mine in Korea. *Science of the Total Environment*; Vol. 198, p. 105–121.

KABATA-PENDIAS, A. & PENDIAS, H. (2001): *Trace Elements in Soils and Plants (3rd ed.)*. Boca Raton: CRC Press.

KORRE, A., DURUCAN, S., KOUTROUMANI, A. (2002): Quantitative-spatial assessment of the risks associated with high Pb loads in soils around Lavrio, Greece. *Applied Geochemistry*; Vol. 17, p. 1029–1045.

LEE, C. G., CHON, H. T., JUNG, M. C. (2001): Heavy metal contamination in the vicinity of the Daduk Au-Ag-Pb-Zn mine in Korea. *Applied Geochemistry*; Vol. 16, p. 1377–1386.

LI, X. D., COLES, B. J., RAMSEY, M. H., THORNTON, I. (1995): Sequential extraction of soils for multielement analysis by ICP-AES. *Chemical Geology*; Vol. 124, p. 109–123.

LIU, H., PROBST, A., LIAO, B. (2005): Metal contamination of soils and crops affected by the Chenzhou lead/zinc mine spill (Hunan, China). *Science of the Total Environment*; Vol. 339, p. 153–166.

LOSKA, K., WIECHULA, D., KORUS, I. (2004): Metal contamination of farming soils affected by industry. *Environment International*; Vol. 30, p. 159–165.

LU, X., ZHANG, X. (2005): Environmental geochemistry study of arsenic in Western Hunan mining area, P.R. China. *Environmental Geochemistry and Health*; Vol. 27, p. 313–320.

ROGAN, N., SERAFIMOVSKI, T., DOLENEC, M., TASEV, G., DOLENEC, T. (2009): Heavy metal contamination of paddy soils and rice (*Oryza sativa* L.) from Kočani field (Macedonia). *Environmental Geochemistry and Health*; Vol. 31, p. 439–451.

ROGAN ŠMUC, N., DOLENEC, T., SERAFIMOVSKI, T., TASEV, G., DOLENEC, M. (2010): Distribution and mobility of heavy metals in paddy soils of the Kočani Field in Macedonia. *Environmental earth sciences*; Vol. 61, p. 899–907.

SIMMONS, R. W., PONGSAKUL, P., SAIYASITPANICH, D., KLINPHOKLAP, S. (2005): Elevated Levels of Cadmium and Zinc in Paddy Soils and Elevated Levels of Cadmium in Rice Grain Downstream of a Zinc Mineralized Area in Thailand: Implications for Public Health. *Environmental Geochemistry and*

Health; Vol. 27, p. 501–511.

Tessier, A., Campbell, P. G. C., Bisson, M. (1979): Sequential extraction procedure for the speciation of particulate trace metals. *Analytical Chemistry*; Vol. 51, p. 844–851.

Uradni list RS (1996): Uredba o mejnih opozorilnih in kritičnih emisijskih vrednostih nevarnih snovi v tleh. *Uradni list*, 68, p. 5773–5774.

Yang, Q. W., Shu, W. S., Qiu, J. W., Wang, H. B., Lan, C. Y. (2004): Lead in paddy soils and rice plants and its potential health risk around Lechang Lead/Zinc Mine, Guangdong, China. *Environment International*; Vol. 30, p. 883–889.

Wedepohl, K. H. (1974): *Handbook of Geochemistry (1st ed.)*. Berlin : Springer–Verlag.

Whitby, L. M., Gaynor, J., Maclean, A. J. (1978): Metals in soils of some agricultural watersheds in Ontario. *Canadian Journal of Soil Science*; Vol. 58, p. 325–330.

Witte, K. M., Wanty, R. B., Ridley, W. I. (2004): Engelman Spruce (Picea engelmannii) as abiological monitor of changes in soil metal loading related to past mining activity. *Applied Geochemistry*; Vol. 19, 1367–1376.

Wong, S. C., Li, X. D., Zhang, G., Qi, S. H., Min, Y. S. (2002): Heavy metals in agricultural soils of the Pearl River Delta, South China. *Environmental Pollution*; Vol. 119, p. 33–44.

Petrochemical characteristics of the Precambrian rare metal pegmatite of Oke-Asa area, Southwestern Nigeria: implication for Ta-Nb mineralization

Petrološko-kemične značilnosti predkambrijskih pegmatitov z redkimi kovinami območja Oke-Asa, jugozahodna Nigerija: vpliv na Ta-Nb mineralizacijo

Olugbenga A. Okunlola[1,*] & Oluwatoyin O. Akinola[2]

[1]University of Ibadan, Department of Geology, Ibadan Nigeria
[2]University of Ado-Ekiti, Department of Geology, Ekiti State, Nigeria

*Corresponding author. E-mail: gbengaokunlola@yahoo.co.uk

Received: November 22, 2010 **Accepted:** December 3, 2010

Abstract: The Precambrian pegmatite of Oke-Asa area of Ijero Ekiti occurring as steeply dipping intrusives into the older rocks of migmatite gneiss complex and schistose rocks were investigated with a view to elucidating their petrochemical features that may be related to economic rare metal Ta-Nb mineralization.

Thin section petrographic study indicates that the pegmatite samples contain mainly quartz (37.0 %), muscovite (30.4 %), plagioclase (12.0 %) and microcline (7.0 %), with accessory biotite, hornblende and tourmaline.

Geochemical analysis of muscovite extracts from the pegmatite using (ICP-AES) analytical methods in Activation Laboratories, Ontario Canada; shows that the pegmatite is siliceous with average SiO_2 content of 71.79 %, Al_2O_3 (13.9 %), Fe_2O_3 1.49 %, K_2O 8.77 %, Na_2O 2.08 % and CaO 1.11 % while other oxides MnO, MgO, TiO_2 and P_2O_5 are generally less than 0.3% in each case. Trace element analysis of the pegmatite shows a significant enhancement in Rb, Ba, Zr and Sr as against lower values for Ta, Sn, and Nb. Bulk chemistry, geochemical signatures and variation plot of Ta/(Ta+Nb) vs Mn/(Mn+Fe) indicate that the muscovite-quartz-microcline pegmatite of Oke-Asa area is of rare-element class, lepidolite subtype

Original scientific paper

and are essentially peraluminous in composition. Ta-Nb mineralization trend using variation plots of Ta vs Cs+Rb, Ta vs K/Cs, Ta/W vs Cs and Ta vs Cs plots shows that the pegmatites are relatively poorer than the mineralized Tanco deposits of Canada, and those of Igbeti, Nigeria but are similar to the marginally endowed Noumas pegmatites of South Africa.

Povzetek: Predkambrijske pegmatite območja Oke-Asa iz Ijero Ekitija, ki se pojavljajo kot strmo vpadajoče intruzije v starejših kamninah mignatitno gnajsnega kompleksa in v skrilavcih, smo raziskali, da bi ugotovili njihove petrološke in kemične značilnosti, ki morda kažejo na ekonomsko pomembno mineralizacijo s Ta in z Nb.

Mikroskopske petrografske raziskave kažejo, da so pegmatiti pretežno iz kremena 37.0 %), muskovita (30.4 %), plagioklaza (12.0 %) in mikroklina (7.0 %), z akcesornim biotitom, rogovačo in turmalinom.

Geokemične analize muskovita z metodo ICP-AES, izvedene v Activation Laboratories, v Ontariju v Kanadi, so pokazale, da je v pegmatitu povprečna vsebnost SiO_2 71.79 %, Al_2O_3 (13.9 %), Fe_2O_3 1.49 %, K_2O 8.77 %, Na_2O 2.08 % in CaO 1.11 %, preostalih oksidov MnO, MgO, TiO_2 in P_2O_5 pa je navadno manj kot 0.3 %.

Analiza vsebnosti slednih prvin je pokazala precejšno obogatitev z Rb, Ba, Zr in Sr v primerjavi z z majhno vsebnostjo Ta, Sn, in Nb. Glede na celotno kemijsko sestavo, geokemične značilnosti ter variacijske diagrame Ta/(Ta+Nb) z Mn/(Mn+Fe) se muskovitno-kremenovo-mikroklinov pegmatit Oke-Asa območja uvršča v razred pegmatiov, obogatenih z redkimi zemljami lapidolitnega podtipa in ima peraluminijski značaj. Ugotavljanje Ta-Nb mineralizacijske težnje na diagramih Ta s Cs+Rb, Ta s K/Cs, Ta/W s Cs in Ta s Cs kaže, da so pegmatiti relativno siromašnejši v primerjavi z mineraliziranimi iz Tanaca v Kanadi ter Igbeti v Nigeriji, a podobni nizko orudenim pegmentitom Noumas iz Južne Afrike.

Key words: precambrian, pegmatite, geochemical, rare metal, economic, mineralisation

Ključne besede: predkambrij, pegmentit, geokemija, redke kovine, ekonomično, mineralizacija

Introduction

The world economy at present is growing at a rate that necessitates an increasing demand for rare metals, with this trend likely to continue into the future (Patrick de St. Simmons, 1999). In recent times, there has been a resurgence of interest in the study of rare metal pegmatite occurrences in Nigeria (Garba, 2002, Okunlola, 2005, 2008 Okunlola & Jimba 2006, Okunlola & Oyedokun, 2009, Oden, 2010,). Granite pegmatite is one of the classic sources of a broad spectrum of rare metals: Li, Rb, Cs, Be, Ga, Sc, Y and Rare Earth Elements: Sn, Nb, Ta, U and Th (Cerny, 1994). In Nigeria, Pan-African intrusive suites which comprise mainly granites, granodiorites and tonalities are intruded by numerous veins of pegmatites and aplites (Okunlola, 2005). The pegmatite belongs to the terminal stage of Pan-African magmatism (Rahaman et al., 1988; Elueze, 2002). Rare metal pegmatite were hitherto thought to be known almost exclusively along the SW-NE striking belt covering about

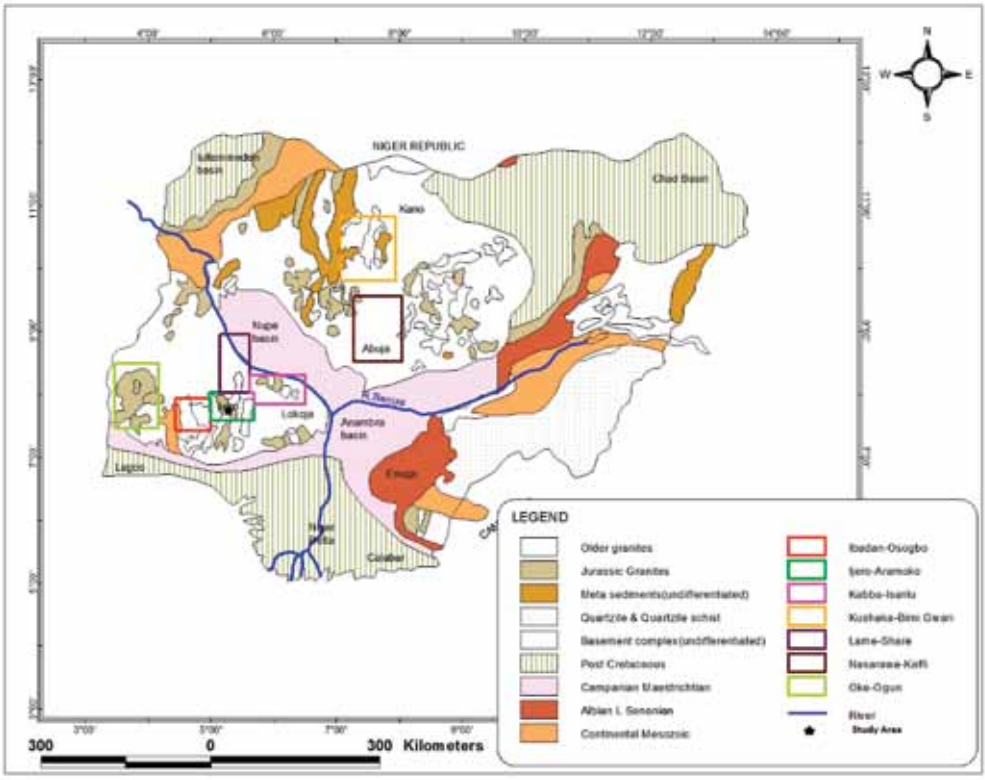

Figure 1. Geological map of Nigeria showing the study area located in the Ijero- Aramoko Pegmatite field (Okunlola, 2005)

400 km long and terminating in the Jos plateau tin field (Jacobson & Webb, 1946, Wright,1970). However, recent studies (Garba, 2003; Okunlola, 2005) have shown that they are not restricted only to these confines. The Ta-Nb pegmatites of Nigeria are generally complex albitised muscovite-quartz-microcline pegmatites with indiscernible to distinct zonations (Okunlola & Jimba, 2006). Seven fields of these mineralized pegmatites as outlined by Okunlola, (2005) include Kabba-Isanlu, Keffi-Nassarawa, Lema-Ndeji, Oke Ogun, Ibadan-Oshogbo, Kushaka-Birnin-Gwari and Ijero-Aramoko. In line with efforts to appraise into some details the petrography, geochemical features and economic potentials in relation to Ta-Nb mineralization of the pegmatites of these different fields, the Oke-Asa pegmatite veins which belong to the Ijero- Aramoko pegmatite field (Figure 1) are thus being studied. This is expected to add to the knowledge of composition, type and economic peculiarities of these suites of rocks.

Geological Setting

Oke-Asa area within the Ijero pegmatite field lies within the Precambrian basement of southwestern Nigeria). The basement rocks of Nigeria form part of the extensive Pan-African Province of West Africa and are delimited in the west by the West African Craton and east by the Congo Craton. Based on lithological associations and geochronological delineations, the Nigeria basement comprises the Migmatite-gneiss complex, the Schist belts and the Older Granites. The Migmatite Gneiss Complex is the oldest, most widespread and abundant rock type in the basement (Ogezi, 1988). It is of Achean-Proterozoic age and a product of long, protracted and possibly polycyclic evolutionary histories. The Nigerian Schist belts comprise of low-grade metasediments and metamorphosed pelitic and psammitic assemblages that outcrop in a series of N-S trending synformal troughs infolded into the crystalline complex of migmatite-gneiss. The Pan-African Granites referred to as Older Granites include rocks of wide range of composition varying from tonalite, granodiorite, granite and syenite. (Rahaman et al., 1988) The Oke-Asa pegmatite form an intrusion into the older lithology of biotite schist that occupies the central part of the area, covering about three quarter of the total land mass (Figure 2). The schistose rock is grayish, highly fissile and weathered. The topographical configurations are essentially low-lying discontinuous outcrops that have a westerly dip values ranging between 25^{o} and 30^{o}. Mineralogically, they are composed of quartz, biotite and hornblende, while accessory minerals include

apatite and opaques. Biotite gneiss occupies the north central area and extends towards the northwestern direction. Outcrops of the rock are low-lying, highly foliated with characteristic black tints imposed by the preponderance of biotite impregnations. Most of the mineral alignments are conformable with the foliation planes of the adjacent schistose rock.

The pegmatite comprises of quartz (37 %), albite (27 %), muscovite (14 %) and microcline (14 %) while biotite, (1.0 %) hornblende (2.8 %) and tourmaline (3.2 %) minerals occur in subordinate amount. Quartz occurs as irregular masses of euhedral crystals. Microcline occurs as phenocrysts with characteristic strong crosshatched twinning and variable microperthitic intergrowth while Carlsbard-twinning and albite twinning characterizes the albite. Muscovite occurs as large platy grains. Accessory minerals include tourmaline and biotite. Tourmaline crystals exhibit long needle-like prismatic shapes with their long axis aligned parallel to each other.

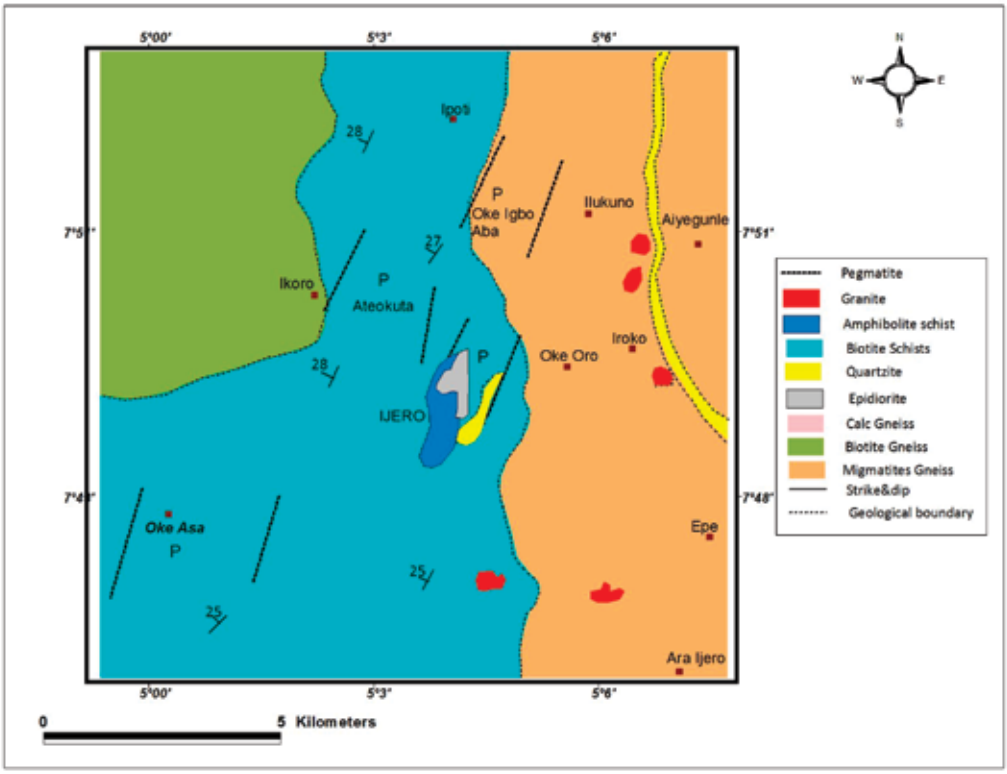

Figure 2. Geologic map of Ijero Ekiti area showing Oke-Asa pegmatite

MATERIALS AND METHODS

Systematic geological mapping was carried out on a scale of 1: 50 000 with grid controlled sampling of the pegmatite veins. Fifteen samples were initially obtained, while ten which were representative of the different veins, fresh and uncontaminated were eventually analyzed. Whole rock analysis of the pegmatite for major, trace and rare earth elements were carried out after they were duly pulverized and homogenized. Many authors including GAUPP et al., (1984) KUSTER, (1990), CERNY et al., (1995) and OKUNLOLA & OYEDOKUN (2009) had established that homogenized and fresh samples of the whole rock pegmatite could be used to establish their genetic features and rare metal potentials, even though the mineral extracts of muscovite, feldspar and tourmaline could also be used effectively. The analysis was carried out using Inductively Coupled Atomic Emission Spectrophotometry (ICP-AES) analytical method at the Activation Laboratories Ltd, Ontario Canada. Rock samples weighing 0.5 g pulverized to 75 μm was put in the platinum crucible. 5 mL perchloric acid, HNO_3 and 15 mL hydrofluoric acid were added. The resulting solution was stirred properly and allowed to evaporate to dryness after warming at low temperature for some hours. 4 mL hydrochloric acid was then added to the cooled solution and warmed to dissolve the salts. On cooling, the solution was diluted to 50 mL with distilled water. The diluted solution was then introduced into the ICP torch as aqueous-aerosol. The light emitted by the ions in the ICP was converted to an electrical signal by a photo multiplier of the spectrometer. The intensity of the electrical signal produced by emitted light from the ions were compared to a standard, which is a previously measured intensity of a known concentration The quality control incorporates a sample prep blank as the first sample and pulp duplicate to monitor analytical precision which is carried all through the stages of preparation to analysis, and the concentration computed. The chemical data are presented in Tables 1 and 2.

GEOCHEMICAL FEATURES IN RELATION TO TA-NB MINERALIZATION.

The analytical results of major, trace and rare elements of pegmatite from Oke-Asa area are presented in Tables 1 and 2. Table 1 shows that the SiO_2 (ca. 71.46 %), Al_2O_3 (ca. 13.9 %), K_2O (ca. 8.77 %) constitute the bulk of the oxide composition. These values are within the range of values of other Ta-Nb pegmatites of Nigeria (OKUNLOLA, 2005). Other major oxides, Fe_2O_3 (ca. 1.49 %), CaO (ca. 1.11 %), Na_2O (ca. 2.08 %) are comparably low while TiO_2 (ca. 0.01 %), MnO (ca. 0.12 %), MgO (ca. 0.03 %) and P_2O_5 (ca. 0.26 %) are much lower.

Table 1. Chemical composition of Oke-Asa pegmatite compared with similar rocks from other locations

Oxides in %	**1**	**2**	**3**	**4**	**5**	**6**	**7**	**8**	**9**	**10**	**Average**	**A***	**B****	**C*****
SiO_2	72.29	72.0	72.46	73.44	72.23	71.58	71.12	71.23	71.62	71.77	**71.46**	**70.17**	**68.26**	**66.17**
Al_2O_3	14.16	13.76	13.79	14.07	13.72	14.21	13.69	13.87	13.87	13.83	**13.90**	**15.68**	**14.02**	**25.51**
Fe_2O_3	1.25	1.58	1.54	1.35	1.69	1.61	1.41	1.49	1.50	1.46	**1.49**	**1.15**	**1.95**	**3.91**
MnO	0.11	0.12	0.13	0.12	0.12	0.13	0.12	0.12	0.12	0.12	**0.12**	**-**	**0.16**	**0.19**
MgO	0.03	0.02	0.03	0.01	0.04	0.04	0.02	0.03	0.03	0.01	**0.03**	**0.13**	**1.49**	**0.37**
CaO	1.30	1.17	1.23	0.72	1.02	1.16	1.41	1.07	1.35	0.75	**1.11**	**1.19**	**1.38**	**0.35**
Na_2O	2.12	2.04	2.04	2.11	2.02	2.14	2.09	2.07	2.13	2.08	**2.08**	**3.26**	**3.42**	**1.18**
K_2O	9.02	8.97	8.86	8.88	8.66	8.64	8.71	8.61	8.78	8.61	**8.77**	**6.05**	**4.64**	**1.16**
TiO_2	0.01	0.01	0.01	0.00	0.02	0.03	0.01	0.02	0.01	0.01	**0.01**	**0.04**	**0.20**	**0.73**
P_2O_5	0.30	0.26	0.26	0.25	0.26	0.25	0.25	0.24	0.25	0.26	**0.26**	**0.02**	**0.03**	**0.20**
LOI	0.15	0.14	0.07	0.04	0.12	0.65	0.36	0.20	0.21	0.24	**0.22**	**-**	**-**	**-**
Total	100.7	100.1	100.4	100.9	99.89	99.12	99.18	98.94	99.87	98.66				
Trace Elements in µg/g														
Ta	27.5	30.3	33.9	33.9	51.8	17.7	17.5	22.9	21.2	24.3	**28.1**	**4.64**	**170.5**	**33.08**
Cs	20.2	20.6	19.9	23.3	25	19.7	22	21.4	22.1	22.7	**21.69**	**1.34**	**105.8**	**72.29**
Rb	576	590	544	600	594	536	571	553	562	580	**570.6**	**115.6**	**1791**	**547.7**
Sn	14.0	6.0	7	6	13	5	7	9.0	7.0	9.0	**8.3**	**1.18**	**202.3**	**50.41**
Nb	23.0	29.0	30	53	39	18	18	27.0	23.0	24.0	**28.4**	**1.28**	**157.5**	**36.73**
Sr	72.0	69.0	54	56	69	90	82	86	78	81	**73.7**		**111.9**	**87.52**
Y	31.0	36.0	39	37	43	28	31	37	33	33	**34.8**	**2.55**	**26.31**	**6.52**
Ba	206	203	213	221	216	205	213	206	213	212	**210.8**	**986.2**	**21.3**	**237.1**
Hf	3.5	3.8	3.3	2.2	2.9	2.4	2.3	2.4	2.6	2.2	**2.76**	**0.47**		
Th	4.0	4.2	4.4	4.8	5	3.8	2.9	3.3	3.7	0.2	**3.63**	**1.93**	**8.28**	
W	1.0	2.0	4.0	5	5	4	4.0	4.0	5.0	4.0	**3.8**	**0.65**	**174.3**	**3.25**
Be	13.0	12	12	12	11	11	12	12.0	11.0	11	**11.8**	**138.4**	**14.8**	**16.56**
Zr	46.0	56	76	39	69	50	51	51.0	52.0	47.0	**53.7**		**23.8**	**41.98**
Ga	22.0	22	22	24	24	22	23	21.0	22.0	23.0	**22.5**	**18.88**	**75.45**	**30.15**
Zn	25	25	25	25	25	25	25	25	25	25	**25**	**15.27**	**111.7**	
U	25.6	27.2	34.8	41.9	50.6	45.5	25.2	31.1	28.5	26.5	**33.6**	**0.56**	**9.96**	
K	19400	20000	6100	4200	6900	4700	19300	20000	19500	5100	**12520**			
Na	960	1050	620	520	350	650	1010	1020	1040	490	**771**			
Ratios	**1**	**2**	**3**	**4**	**5**	**6**	**7**	**8**	**9**	**10**				
K/Rb	33.7	33.90	11.21	7.0	11.62	8.77	33.8	36.17	34.69	8.79	18.3			
Rb/Sr	8.0	8.55	10.07	10.71	8.61	5.96	6.96	6.43	7.21	7.16	7.97			
Na/K	0.05	0.053	0.102	0.124	0.05	0.14	0.05	0.05	0.05	0.096				
Ba/Rb	0.36	0.34	0.39	0.37	0.36	0.38	0.37	0.37	0.38	0.366				
Zr/Hf	13.1	14.74	23.03	17.73	23.79	20.8	22.2	21.3	20.0	21.36				
Sr/Rb	0.13	0.116	0.099	0.093	0.116	0.17	0.14	0.155	0.139	0.14				
Rb/Cs	28.5	28.6	27.34	25.75	23.76	27.2	26.0	25.8	25.43	25.55	26.39			
Ta/W	27.5	15.15	8.48	6.78	10.36	4.43	4.38	4.58	5.3	6.08	9.31			
K/Cs	960	971	306.5	180.3	276	239	877	934.6	882.4	224.7	585.2			

A= Itakpe pegmatite (Okunlola & Somorin, 2006); B= Komu pegmatite (Okunlola & Ofonime, 2006); C= Sepeteri pegmatite (Okunlola & Akintola, 2007). *Average of 11 representative samples.
** Average of 10 representative samples; *** Average of 25 representative samples

Table 2. REE/ Chondrite data for Oke-Asa Pegmatite

REE	1	2	3	4	5	6	7	8	9	10	Range
La	1.4	1.7	1.8	2.5	2.2	1.8	2.3	1.8	1.9	3.7	**1.4–3.7**
Ce	3.3	2.7	3.9	3.0	3.1	2.8	3.3	2.7	2.9	2.9	**2.7–3.9**
Nd	3.1	2.6	3.5	2.8	3.1	2.8	3.3	2.7	2.7	2.9	**2.6–3.5**
Sm	1.1	1.0	1.3	1.0	1.2	1.1	1.3	1.1	1.2	1.4	**1.0–1.4**
Eu	0.13	0.11	0.14	0.12	0.13	0.11	0.14	0.13	0.13	0.13	**0.11–0.14**
Gd	2.0	1.3	2.3	1.4	1.7	1.6	1.8	1.5	1.6	2.0	**1.3–2.3**
Tb	0.4	0.4	0.5	0.4	0.4	0.4	0.4	0.4	0.4	0.5	**0.4–0.5**
Dy	2.8	2.7	3.3	2.8	3.4	3.1	3.5	3.0	3.3	4.1	**2.7–4.1**
Ho	0.7	0.6	0.8	0.6	0.8	0.7	0.8	0.7	0.8	1.0	**0.6–1.0**
Er	2.4	2.1	2.7	2.1	2.7	2.5	2.9	2.4	2.8	3.2	**2.1–3.2**
Tm	0.45	0.39	0.49	0.38	0.48	0.44	0.51	0.43	0.49	0.53	**0.38–0.51**
Yb	3.4	0.45	0.56	0.43	0.53	0.48	3.8	3.1	3.5	3.8	**0.43–3.8**
Lu	0.55	0.45	0.56	0.43	0.53	0.48	0.55	0.47	0.54	0.57	**0.43–0.57**

Trace element data (Table 2) shows a pronounced enrichment in trace elements like Rb (570.6 μg/g), Ba (209.8 μg/g) and Li (1285 μg/g). However, fairly lower values are recorded for Ta (ca. 28.1 μg/g), Nb (ca. 28.3 μg/g) and Sn (ca. 83 μg/g). These values are significantly lower compared to those for rare metal pegmatites of Nasarawa-Keffi (OKUNLOLA, 2005). Following the classification system of pegmatites based on bulk chemistry and geochemical signatures (CERNY, 1991) and Ta/(Ta+Nb) versus Mn/(Mn+Fe) plot, (Figure 3), The Oke-Asa pegmatites are of rare element complex pegmatite type, LCT petrogenetic (Li, Rb, Cs, Be, Ga, Sn, Ta> N(B, P, F)) family, and of the lepidolite sub type. The pegmatite are of peraluminous bulk composition (Al_2O_3>CaO+Na_2O+K_2O) (Figure 4). CERNY (1992), states that the LCT family has a mildly to extremely peraluminous parent granitic composition. Based on this, there is a strong possibility that the Oke-Asa pegmatites are derived from the anatexis of crustal protoliths or supracrustal rocks with evidence of sodic metasomatic alteration. Using the K/Rb versus Rb plots (Figure 5) shows the pegmatite of Oke-Asa area are rare metal bearing. (MATHEIS, 1987; CERNY, 1994) Also, the relatively low Mg and Ti with attendant high Rb, Li, Cs composition indicate a high level of fractionation, as is usual with such pegmatites, While the level of mineralization may be comparable to those for some Nigerian pegmatite fields such as Egbe (MATHEIS, 1987), it is lower when compared to that of highly mineralized Tanco Pegmatite of Canada (CERNY, 1982, MOLLER & MORTEANI, 1987). The Ta vs Ga (Figure 6) plot also show the Oke-Asa pegmatite plotting above the BEUS (1966) mineralization line but below the GORDIYENKO (1971) line. The Na/K vs Ta diagram (Figure 7) also in-

dicates that the pegmatite of Oke Asa area are moderately albitised and compares with other mineralized pegmatite of Egbe-Isanlu area (Matheis, 1987) and Komu pegmatite Nigeria (Okunlola & Ofonime, 2006) but lower than those of Tanco and Noumas pegmatites. Chondrite normalized plot of the rare earth element (REE) reveals high light REE (LREE) (La, Ce, Pr) values and lower heavy (HREE) (Er,Lu,Yb). There is a marked negative Europium (Eu) anomaly (Figure 8) which according to Taylor et al., (1986) suggests fractionation and intense late metasomatic effect.

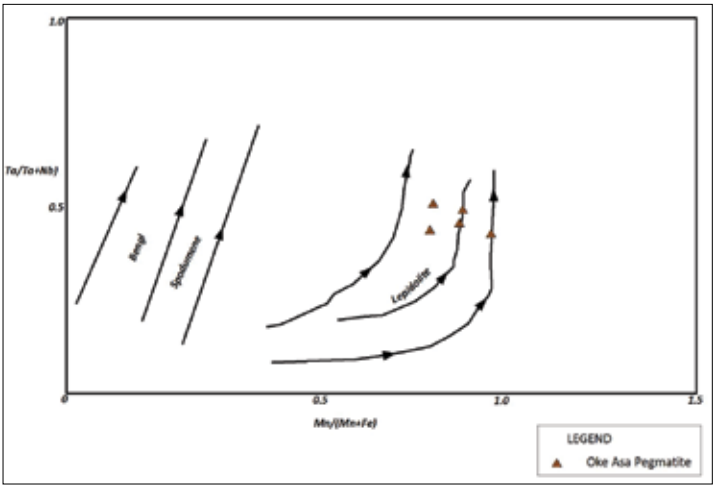

Figure 3. Ta/(Ta+Nb) vs Mn/ (Mn+Fe) plot of Oke Asa pegmatite indicating Lepidolite subtype

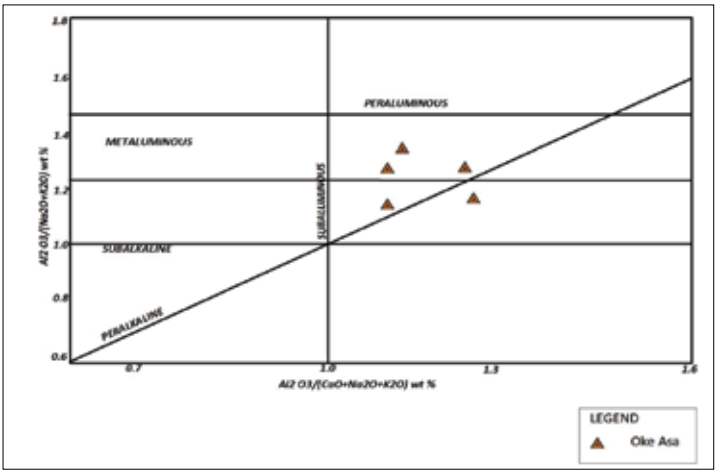

Figure 4. $Al_2O_3/(Na_2O+K_2O)$ vs $Al_2O_3/ (CaO+Na_2O+ K_2O)$ plot of Oke-Asa pegmatite showing it as having Peraluminous composition

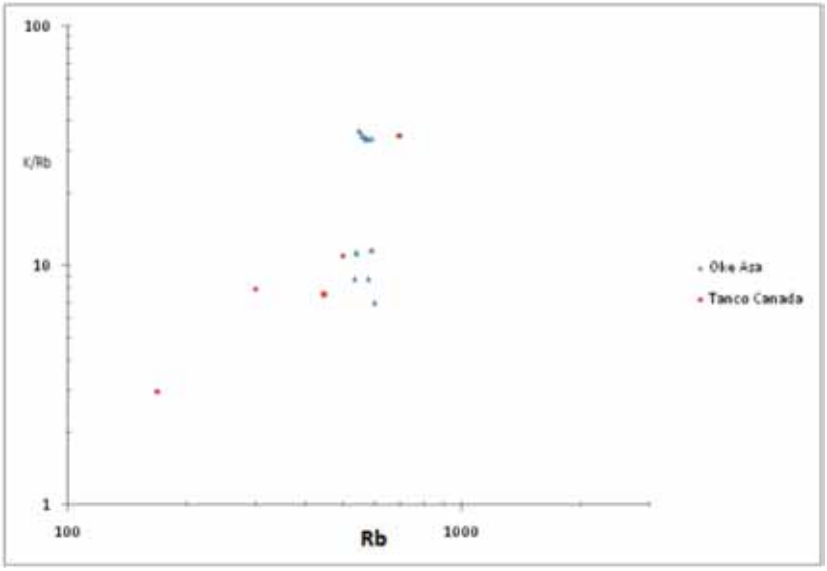

Figure 5. K/Rb/Rb plot of the Oke Asa pegmatite

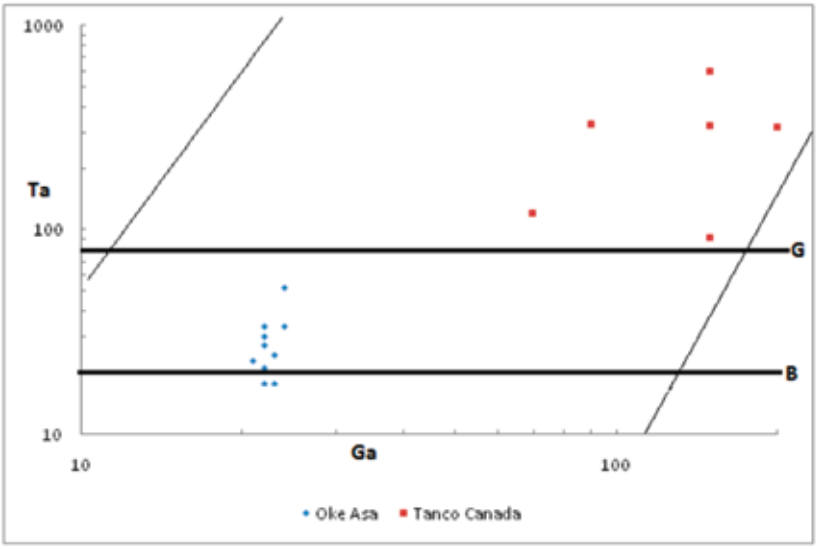

Figure 6. Ta/Ga plot of the Oke Asa pegmatite.
B=BEUS (1966) line , G=GORDIYENKO (1971) line

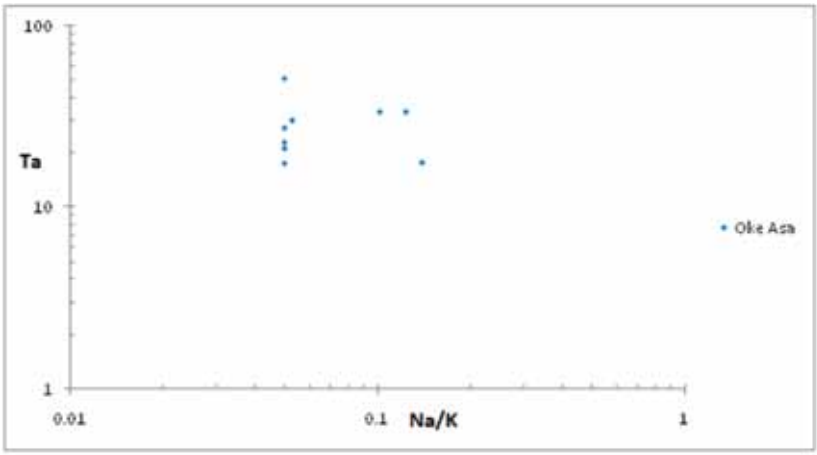

Figure 7. Ta vs Na/K plot for Oke-Asa pegmatite (OKUNLOLA, 2008).

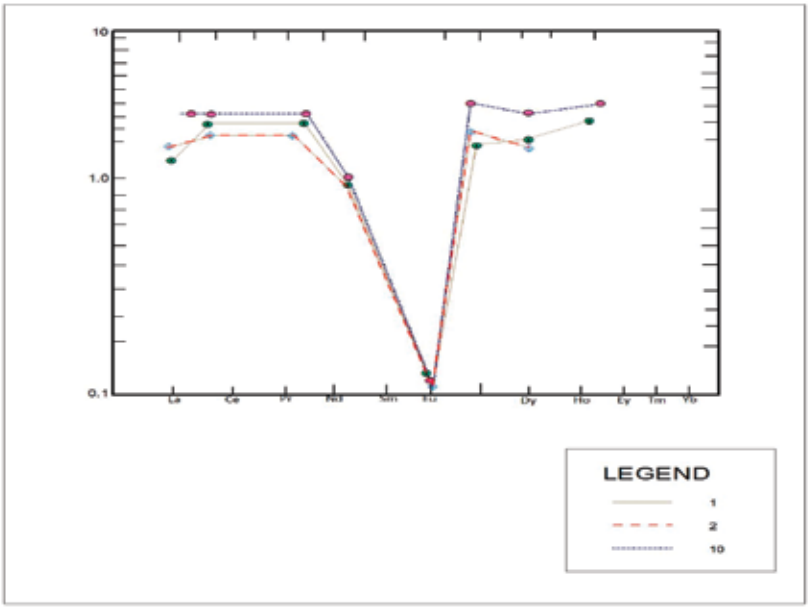

Figure 8. REE /chondrite plot for Oke Asa pegmatite

CONCLUSIONS

Systematic field mapping reveals that the the Precambrian pegmatite of Oke-Asa area are hosted by biotite gneiss and biotite schist. Petrographic analysis also shows that they contain mainly quartz, plagioclase, microcline and muscovite with accessory biotite, hornblende, tourmaline and opaque. From geochemical studies of the muscovite extracts, the pegmatite are siliceous, with a peraluminous composition, while trace elements analysis indicate that the pegmatite are variably enriched in rare metals Ta, Nb including Li, Rb and Sr. Variation plots for Ta versus K/Cs, Ta/W versus Cs, Ta versus Ga, Na/K versus Sn, Nb, Ta of the samples indicate a lower mineralization potentials when compared to Tanco pegmatite (Canada), Nassarswa-Keffi pegmatite field of Nigeria, but are comparable to those of Wodgina pegmatite (Australia), Hergendorf pegmatite (Western Germany) and Noumas pegmatite (South Africa). In addition to the major and minor element compositional features, consistent negative Eu signature of the chondrite normalized REE plots suggest the possibility of Oke-Asa pegmatites being derived from anatexis of undepleted upper to middle crustal protoliths or supracrustals with possible later metasomatic alterations.

Acknowledgement

The authors wish to acknowledge Prof. A. O. Oyinloye of the University of Ado -Ekiti, Mr. O. Olaifa of the department of Earth Sciences, Olabisi Onabanjo University Ago-Iwoye and Mr. Nasirudeen of Obafemi Awolowo University, Ile-Ife for their considerable support. Numerous colleagues and friends who contributed in various ways are also acknowledged. Chemical analysis was executed at Actlabs laboratories, Canada. Dr. A.F. Abimbola was exceptionally supportive.

REFERENCES

BEUSS, A. A. (1966): Distribution of Tantalum and Niobium in muscovites from granite pegmatites. *Geokhimiya*; Vol. 10, pp. 1216–1220.

CERNY, P. (1982): Mineralogy of Rubidium and Cesium. Granitic pegmatite in Science and Industry. *Mineralogical Assoc. of Canada Short Course handbook*; Vol. 8, pp. 148–161.

CERNY, P. (1991): Fertile Granites of Precambrian pegmatite fields: Is geochemistry controlled by tectonic setting or source lithologies? *Prec. Res.*; Vol. 51, pp. 429–468.

CERNY, P. (1992): Geochemical and petrogenetic features of mineralization in rare element granitic pegmatites in the light of current research. *Applied Geochemistry*; Vol. 7, pp. 393–416.

Cerny, P. (1994). Rare-element Granitic Pegmatites. Part 1: Anatomy and Internal Evolution of Pegmatite Deposits. *Prec. Res.*; Vol. 53, pp. 29–62.

Cerny, P, Stanck, J., Novak, N., Baadsgaard, H., Rieder, M.,Ottolini, I. & Shapman, R. (1995): Geochemical and structural evolution of Micas of Rozna and Dubravodal pegmatites, Czech. Republic. *Mineralogy and Petrology*; Vol. 52, pp. 4–9.

Elueze, A. A. (2002): Compositional character: A veritable tool in the appraisal of geomaterials. An inaugural lecture. University of Ibadan; 43p.

Garba, I. (2003): Geochemical discrimination of newly discovered rare-metal bearing and barren pegmatites in the Pan-African 600 ± 150 Ma basement of Northern Nigeria. A*pplied Earth Sc. Transaction Inst. Of Mining and Metallurgy*; 13: Vol. 112, pp. 287–292.

Gaupp, R., Moller, P., Moteani, G. (1984). Tantalum Pegmatites: *Geologische, Petrologische and Geochemische unterschungen*; Monograph Series Min.

Gordiyenko, L. (1971): Concentration of Li, Rb and Cs in potash feldspar and muscovite as criteria for assessing the rare metal mineralization in granite pegmatites, Southwestern Australia. *Min. Assoc. Can. Short course*; Vol. 8, pp. 513–525.

Jacobson, R. R. E. & Webb, J. S. (1946): The pegmatites of Central Nigeria. *Geol. Surv. Nig. Bull.*; Vol. 17, pp. 40–61.

Kuster, D. (1990): Rare-metal pegmatites of Wamba, Central Nigeria: their formation in relationship to late Pan-African granite. Journ. of Mineral Dep. 25,pp 25–33.

Matheis, G. (1987): Nigerian rare metal pegmatites and their lithologic framework. *J. Geol.*; Vol. 22 pp. 271–291.

Moller, P. & Morteani, G. (1987): Geochemical guide for Tantalum Pegmatites Economic Geology; Vol. 12, pp. 1885–1897.

Oden, M. I. (2010): The pegmatite veins of western Oban Massif: tectonic and lithologic controls of physical property. *Book of abstarcts, 46th NMGS Annual Internatoional conference calabar*; 7p.

Ogezi, A. E. O. (1988): Geochemistry and origin of Ensialic Alpines - type serpentine Associations from Mallam Tanko (Shemi) and Ribah Northern Nigeria. *In Prec. Geo. of Nigeria*; GSN, Esho Pub. Kaduna.

Okunlola, O. A. (2005): Metallogeny of Ta-Nb mineralization of Pre Cambrian pegmatite of Nigeria. *Mineral Wealth*; 137/2005, pp. 38–50.

Okunlola, O. A. & Jimba, S. (2006): Compositional trends in relation to Tantalum-Niobium mineralization in PreCambrian pegmatites of Aramoko-Ara-Ijero area, Southwestern Nigeria.

Okunlola, O. A. & Ofonime, B. U. (2006): Geological setting and petrochemical features of Rare metal Ta-Nb) Mineralisationof pegmatites of

Komu area southwestern Nigeria. *African Journal of Science and Technology*; *Science and engineering Series*; Vol. 7, No. 1, pp. 96–110.

OKUNLOLA, O. A. & OYEDOKUN, M. O. (2009): Compositional trends and raremetal Ta-Nb mineralization potential of pegmatite and associated lithologies of Igbeti area, south-western Nigeria. *RMZ - Materials and Geoenvironment*; Vol. 56, No. 1, pp. 38–53.

OKUNLOLA, O. A. & SOMORIN, E. B. (2006): Compositional characteristics of Precambrian pegmatites of Itakpe area, central Nigeria. *Global Journal of Geological Siences*; 4.2: p 23–32.

OKUNLOLA, O. A. & AKINTOLA, A. I.. (2008): Geochemical features and rare metal (Ta-Nb) potentials of Precambrian Pegmatite of Sepeteri area, southwestern Nigeria. *Ife Journal of Science*; Vol. 9, No. 2, pp. 203–214.

OKUNLOLA, O. A. (2008): Compositional characteristics and functional industrial applications of Itakpe clay occurrence, central Nigeria. *European Journal of Scientific Research*; Vol. 19, No. 3, pp. 453–461.

OVERSBY, V. N. (1975): Lead isotope study of Aplites in the Precambrian basement rocks near Ibadan, southwestern Nigeria. *Earth and Planetary Science Letters*; Vol. 27, pp. 177–180.

PATRICK DE ST. SIMMON (1999) Specialty metals of Nigeria. Potentials for world Class Deposits. In. Uche, J., Ohiwerei, F. and Bassey, E., (eds); *Proceedings of First Mining in Nigeria Conference*; pp. 91–100.

RAHAMAN, M. A., AJAYI, T. R., OSHIN, I. O. & ASUBIOJO, F. O. (1988): Trace element geochemistry and geotechtonic setting of Ile-Ife schist belts. *PreC. Geol. of Nigeria*, GSN pub. Kaduna., pp 241–256.

TAYLOR, S. R. & ROBERTA, L. R., MCLENNAN, S. C. & ERIKSSON, K. A. (1986): Rare Earth Elements patterns in Archean high grade metasediments and their tectonic significance. *Geochemical et.Cosmochimica Acta*; Vol. 50, pp. 2267–2279.

WRIGHT, J. B. (1970): Controls of Mineralization in the Older and Younger tin fields in Nigeria. *Economic Geology*; pp. 943–951.

Dokumentiranje oblik propadanja naravnega kamna na objektih kulturne dediščine

Documentation of weathering forms of natural stone on monuments

Sabina Kramar[1,*] & Breda Mirtič[2]

[1]Institute for the Protection of Cultural Heritage of Slovenia, Conservation Centre, Restoration Centre, Poljanska cesta 40, 1000 Ljubljana, Slovenia
[2]University of Ljubljana, Faculty of Natural Sciences and Engineering, Department of Geology, Aškerčeva cesta 12, SI-1000 Ljubljana, Slovenia

*Corresponding author. E-mail: sabina.kramar@rescen.si

Received: October 22, 2010 **Accepted:** December 3, 2010

Abstract A detailed investigation of stone monuments makes an important contribution to damage diagnosis on stone monuments. Paper presents a review of weathering form groups and main weathering forms, which represent classification scheme of individual weathering forms. Documentation of weathering forms of natural stone and mapping of weathering forms is shown for the case of black limestone Drenov Grič.

Izvleček Izčrpna dokumentacija o propadanju naravnega kamna je ključnega pomena na področju ohranjanja objektov kulturne dediščine. V prispevku je podan pregled skupin in glavnih oblik propadanja naravnega kamna, na podlagi katerih klasificiramo posamezne oblike propadanja. Dokumentacija in vrednotenje oblik propadanja naravnega kamna in grafični prikaz le-teh so podani na primeru črnega apnenca Drenov Grič.

Key words: weathering forms, limestone, deterioration, natural stone, cultural heritage
Kjučne besede: oblike propadanja, apnenec, propadanje, naravni kamen, kulturna dediščina

Professional Paper

UVOD

Razpadanje naravnega kamna kot manifestacija preperevanja je naraven odziv sestavin kamnine na razmere v okolici, ki zajemajo atmosferske spremembe, antropogene dejavnike in vpliv živega sveta. Propadanje kamna zmanjšuje njegovo uporabno vrednost in funkcionalnost, saj vpliva na dimenzije, obliko, videz, fizikalno-mehanske lastnosti, na kemično obstojnosti ipd. (BILBIJA & GRIMŠIČAR, 1987). Pojav posameznih oblik propadanja na določenem objektu oz. spomeniku iz naravnega kamna je odvisen od zunanjih dejavnikov ter lastnosti kamnine. Določene poškodbe so vezane izključno na intrinzične lastnosti kamnine, ki so posledica njenega nastanka in geološke zgodovine. Pojem »oblika propadanja« uporabljamo za vidno propadanje kamnin na mezoskali (cm–m) (FITZNER & HEINRICHS, 2002).

Sodoben način ohranjanja spomenikov iz naravnega kamna delimo na: (a) anamnezo (umetnostna zgodovina objekta, lokacija, umestitev v okolje), (b) diagnozo (določanje materialov, lastnosti materialov, identifikacija stanja propadanja ter določanje procesov propadanja) in (c) terapijo (nadzor, vzdrževanje) (FITZNER & HEINRICHS, 2002). Upoštevajoč mednarodne direktive je dokumentacija oblik propadanja nujen del vseh treh korakov. Metodologija v okviru diagnoze zajema preiskave na samem objektu (preiskave *in situ*), skupaj z vrednotenjem in grafično dokumentacijo propadanja naravnega kamna ter laboratorijske analize.

Dokumentiranje makroskopskih sprememb oziroma karakterizacija, kvantifikacija in interpretacija oblik propadanja naravnega kamna na določenem objektu je eden od ključnih korakov pred restavratorsko-konservatorskim posegom, saj je osnova za konservatorsko-restavratorske smernice. Detajlna analiza oblik propadanja je prvi pogoj za razumevanje vzrokov, procesov ter karakteristik poškodb naravnega kamna ter celostnega ohranjanja spomenikov. Učinkovit nedestruktivni postopek za preiskave *in situ* oz. preučevanje poškodovanosti naravnega kamna na objektih kulturne dediščine je metoda kartiranja oblik propadanja (FITZNER in sod., 2002; FITZNER & HEINRICHS, 2003; FITZNER, 2004; FITZNER in sod., 2004; ROTHERT in sod., 2007). Na podlagi prepoznanih oblik propadanja lahko ugotovimo vzroke zanj ter stopnje in procese propadanja. Objektiven opis, prepoznavanje in dokumentacija oblik propadanja zahtevajo natančno klasifikacijsko shemo teh oblik. Na razpolago so različne klasifikacije, ki so jih podali: italijanska komisija NORMAL (Normative materiali lapidei, 1988), nemška delovna skupina *Natural stones and weathering* (Classification scheme of weathering forms (FITZNER & HEINRICHS, 2002) in Photo

atlas of weathering forms on stone monuments (Fitzner & Heinrichs, 2004) in nedavno tudi ICOMOS-ISC (Illustrated glossary on stone deterioration patterns, 2008).

V slovenskem prostoru se ne uporablja klasifikacije, ki bi vsebovala popis vseh oblik propadanja naravnega kamna na objektih kulturne dediščine. Zato se pogosto za isti tip oblik propadanja uporabljajo različni izrazi, poleg tega oblike propadanja niso razdeljene po skupinah, kar je pogoj za pregledno dokumentiranje.

V prispevku so podani pregled skupin in glavnih oblik propadanja naravnega kamna, na podlagi katerih klasificiramo posamezne oblike propadanja, ter opis določenega pojava, nabor izrazov ter razlaga procesov propadanja. Opis temelji na klasifikaciji nemške delovne skupine Natural stones and weathering (Fitzner & Heinrichs, 2002; Fitzner & Heinrichs, 2004). Definicije posameznih pojmov se navezujejo izključno na makroskopske analize, ne glede na vzroke za nastanek sprememb oz. oblik razpadanja. Namen tega prispevka je zbrati in poenotiti različne klasifikacije, vpeljati slovenske izraze za različne primere oblik propadanja, ki bi jih pri svojem delu nato uporabljali vsi, ki se ukvarjajo s problemom propadanja naravnega kamna na spomenikih in drugih objektih iz naravnega kamna. Prikaz določanja oblik propadanja naravnega kamna na objektih kulturne dediščine in grafična prestavitev le-teh je podana na primeru črnega apnenca Drenov Grič.

Klasifikacija oblik propadanja naravnega kamna

Osnovno klasifikacijsko shemo, uporabljeno v prispevku, po vzoru nemške klasifikacije (Fitzner & Heinrichs, 2002) sestavljajo štiri skupine propadanja, ki so nadalje razdeljene v glavne oblike, le-te pa v posamezne oblike propadanja. Klasifikacijo bo z nadaljnjim delom smiselno izboljševati in dopolnjevati. Predlagana klasifikacija omogoča na objektu kartirati posamezne oblike propadanja, ki jih označimo z ustreznim grafičnim simbolom in razdelimo po glavnih oblikah propadanja in po skupinah. Razdelitev oblik propadanja v štiri skupine poda pregled nad različnimi načini propadanja in s tem prvo informacijo o določeni obliki propadanja in njeni lokaciji na objektu.

Grafični prikaz zato omogoča takojšnjo oceno stopnje poškodb na določenem objektu. V naslednji fazi izdelamo načrt o vrsti in količini preiskav, katerih rezultati nam nato omogočajo določiti potrebne konservatorsko-restavratorske posege. Iz kartiranja oblik propadanja je razvidno, na katerih delih kamnitega objekta prevladuje izguba materiala (prva skupina), kje so barv-

ne spremembe in nalaganje materiala (druga skupina), kje material odstopa (tretja skupina) in kje gre za poškodbe v obliki razpok in deformacij (četrta skupina). Na podlagi litološkega kartiranja na objektu lahko točno razberemo, kateri tipi oblik propadanja se pojavljajo na posamezni kamnini. Poleg tega lahko ugotovimo, kje je največja stopnja poškodb in kateri del spomenika je najbolj poškodovan.

Pregled skupin in glavnih oblik propadanja

Oblike propadanja naravnega kamna so razdeljene v štiri glavne skupine, v njih pa je izvedena dodatna delitev glede na prevladujočo obliko propadanja.

- *1. skupina* »Odpadanje delov kamnine« se deli na:

a) odpadanje površinskih plasti kamnine

Debelina odpadle površinske plasti je odvisna od globine, na kateri je nastala dekohezija kamnine.

b) nastanek reliefa

Nastanek reliefa na površini, ki ga lahko povzročajo različni dejavniki in se izraža kot površinsko odpadanje. Odpadajo manjši, bolj izpostavljeni deli površine objekta – erozija, zaradi česar se na objektu pojavi relief. Posamezne oblike propadanja so zaobljevanje in dolbenje, izbirno propadanje in luknjičasto razpadanje.

c) odlom

To je odpadanje delov kamnine zaradi kratkotrajnega delovanja mehanske sile na kamniti objekt (zunanja mehanska sila). Velikost in oblika odlomljenega dela kamnine ter smer, po kateri se je kamnina odlomila, so odvisni od vrste sile, od tipa kamnine, njene orientacije pri gradnji ter tehnologije izdelave kamnitega elementa.

- *2. skupina* »Sprememba barve in odlaganje materiala« se deli na:

a) spremembo barve

Zajema spremembo tona, čistosti in kromatičnosti (intenzitete) barve na površini kamnine. Številne vrste propadanja kamna spremlja tudi sprememba njegove barve (obarvanje in razbarvanje).

b) odlaganje materiala v obliki tankih plasti na površini kamnine

Te plasti so posledica odlaganja aerosolov, atmosferskih delcev, ptičjih iztrebkov itd.

c) nevezane usedline soli na površini kamnine

Trdni delci soli, ki se odlagajo na površini in s tem spremenijo osnovno barvo kamnine, imajo svoj izvir v kamnini, na katere površini so se odlagali. Nastanek soli in njihova migracija na površino kamnine sta posledica drugih vrst propadanja kamnine.

č) obloge

Oblogo sestavlja material, ki se je usedel na površino kamnine in se je vezal na kamnino s procesi mineralizacije. Vzroki za nastanek materiala, ki tvori

skorjaste prevleke, so različni. Lahko imajo izvir v kamnini sami ali pa je bil material prinesen od drugod (polutanti). Obloge so lahko slabo ali dobro vezane.

d) otrdevanje površine

Površinsko plast kamnine kompaktirajo sekundarni minerali, ki so se odlagali v njej in imajo izvir v kamnini sami. Plast je bolj gosta in ima večjo trdnost od kamnine v notranjosti, zato odstopi od nespremenjenega dela kamnine.

e) zaraščanje površine kamnine z vegetacijo

Na površini kamnine se lahko naselijo mikroorganizmi in višje vrste rastlin.

- *3. skupina* »Odstopanje površine kamnine« se deli na:

a) zrnato razpadanje materiala na površini kamnine

S površine kamnine lahko odpadajo posamezna mineralna zrna, lahko pa tudi večji kosi kamnine. Vzrok je zmanjšanje kohezijskih sil v kamnini. Posamezne oblike propadanja so razpadanje v prah, v zrna ali v zrnate agregate.

b) drobljenje

Površina kamnine se drobi, ker se je zmanjšala kohezijska sila v površinski plasti primarno razpokane kamnine. Zdrobljeni deli kamnine sicer niso mineraloško in kemično spremenjeni.

c) luščenje

Material, ki odpada s površine kamnine, je v obliki tankih kosov kamnine – lusk, pri čemer luska ne sledi teksturi kamnine. Luščenje je lahko neoslojno ali večslojno. Vzroki za nastanek lusk so različni.

č) napihovanje

Površinska plast se zaradi napihovanja loči od kamnine, kasneje pa lahko v celoti odpade. Vzroki za napihovanje so različni. Ločimo napihovanje, ki je odvisno od teksture kamnine, in napihovanje, ki ne sledi teksturi kamnine.

d) konturno luščenje

To je luščenje površinske plasti kamnine v obliki lusk, ki sledi konturam kamnitega objekta. Lahko se lušči v eni – enoplastno luščenje ali v več plasteh – večplastno luščenje.

e) razslojevanje

Odstopanje površinskega dela kamnine, ki sledi teksturi kamnine.

f) odstopanje skorij

Na kamnini, ki ima skorjo, lahko prihaja do odstopanja le-te. Po navadi prihaja do odstopanja skorij s kamnino. Če je kohezivna sila med skorjo in kamnino večja, kot je kohezivna sila med delci kamnine, pri odstopanju skorje le-ta odstopi tako, da s sabo povleče še stično plast kamnine. Le-ta je zaradi dejavnikov preperevanja fizikalno, kemično in mineraloško spremenjena v odnosu do matične kamnine. Skorjo pa lahko tvorijo tudi samo sekundarni minerali, nastali kot posledica dejavnikov preperevanja iz okolja.

- *4. Skupina* »Razpoke in deformacije« se delijo na:

a) razpoke

Razpoke so posledica različnih vzro-

kov in lahko sledijo teksturi kamnine ali pa ne. Razpoke so nastale izključno zaradi delovanja zunanje mehanske sile na kamnino. Ob razpoki lahko pride do premika med deloma kamnine na obeh straneh razpoke.

b) zlomi

Po razpoki se oba dela kamnine ločita (kamnina razpade na vsaj dva dela).

c) deformacije

Deformacija je sprememba profila kamnitega objekta. Izražena je predvsem na kamnitih objektih v obliki plošč oz. tam, kjer je močno izražena geometrijska anizotropnost kamnine. Ločimo konveksno in konkavno deformacijo.

DOKUMENTIRANJE OBLIK PROPADANJA APNENCA DRENOV GRIČ

Osnovne karakteristike in uporaba črnega apnenca Drenov Grič

Črni karnijski (zg. trias) apnenec (GRAD & FERJANČIČ, 1968) velja za enega izmed najlepših slovenskih naravnih kamnov. Zaradi njegove velike gostote in doseganja visoke stopnje politure ga pogosto imenujejo s komercialnim imenom črni marmor. Znani so trije, sedaj opuščeni kamnolomi črnega apnenca iz Drenovega Griča, ki se nahajajo zahodno od Ljubljane: (i) najstarejši kamnolom, opuščen kmalu po 2. svetovni vojni, (ii) Kuclerjev kamnolom in (iii) Mineralov kamnolom (slika 1a). V kamnolomih se menjavajo različno debeli skladi kamnine, od nekaj 10 cm do 80 cm, redko celo do poldrugega metra, z večinoma tankimi polami laporovca (RAMOVŠ, 2000). Apnenec je mikriten z značilnimi belimi žilami (slika 1b), vsebuje bituminozno in organsko snov (RAMOVŠ, 2000; JARC, 2000; KRAMAR, 2010), ki je vzrok za njihovo črno barvo, kar velja tudi za podobne črne apnence po svetu (WINKLER, 1997; MARINONI in sod. 2007; MARSZAŁEK, 2007). Med fosili so za apnenec značilne školjke, polži, alge, luknjičarke, ostrakodi in korale (RAMOVŠ, 2000). Apnenec ima zelo majhno poroznost, majhno vpijanje vode in veliko trdnost (KRAMAR, 2010).

Uporaba črnega apnenca z Drenovega Griča naj bi se uveljavila v poznem 17. st., v kiparski modi je ostal tudi v 18. st. Zaradi njegove tipične barve so apnenec veliko uporabljali v baročni arhitekturi ne samo v Ljubljani, temveč tudi v drugih krajih po Sloveniji. Uporabljali so ga ugledni kamnoseški in kiparski mojstri, kot sta Mihael Cussa in Luka Mislej ter vrsta njunih sodobnikov v kamnoseški obrti (RAMOVŠ, 2000). Znani so portali in baročni oltarji, večinoma na območju Ljubljanskega barja in Polhograjskega hribovja. Iz omenjenega apnenca so bili izklesani tudi številni kropilniki ter pohodne plošče (RAMOVŠ, 2000). Široka uporaba črnih apnencev, predvsem v baročni arhitekturi, je znana tudi iz drugih krajev po Evropi (MARINONI in sod., 2002; ZEHNDER, 2003; ZEHNDER, 2006; MARINONI in sod., 2007; MARSZAŁEK, 2007).

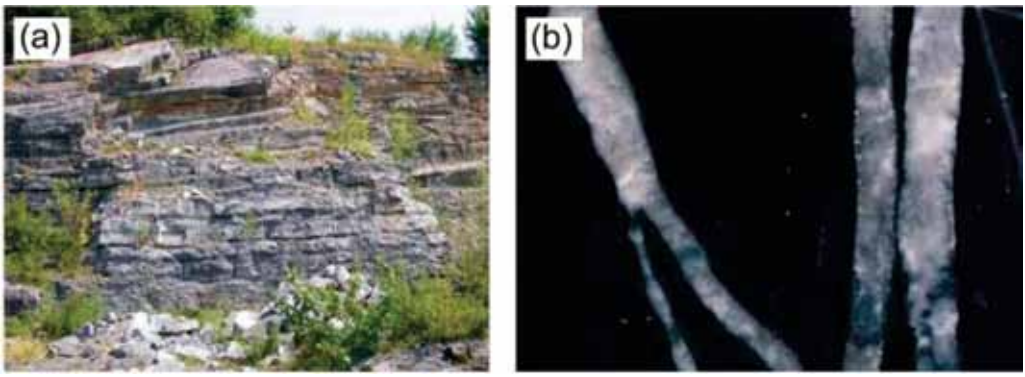

Slika 1. Črni apnenec Drenov Grič; a) opuščeni Mineralov kamnolom črnega apnenca; b) polirana površina črnega apnenca z belimi žilami (dolžina fotografije 4 cm)

Slika 2. Oltar v kapeli sv. Frančiška Ksaverja, Cerkev Sv. Jakoba, Ljubljana. EŠD 332; a) fotografija oltarja (foto: Valentin Benedik, fotodokumentacija ZVKDS, RC); b) prikaz delov oltarja s črnim apnencem iz Drenovega Griča (izris grafične podloge oltarja: Martin Kavčič, ZVKDS, RC). Sivi deli so apnenec Drenov Grič.

Iz črnega apnenca iz Drenovega Griča je izdelan tudi velik del kamnitega oltarja v kapeli sv. Frančiška Ksaverja v cerkvi Sv. Jakoba v Ljubljani (slika 2), kjer je bila v okviru konservatorsko-restavratorskih del izvedena dokumentacija oblik propadanja. Kamniti oltar je nastal v kamnoseški delavnici Franca Grumnika, kjer so delovali nekateri italijanski kiparji (Matthias Hendrichx, Paolo Gropelli, Jacopo Contieri, Angelo Putti) (DREŠAR in sod., 2005). Na podlagi litološkega kartiranja je bilo ugotovljeno, da oltar sestavljajo številne različne kamnine, izmed katerih prevladujejo sedimentne (apnenci in breče) ter metamorfne (marmor) (KRAMAR, 2006). Poleg kamnin slovenskega izvora so uporabljene tudi take, ki so najverjetneje tujega izvora.

Oblike propadanja črnega apnenca Drenov Grič

Oblike propadanja črnega apnenca z Drenovega Griča so določene na podlagi preiskave *in situ* na oltarju sv. Frančiška Ksaverja v cerkvi Sv. Jakoba. Oblike propadanja so bile dokumentirane po Fitzner-Heinrichsovi klasifikaciji (FITZNER & HEINRICHS, 2002). Primeri oblik propadanja so prikazani na slikah 3, 4, 5 in 6. Vse ugotovljene oblike propadanja so prikazane na grafičnih prilogah (priloge 1, 2, 3 in 4), iz katerih je razvidno, da so te značilno razporejene po oltarju. Največji obseg propadanja apnenca je vezan na spodnji del oltarja, medtem ko so površine apnenca v zgornjih predelih oltarja manj poškodovane. V spodnjem delu oltarja na propadanje apnenca močno vpliva vlaga v območju kapilarnega dviga, kjer se pojavljajo tudi topne soli. Posebno spodnji deli oltarja so močno poškodovani zaradi kristalizacije topnih soli, medtem ko je v zgornjih predelih prvotna črna barva apnenca obledela.

Po vrsti si na oltarju sledijo naslednje oblike propadanja črnega apnenca:

(1) Najpogostejše oblike propadanja, ki spadajo v skupino *Izgube materiala (priloga 1)* so odpadanje površinskih slojev kamnine, nastanek reliefa (zaobljevanje in dolbenje ter izluževanje komponent kamnine) in odlom. Predvsem v spodnjem delu oltarja se odpadanje površinskih slojev izraža še posebej pogosto v obliki odpadanja lusk ali drobcev kamnine.

Odpadanje površinskih slojev zajema odpadanje materiala vzporedno z izpostavljeno površino kamnine zaradi izgube kohezijske sile. Debelina plasti je odvisna od globine, v kateri je kamnina izgubila kohezijsko silo do take stopnje, da je površinska plast kamnine lahko odpadla.

Pri *odpadanju lusk* gre za enovito izgubo materiala v smeri vzporedno z izpostavljeno površino kamnine (slika 3a). Ta se na površini lušči in nato sloj

kamnine odpade, pri čemer je luščenje neodvisno od teksture kamnine. Vzroki so po navadi v zmanjšanju kohezijske sile pod slojem zaradi pritiskov, ki so nastali pod površino kamnine zaradi fizikalnega in kemičnega preperevanja kamnine, npr. kristalizacije soli, zaradi termohidričnega pritiska, zmrzali (Kramar, 2010). Pojav je sicer značilen predvsem za zrnate kamnine, kot so sedimentne kamnine, npr. peščenjaki in magmatske kamnine, npr. granodiorit (Fitzner in Heinrichs, 2002).

Pri *odpadanju kosov kamnine* gre za enovito izgubo materiala vzporedno z izpostavljeno površino kamnine (slika 3b). Kamnina se na površini drobi.

Pri *nastanku reliefa* gre za morfološke spremembe površine kamnine zaradi delnega ali izbirnega odpadanja materiala.

Zaobljevanje in dolbenje vključuje nastanek reliefa na izpostavljeni površini, ki je nastal zaradi zaobljevanja robov, kar imenujemo pozitivni relief. Lahko nastane tudi zaradi zarezovanja oz. dolbenja, kar imenujemo negativni relief (slika 3c). Nastajajo naključne mehke konkavne ali konveksne oblike. Na nastanek te oblike propadanja lahko vpliva geografska lega vgrajene kamnine, ki omogoča npr. stalno izpostavljenost vetru, osončenju, padavinam, kar povzroča ponavljajoče se ogrevanje/hlajenje in vlaženje/sušenje. Pojav je značilen za vse kamnine s homogeno teksturo.

Pri *izbirnem (selektivnem) odpadanju* nastaja izluževanje oz. raztapljanje manj obstojnih sestavin (glinene in laporнate leče, limonitne nodule itd.) ali pa izpadajo obstojnejše sestavine (prodniki, delci fosilov itd.) – negativni relief (slika 3č). S časom obstojnejše sestavine (prodniki, delci fosilov, konkrecije) vedno bolj izstopajo iz površine – nastaja pozitiven relief. Vzrok je v različni obstojnosti komponent zaradi razlike v sestavi. Pojav je značilen za kamnine, ki vsebujejo različno obstojne komponente (mineralna zrna ali večji skupki kamnine) in razne manj obstojne vključke (žile, razpoke, prodniki, leče), kot so apnenci in konglomerati.

Odlom pomeni odpadanje kompaktnih delov kamnine zaradi delovanja zunanje mehanske sile (slika 3d). Odlom dela kamnine nastane zaradi različnih vzrokov, kot je odlom zaradi antropoloških dejavnikov, odlom zaradi naravnih vzrokov, kot je rast višjih rastlin, potresov, prepleta razpok, ki zmanjšajo trdnost kamnine pod vrednost nosilne trdnosti, naravni pojavi z destruktivnimi posledicami, npr. rast višjih rastlin, potresi. Odlom lahko nastane tudi zaradi konstrukcijskih vzrokov. Le-ti so posledica nepravilnega načina vgrajevanja kamnitega segmenta, zaradi česar nastanejo napetosti, ki povzročijo

odlom kamnine (oksidacija kovinskih vezi v kamnitem objektu) (FITZNER & HEINRICHS, 2002). Nemalokrat pa povzročitelja ne moremo ugotoviti. Pojav ni odvisen od vrste kamnine.

(2) Sprememba barve, nevezane usedline soli ter obloge so najpogostejše oblike iz skupine *Usedanje materiala in sprememba barve* (priloga 2). Eflorescenca (kristalizacija soli na površini kamnine) in subflorescenca (kristalizacija soli pod površino kamnine) sta pogosti v spodnjem delu oltarja v območju kapilarnega dviga, v območju, kjer so bili kamniti elementi spojeni z malto ter ob stiku z zidom. Bele obloge so v večji meri predvsem v pasu na višini okoli 1 m od tal. Sprememba barve črnega apnenca je vidna predvsem v zgornjem delu oltarja.

Sprememba prvotne barve kamnine opisuje spremembe, ki se kažejo z variiranjem enega ali več parametrov, ki definirajo barvo. To so ton, čistost in kromatičnost. Sprememba se lahko pojavi na večjih površinah ali pa lokalno. Sprememba barve obravnavanega apnenca je opazna predvsem v zgornjih delih oltarja.

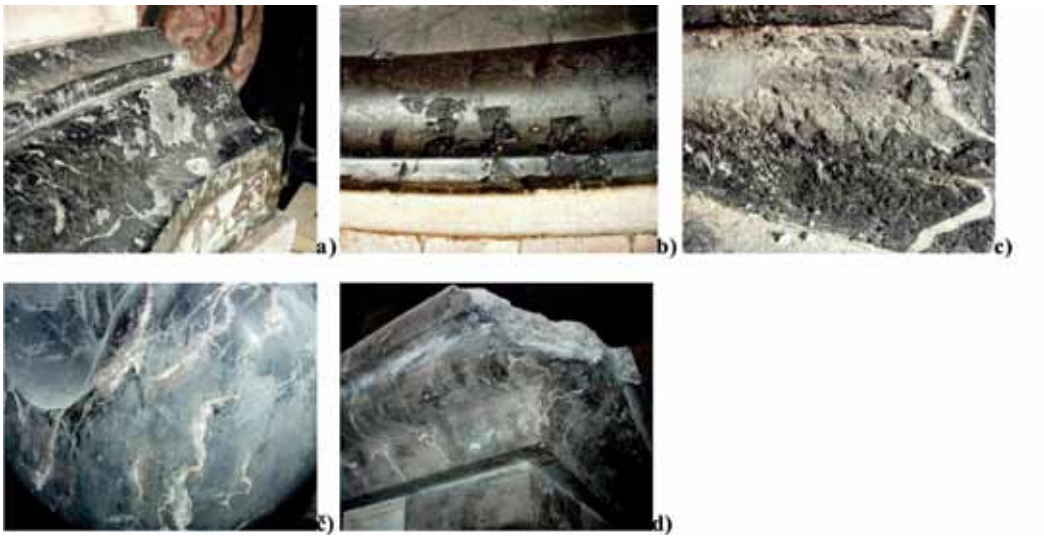

Slika 3. Oblike propadanja apnenca Drenov Grič iz skupine Izguba materiala: a) odpadanje lusk. Kristalizacija soli pod površino (subflorescenca) vodi do luščenja in posledično do izgube materiala zaradi odpadanja lusk (dolžina slike 20 cm). b) Izguba materiala zaradi odpadanja drobcev kamnine (dolžina slike 30 cm); c) zaobljevanje/dolbenje (dolžina slike 30 cm); č) izluževanje komponent zaradi izbirnega propadanja (dolžina slika 20 cm); d) odlom (dolžina slike 50 cm).

Razbarvanje (slika 4a) opisuje spremembo barve zaradi kemičnega preperevanja mineralov, ki vsebujejo barvajoče prvine (redukcija železovih in manganovih komponent, oksidacija organske snovi) ali izločanja barvajoče snovi (izluževanje, izpiranje). Razbarvanje se pojavi tudi zaradi nastanka razpok na površini kamnine (izguba kohezije med zrni) oz. zaradi povečanja specifične površine zrn, ki sestavljajo kamnino, kar ima za posledico drugačno sipanje svetlobe (Zehnder, 2006). Razbarvanje se pojavi tudi, če se na površini ali po razpokah nalagajo sekundarni brezbarvni minerali. Vzroki za nastanek pojava sta lahko tako kemično kot fizikalno preperevanje kamnin. Pojav razbarvanja nastaja pri preperevanju barvastih kamnin, kjer nastaja redukcija železovih in manganovih spojin, medtem ko je razbarvanje zaradi nastanka razpok in zaradi nalaganja brezbarvnih sekundarnih mineralov na površini kamnine značilno za vse vrste kamnin. Pojav pri obravnavanem apnencu pripisujemo dekoheziji med zrni v površinskih delih apnenca, kar je bilo ugotovljeno z elektronskim mikroskopom (Kramar, 2010). Na nekaterih področjih oltarja je sprememba barve vezana na nastanek tanke plasti sadre na površini apnenca (Kramar, 2010). Marinoni (2007) navaja, da je dekohezija med zrni in s tem večja poroznost na površini apnenca rezultat termičnega propadanja, ki se nato kaže v razbarvanju črnega apnenca. Zadnji navedeni mehanizem je predlagal tudi Zehnder (2003), medtem ko nekateri drugi raziskovalci razbarvanje črnega apnenca pripisujejo oksidaciji organske snovi, saj naj bi bili ogljikovodiki eden izmed manj stabilnih pigmentov (Winkler, 1997).

Nevezane usedline soli so slabo vezane usedline zrn (delcev) soli, ki imajo svoj izvir v kamnini. Soli, ki bodo kristalizirale na površini apnenca kot eflorescenca, so odvisne od sestave raztopine soli, lastnosti podlage (površina apnenca) in okoljskih razmer med procesom kristalizacije (Bläuer-Böhm in sod., 2001). Pri oltarju je pojav eflorescence vezan na spodnjih 0,5 m višine, kar je razvidno s priloge 2.

Pri *eflorescenci* se na površini kamnine koncentrirajo drobnozrnate (kristalne ali amorfne) snovi, ki so navadno belkaste barve (slika 4b). Pri kristalizaciji soli se sestavine izlužujejo iz kamnine zaradi kemičnega preperevanja kamnine. Pojav je značilen za kamnine, ki vsebujejo minerale, topne v vodni raztopini. Lahko pa soli v kamnino prihajajo tudi iz okolice (tla, omet). Vse kamnine so bolj ali manj porozne, zato je mogoč transport soli po kamnini. Po drugi strani pojav eflorescence omogoča majhna poroznost preiskovanih apnencev, saj le-te po navadi nastajajo na gostih površinah (Arnold

& KUENG, 1985). Prisotnost vlaknate oblike topnih soli (angl.: whiskers) na površini preiskovanih apnencev izraža bodisi rahlo vlažno do skoraj suho površino apnencev, zelo omejen vir vode ali pa majhno hitrost evaporacije v primerjavi z nastankom oblog, ki zahtevajo veliko zalogo raztopine (ZEHNDER & ARNOLD, 1989). Eflorescenco na apnencu Drenov Grič sestavljajo sadra in magnezijevi sulfat hidrati (KRAMAR, 2010). Transport soli na površino apnencev poteka v fazi močenja, medtem ko v fazi sušenja soli kristalizirajo na površini. Vsako zmanjšanje relativne vlage v prostoru bo povzročilo, da bodo raztopljene soli potovale proti površini kamnine, kjer površinska voda izhlapeva in tako kompenzira spremembe v relativni vlažnosti okolja (COLSTON in sod., 2001).

Pri *subflorescenci* nastane kristalizacija soli v porah pod površino (slika 4c). Pojav vodi do odstopanja površinskih delov kamnine. Vzrok je kristalizacija topnih soli, ki se izlužujejo iz kamnine zaradi njenega kemičnega preperevanja kamnine. Soli lahko v kamnino prihajajo tudi iz okolice (tla, omet). V odvisnosti od atmosferske vlage se lahko izločajo na površini ali v kamnini. Porazdelitev topnih soli na objektu je odvisna od vrste soli v raztopini in od njihovega izvora (CHAROLA, 2000). Soli se načeloma koncentrirajo na področjih, ki zadržujejo vlago dlje časa. To območje se po navadi nahaja 1–5 cm pod površino in je odvisno predvsem od poroznosti kamnine (CHAROLA, 2000). Pri apnencu z Drenovega Griča je to območje omejeno le na nekaj zgornjih kvadratnih milimetrov površine, verjetno zaradi njegove majhne poroznosti. Na tem območju nastajajo mehanski pritiski, ki vodijo do nastanka površinskih lusk in s tem razpada apnenca. Zaradi majhne poroznosti apnenca se voda laže zadržuje v kapilarah, saj je gibanje vode oteženo, s površine apnencev pa je omogočena hitrejša evaporacija (AMOROSO & FASSINA, 1983). Kristalizacija soli onemogoči reverzibilno dilatacijo apnenca, kar se pri preiskovanih apnencih izraža v obliki luščenja in drobljenja. Kristalizacija sadre (KRAMAR, 2010) pod površino (subflorescenca) vodi do razpada apnenca, kar se izraža v obliki luščenja in drobljenja ter s tem izgube materiala. Ko kristali sadre presežejo velikost pore, nastanejo pritiski, ki so lahko večji od natezne trdnosti preiskovanih apnencev. Mehanizmi propadanja zaradi kristalizacije soli temeljijo namreč na nastanku pritiskov na pore kamnine, ko sol kristalí pri ponavljajočih se ciklih kristalizacije/raztapljanja soli. Kristali sadre dokazujejo, da je hitrost evaporacije večja od dovajanja vode v območju oltarja, kjer nastaja intenzivno luščenje. Medtem ko so v spodnjem delu soli na površini kamnine, se v zgornjem delu nahajajo pod površino. Iz tega sklepamo, da se razmerje evaporacija/transfer vode spreminja v odvisnosti od višine. Sadra zunaj dosega kapilarnega dviga

nakazuje na možnost transferja raztopine tudi z drugimi mehanizmi, kot je npr. kondenzacija. Pri relativni vlažnosti nad 75 % je namreč omogočena površinska penetracija s kapilarno sukcijo in kristalizacijo sadre v porah in razpokah pod površino kamnine (Chabas & Jeanette, 2001). Ko petrofizikalne lastnosti kamnine omogočajo hiter in dolg transfer vode, po drugi strani pa poroznost kamnine kot druga petrofizikalna lastnost kamnine omogoča, da je dotok vode enak količini vode, ki je odparela, soli kristalijo na površini. Eflorescenca v tem primeru ne povzroča dekohezije kamnine na površini objekta. Po drugi strani v primerih, ko odpari večja količina vode, kot je s kapilarnim dvigom migrira v površinsko plast kamnine, soli precipitirajo v kamnini pod površino, kar vodi do izgube materiala na površini (Lewin, 1982; Chabas & Jeanette 2001). Zniževanje relativne vlažnosti močno vpliva na propadanje, kombinacija nizke relativne vlažnosti in daljšega sušnega obdobja pa povzroča nastanek večjih poškodb (Colston in sod., 2001). Pri spremljanju nihanja temperature (T) in relativne vlažnosti (RH) v kapeli ugotavljamo, da v obdobju enega leta RH variira od 40 % do 100 %, medtem ko se T giblje v območju od –0,6 °C do 28,1 °C (Kolenc, 2006).

Obloge so kompaktne usedline, močno vezane na površino kamnine, imajo lahko svoj izvir v kamnini ali prihajajo kot polutanti iz okolja. Obloge se pojavljajo v pasu oltarja okoli 1,5 m nad tlemi (priloga 2).

Obloga, ki sledi površini kamnine, je kompaktna usedlina (slika 4č). Lahko je različnih barv, npr. črna, siva, bela ali rjava. Kompaktiranje usedline so omogočile soli, ki so se izluževale iz kamnine ali so se obarjale iz vode, ki je prinašala raztopljene soli iz zunanjega okolja – kemično preperevanje. Večinoma nastanejo zaradi procesov precipitacije brezbarvnih sekundarnih mineralov kalcita ali kremenice in drugih soli. Vzroki so polutanti iz atmosfere, interakcija polutantov s kamnino, izluževanje soli (npr. sadre) iz kamnine, obarjanje kalcita iz vode pri vodnjakih, ki vsebuje raztopljene minerale. Pojav načeloma ni odvisen od vrste kamnine, čeprav ga lahko favorizirajo kamnine, ki vsebujejo v vodi topne minerale. Lahko so v stiku z vodo, ki vsebuje raztopljene brezbarvne soli, oz. so v stiku z vodo, ki vsebuje raztopljene barvaste soli. Bele obloge na črnem apnencu, ki jih tvori sadra, se pojavljajo v pasu v spodnjem delu oltarja. Ker obloge nastajajo na mestih, kjer je substrat vlažen ali moker (Arnold & Zehnder, 1985), nakazujejo območja na oltarju, v katerih se v kamnini zadržuje več vode. Nekatere obloge sestavlja več vzporednih plasti sadre, ki izražajo ritmično kristalizacijo sadre iz raztopine zaradi ponavljajočih se ugodnih razmer za kristalizacijo (nasičenje, temperatura).

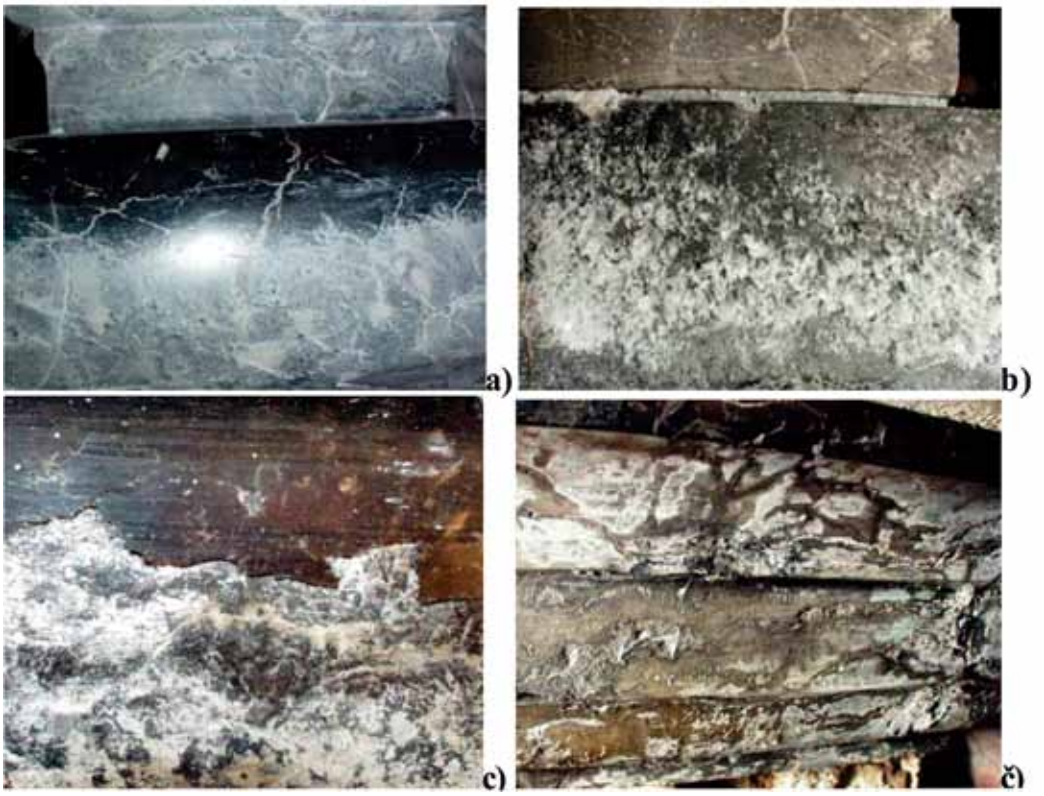

Slika 4. Oblike propadanja apnenca Drenov Grič iz skupine Usedanje materiala in sprememba barve: a) Razbarvanje – sprememba prvotne črne barve v siv odtenek (dolžina slike 30 cm); b) eflorescenca-kristalizacija soli na površini (dolžina slike 30 cm); c) subflorescenca-kristalizacija soli pod površino, ki vodi do luščenja apnenca (dolžina slike 10 cm); č) bela obloga na povšini apnenca (dolžina slike 20 cm)

(3) Drobljenje, luščenje in cepljenje so najpogostejše oblike propadanja v skupini *Odstopanje materiala*. V odvisnosti od orientacije plastnatosti apnenca, vgrajenega v spomenik, je odstopanje bodisi izraženo kot cepljenje (ni vzporedno izpostavljeni površini) ali kot luščenje (vzporedno površini apnenca). Luščenje je stopnja propadanja apnenca pred odpadanjem materiala, še prej pa se pojavijo razpoke, ki so posledica ekspanzije zaradi kristalizacije soli pod površino. Odpadanje materiala je zadnja faza propadanja, ki sledi po luščenju kamnine. Najbolj intenzivno luščenje se pojavlja okoli 0,5 m od tal, čeprav je v manjši meri po vsem oltarju. V tem območju oltarja so po površini apnenca razpoke, ki so posledica kristalizacije soli pod površino preiskovanega apnenca.

Drobljenje zajema odstopanje večjih kosov kamnine nepravilnih oblik, ki mu kasneje sledi odpadanje.

Drobljenju so izpostavljene kamnine z izrazito nehomogeno sestavo. Odpadli kosi, ki jih sestavlja nespremenjen material, so trdi in nepravilnih oblik. Degradacija se kaže z delnim ali popolnim odstopanjem. Vzroki so v fizikalnem preperevanju kamnin z nehomogeno strukturo. Največkrat nastane razpad zaradi zmrzovanja vzdolž manj odpornih plasti in v območju kapilarnih por. Pojav je značilen za zrnate kamnine karbonatnega in silikatnega izvora. Drobljenje in posledično izguba materiala je pri apnencu Drenov Grič vezana na žile, ki so zapolnjene s filosilikati. Minerali glin lahko nabrekajo, kar lahko vodi do nepovratnega razpada kamnine. Soli se nahajajo na območjih, ki zadržujejo vlago dlje, tako lahko ti minerali glin povzročijo razpad kamnine tudi zaradi kristalizacije soli. Izmenično nabrekanje in krčenje glin lahko prav tako prispevata k drobljenju apnencev (Rodríguez-Navarro in sod., 1998). Transport vode je zaradi majhne poroznosti apnencev zmanjšan, kar ima za posledico večjo hitrost evaporacije s površine kamnine v primerjavi s hitrostjo kapilarnega dviga. Takšno območje je zato mehansko obremenjeno in vodi do razpada apnencev. Kristalizacijski pritiski topnih soli so mnogo večji od natezne trdnosti preiskovanih apnencev.

Luščenje zajema odstopanje majhnih, tankih kosov kamnine (lusk) neodvisno od njene teksture. Luščenje se pojavlja v pasu okoli 0,5 m nad tlemi, v manjši meri tudi mestoma po celotni površini oltarja.

Posamezne luske – *enoplastno luščenje* pomeni odstopanje ene plasti v obliki posameznih lusk, ki se kasneje odluščijo od nespremenjene kamnine. Vzroki so v fizikalnem ali kemičnem preperevanju kamnine, ki povzroči, da popusti kohezijska sila tanke površinske plasti kamnine. Pojav je sicer značilen za drobnozrnate goste kamnine.

Cepljenje (lamelarno odstopanje) opisuje odstopanje slojev kamnine, ki ni vzporedno s površino kamnine (slika 5b). Odstopanju kasneje sledi odpadanje slojev kamnine. Vzroki so v fizikalnem preperevanju kamnine, zaradi česar odstopajo sloji kamnine po ravninah foliacije, plastnatosti, laminarnosti. Značilno je za plastnate in laminirane kamnine ter kamnine z izraženo foliacijo, npr. peščenjake.

(4) Oblike propadanja četrte skupine, to so *razpoke in deformacije*, so zastopane z zlomi, ki so na nekaterih kamnitih elementih, ki delijo kamnit element na dva dela (mehanska poškodba).

Zlomi nastajajo v primeru, ko zaradi razpok nastane delitve kamnine na dva ali več delov. Vzroki za nastanek zlo-

mov so fizikalne narave, ko je mehanska sila, ki deluje na kamnino, večja od kohezijske sile kamnine. Razpoka je tako velika, da kamnina razpade na več ločenih delov. Pojav ni odvisen od vrste kamnine.

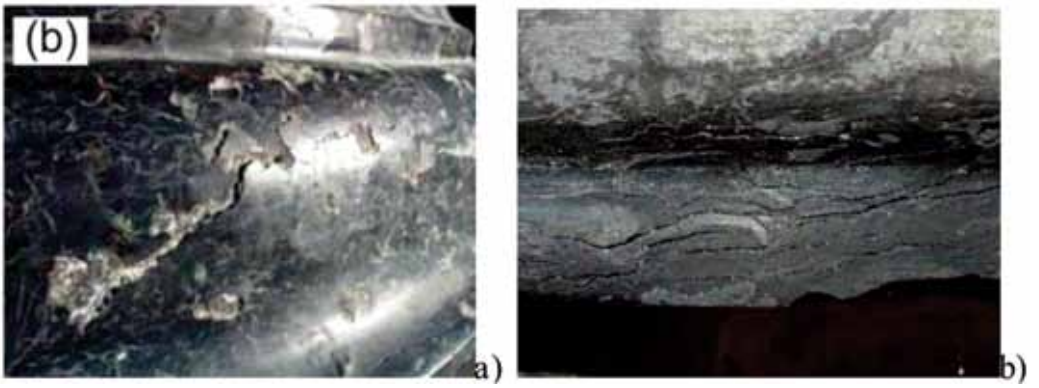

Slika 5. Oblike propadanja apnenca Drenov Grič iz skupine Odstopanje materiala: a) luščenje apnenca (dolžina slike 10 cm); b) cepljenje apnenca (dolžina slike 5 cm)

Slika 6. Oblike propadanja apnenca Drenov Grič iz skupine Razpoke in deformacije: a) razpoke, neodvisne od teksture kamnine (dolžina slike 100 cm)

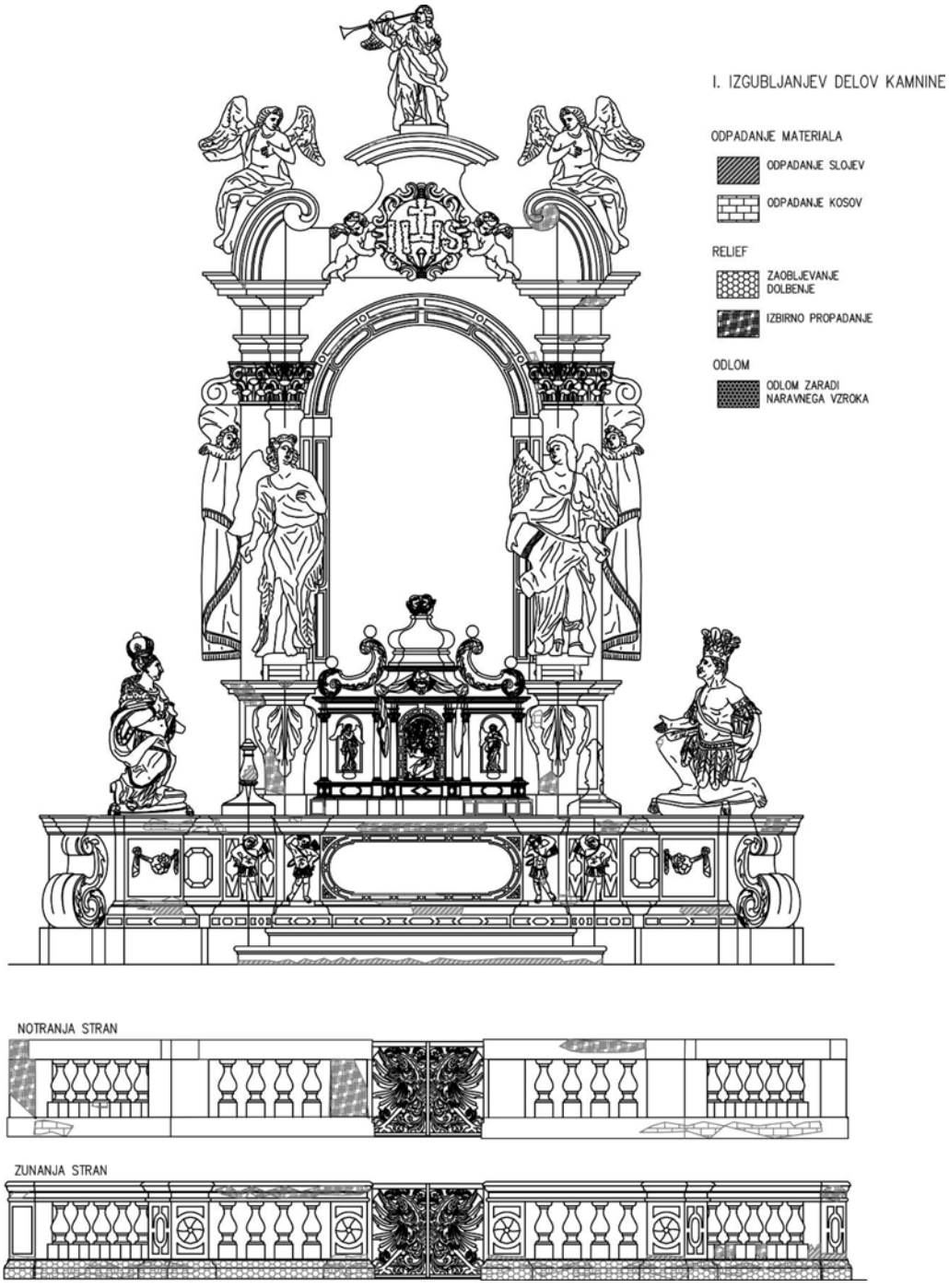

Priloga 1. Karta oblik propadanja v skupini Izguba materiala

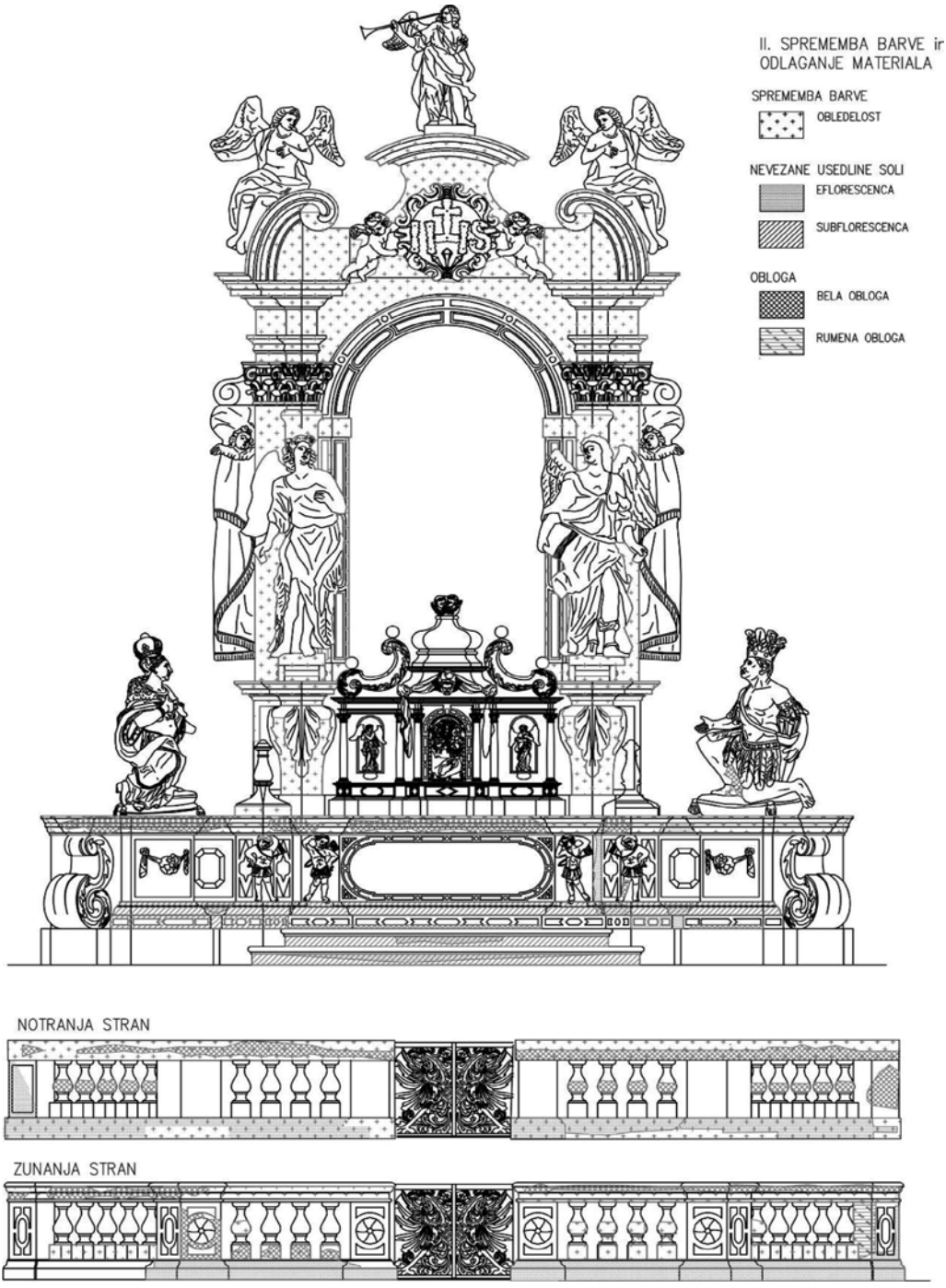

Priloga 2. Karta oblik propadanja v skupini Sprememba barve in odlaganje materiala

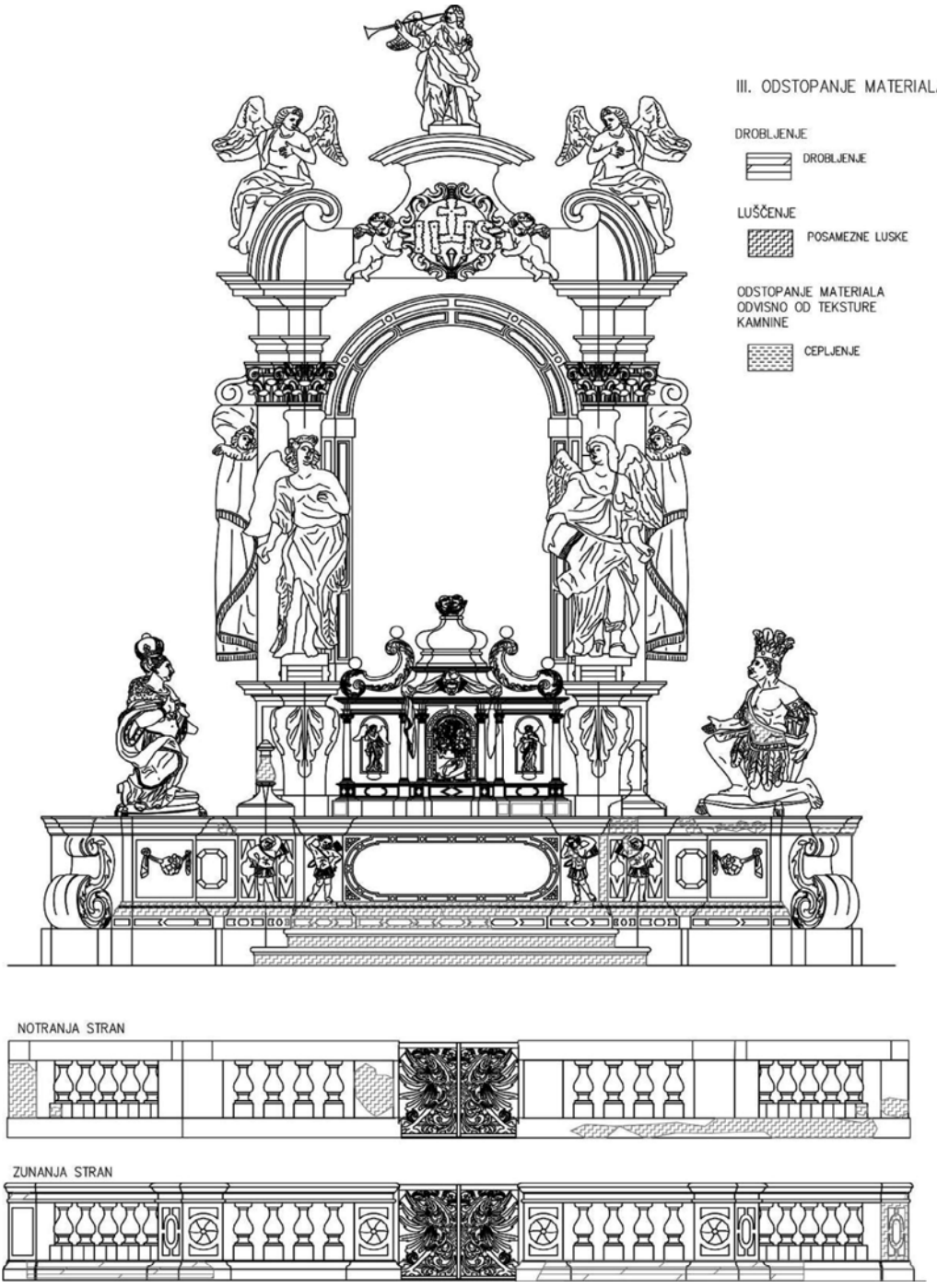

Priloga 3. Karta oblik propadanja skupine Odstopanje materiala

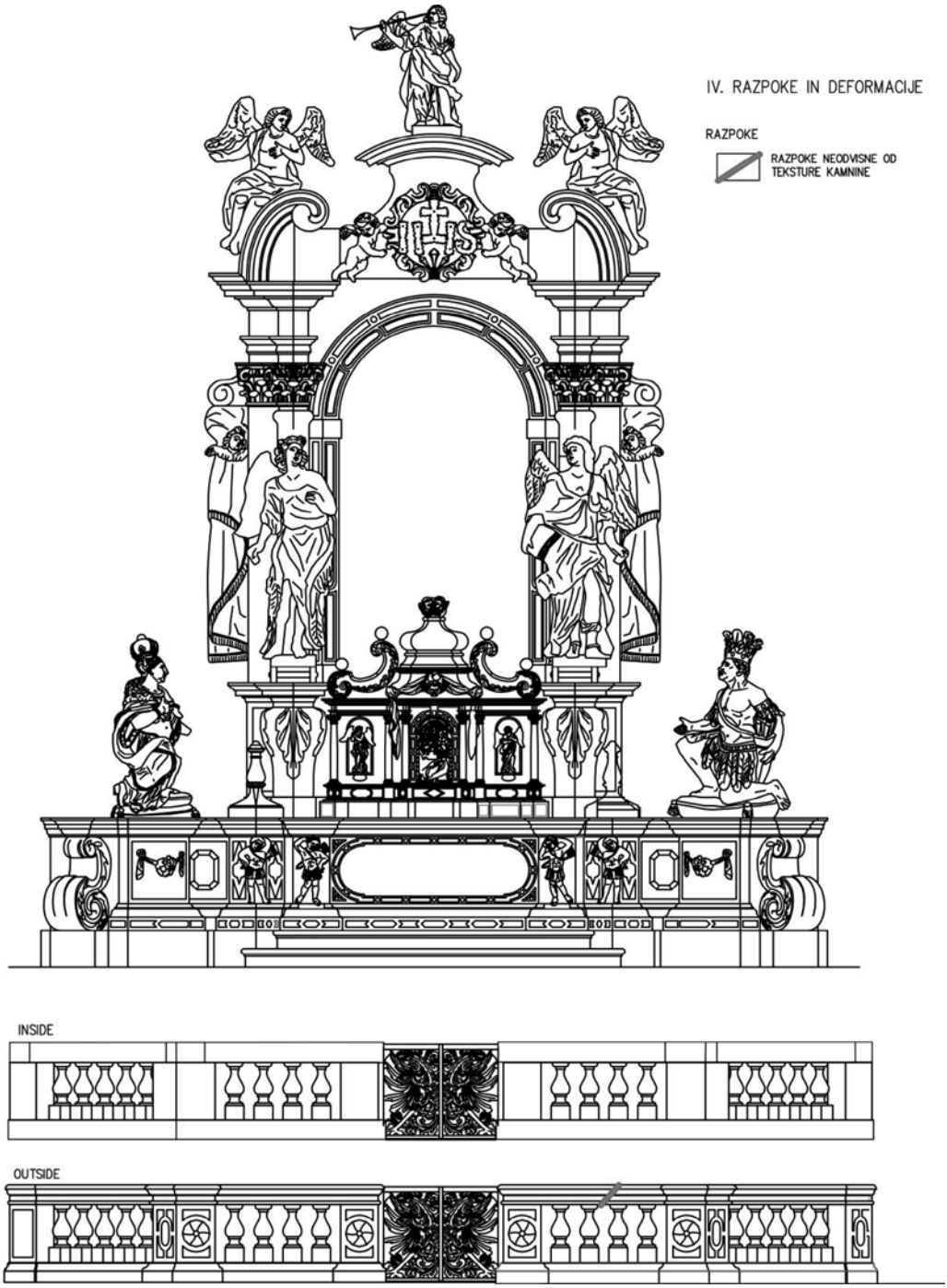

Priloga 4. Razpoke in deformacije

Sklepi

Izčrpne raziskave o vzrokih in mehanizmih propadanja naravnega kamna so ključnega pomena na področju ohranjanja objektov kulturne dediščine. Dokumentiranje makroskopskih sprememb oziroma karakterizacija, kvantifikacija in interpretacija oblik propadanja naravnega kamna na določenem objektu je eden osnovnih korakov pred restavratorsko-konservatorskim posegom. V prispevku je podan pregled skupin in glavnih oblik propadanja naravnega kamna, ki je prirejen po nemški klasifikacijski shemi, na podlagi katere klasificiramo posamezne oblike propadanja. Prikaz določanja oblik propadanja naravnega kamna na objektih kulturne dediščine in grafična prestavitev le-teh sta podana na primeru črnega apnenca Drenov Grič.

Kot je razvidno z grafičnih prilog, so oblike propadanja značilno razporejene po oltarju. Največji obseg propadanja apnenca je vezan na spodnji del oltarja, medtem ko so površine apnenca v zgornjih predelih oltarja manj poškodovane. Prepoznanih je bilo veliko različnih oblik propadanja v skupini izgube materiala, razbarvanja/odlaganja, odstopanja materiala ter razpok/deformacij.

Glavni dejavnik propadanja je kristalizacija topnih soli, ki ima za posledico številne različne oblike propadanja apnenca. Zaradi različnih okoljskih dejavnikov se soli pojavljajo v več oblikah, in sicer kot eflorescenca, subflorescenca ali kompaktna obloga. Glavni vzrok propadanja je lahko kapilarni dvig in posledično kristalizacija topnih soli. Največja poškodovanost kamnine je bila identificirana prav v območju kapilarnega dviga. Raztopine soli potujejo skozi kamnino s kapilarnim dvigom, nato pa ob evaporaciji kristalizirajo bodisi na površini ali pod površino apnencev. Obloge so vezane na vlažnejše predele oltarja.

Zahvale

Raziskavo je finančno omogočil ARRS; številka pogodbe 3211-05-000545. Avtorici se zahvaljujeta g. Jožetu Drešarju, ki je omogočil preiskave oblik propadanja na oltarju v kapeli Sv. Frančiška Ksaverja, kjer pod njegovim vodstvom potekajo konservatorsko-restavratorska dela.

Viri

Amoroso, G. G. & Fassina, V. (1983): Stone decay and conservation, Amsterdam. *Elsevier Science Publisher*, 453 str.

Arnold, A. & Kueng, A. (1985): Crystallization and habits of salt efflorescences on walls, I., Methods of investigation and habits. V

Proceedings of 5th International Congress on Deterioration and Conservation of Stone. Editor G. Felix. Laussane: Presses Polytechniques et Universitaires Remandes, str. 255–267.

ARNOLD, A. & ZEHNDER, K. (1988): Decay of stony materials by salts in humid atmosphere. V Proceeding of 6th International Congress on the Deterioration and Conservation of Stone. Editor J. Ciabach. Torun: Nicolas Copernicus University Press Department, str. 138–148.

BILBIJA, N. & GRIMŠIČAR, A. (1987): Obstojnost arhitektonskega naravnega kamna iz Slovenije. *Geološki zbornik*; št. 8, str. 151–160

BLÄUER-BÖHM, C., KÜNG, A. & ZEHNDER, K. (2001): Salt Crystal Intergrowth in Efflorescence on Historic Buildings. *Chimia*, Vol. 55, str. 996–1001.

CHABAS, A. & JEANETTE, D. (2001): Weathering of marbles and granites in marine environment: petrophysical properties and special role of atmospheric salts. *Environmental Geology*; Vol. 40, str. 359–368.

CHAROLA, E. A. (2000): Salts in the deterioration of porous materials: an overview. *Journal of the Institute of American Conservators*; Vol. 39, str. 327–343.

COLSTON, B. J., WATT, D. S. & MUNRO, H. L. (2001): Environmentally-induced stone decay: the cumulative effects of crystallization-hydration cycles on a Lincolnshire oopelsparite limestone. *Journal of Cultural Heritage*; Vol. 4, str. 297–307.

DREŠAR, J., KLAJDER, M., HIRCI, B. (2005): Restavratorski projekt za obnovo kapele Sv. Frančiška Ksaverja, Ljubljana, Cerkev Sv. Jakoba. Ljubljana: Restavratorski center, 12. str.

FITZNER, B. & HEINRICHS, K. (2002): Damage diagnosis on stone monuments - weathering forms, damage categories and damage indices. V Understanding and managing stone decay, Proceeding of the International Conference "Stone weathering and atmospheric pollution network (SWAPNET 2001)". Editors R. Prikřyl in H. A. Viles. Charles University in Prague: The Karolinum Press, 2002, str. 11–56.

FITZNER, B., HEINRICHS, K. & LA BOUCHARDIERE, D. (2002): Limestone weathering of historical monuments in Cairo, Egypt. V Natural stone, weathering phenomena, conservation strategies and case studies. Editors S. Siegesmund, T. Weiss, in A. Vollbrecht. *Geological Society*; Special Publication, Vol. 205, str. 217–239.

FITZNER, B., HEINRICHS, K. & LA BOUCHARDIERE, D. (2003): Weathering damage on Pharaonic sandstone monuments in Luxor-Egyt. Building and Environment, Vol. 38, str. 1089–1103.

FITZNER, B. & HEINRICHS, K. (2004): Photo atlas of weathering forms on stone monuments. http://www.stone.rwth-aachen.de

FITZNER, B. (2004): Documentation and evaluation of stone damage on monuments. V Proceedings of the 10th International congress on

deterioration and conservation of stone. Editors D. Kwiatkowski in R. Löfvendahl. Stockholm: ICOMOS; str. 677–690.

Fitzner, B., Heinrichs, K. & La Bouchardiere, D. (2004): The Bangudae Petroglyph in Ulsan, Korea: studies on weathering damage and risk prognosis. *Environmental Geology*; Vol. 46, str. 504–526.

Grad, K. & Ferjančič, L. (1968): Osnovna geološka karta. Tolmač za list Kranj. L33–65. Socialistična Federativna Republika Joguslavija. Geološki zavod Ljubljana.

Jarc, S. (2000): Vrednotenje kemične in mineralne sestave apnencev kot naravnega kamna: magistrsko delo. Ljubljana, 88 str.

Kolenc, I. (2006): Sv. Jakob, Prikaz meritev temperature in vlage. Ljubljana : *Restavratorski center*.

Kramar, S. (2006): „Cerkev Sv. Jakoba" Kapela Sv. Frančiška Ksaverja: mnenje o vrsti in izvoru kamnin. Ljubljana: ZVKDS, *Restavratorski center*, 12 str.

Kramar, S. (2010): Vrednotenje apnencev z vidika vpliva okoljskih dejavnikov na njihovo propadanje: doktorska disertacija. Ljubljana, 119 str.

Lewin SZ. (1982): The Mechanism of Masonry Decay through Crystallization. V Conservation of Historic Stone Buildings and Monuments. Editro N. S. Baer. Washington DC: National Academic Press, str. 120–144.

Marinoni, N., Pavese, A., Bugini, R. & DI SILVESTRO, G. (2002): Black limestone used in Lombard architecture. *Journal of Cultural Heritage*; Vol. 3, str. 241–249.

Marinoni, N., Pavese, A., Riva, A, Cella, F. & Cerulli, T. (2007): Chromatic weathering of black limestone quarried in Varenna (Lake Como, Italy). Building and Environment, Vol. 42, str. 68–77.

Marszałek, M. (2007): The mineralogical and chemical methods in investigations of decay of the Devonian Black »marble« from Dębnik (Southern Poland). V Building Stone Decay: From Diagnosis to Conservation. Editors R. Přikryl in B. J. Smith. London: Geological Society, Special Publications 2007, Vol. 271, str. 109–115.

Ramovš, A. (2000): Podpeški in črni ter pisani lesnobrdski apnenec skozi čas. *Mineral*; 115 str.

Rodríguez-Navarro, C., Sebastian, E., Doehne, E. & Ginell, W. S. (1998): The role of sepiolite-palygorskite in the decay of ancient Egyptian limestone sculptures. *Clays and Clay Minerals*; Vol. 46, str. 414–422.

Rothert, E., Eggeers, T., Cassar, J., Ruedrich, J., Fitzner, B. & Siegsmund, S. (2007): Stone properties and weathering induced by salt crystallization of Maltese Globigerina Limestone. V Building Stone Decay: From Diagnosis to Conservation. Editors R. Přikryl in B. J. Smith. London: Geological Society. Special Publications; Vol. 271, str. 189–198.

Zehnder, K. & Arnold, A. (1989): Crystal growth in salt efflorescence. *Jour-*

nal of Crystal Growth; Vol. 8, str. 513–521.

ZEHNDER, K. (2003): Grey veils on black polished limestones-nature and conservation concepts, V EUROMAT, Symposium P2 – Materials and Conservation of Cultural Heritage. Lausanne: EPFL.

ZEHNDER, K. (2006): Greying of black polished limestone – a case study to clarify the phenomenon. Zeitschrift fur Kunsttechnologie und Konservirung, Vol. 2, str. 361–367.

WINKLER, E. M. (1997): Stone in Architecture: Properties, Durability. Berlin: *Springer*; 313 str.

UNI 11182:2006, Beni culturali - Materiali lapidei naturali ed artificiali - Descrizione della forma di alterazione - Termini e definizioni, Sostituisce NORMAL 1/88, 1988.

Illustrated glossary on stone deterioration patterns, ICOMOS-ISC: 2008.

Author`s Index, Vol. 57, No. 4

Fazarinc Matevž	matevz.fazarinc@omm.ntf.uni-lj.si
Gandova V.	
Gregorič Asta	asta.gregoric@ijs.si
Grządziel Dominik	
Kochowska Elzbieta	
Kozak Krzysztof	
Kramar Sabina	sabina.kramar@rescen.si
Krušič Vid	vid.krusic@iskra-ae.com
Kugler Goran	goran.kugler@omm.ntf.uni-lj.si
Lavtar Lejla	lavtar@steel.si
Mazur Jadwiga	
Mirtič Breda	breda.mirtic@guest.arnes.si
Olugbenga A. Okunlola	gbengaokunlola@yahoo.co.uk
Oluwatoyin O. Akinola	
Rogan Šmuc Nastja	nastja.rogan@guest.arnes.si
Romanowska J.	
Rotimi Oluwatosin John	orotimi@covenantuniversity.com
Terčelj Milan	milan.tercelj@omm.ntf.uni-lj.si
Vassilev G.	gpvassilev@gmail.com
Vaupotič Janja	janja.vaupotic@ijs.si

Author`s Index, Vol. 57

Adeyeye Ademola David	ademola.adeyeye@mail.ui.edu.ng
Antić Aco	
Barbič Rok	
Bisht Sandeep	
Bombač David	david.bombac@omm.ntf.uni-lj.si
Bratun Julijan	julijan.bratun@e-cono.si
Breda Mirtič	breda.mirtic@guest.arnes.si
Budak Igor	
Choubey V. K.	
Čekada Miha	miha.cekada@ijs.si
Denić Miodrag	miodrag.denic@yahoo.com
Dervarič Evgen	evgen.dervaric@ntf.uni-lj.si
Dolenec Matej	matej.dolenec@ntf.uni-lj.si
Dolenec Tadej	tadej.dolenec@ntf.uni-lj.si
Đukanović Duško	ugaljprojekt@sezampro.rs
Fajfar Peter	peter.fajfar@omm.ntf.uni-lj.si
Fazarinc Matevž	matevz.fazarinc@omm.ntf.uni-lj.si
Ganatea Marco Francesco	
Gandova V.	
Giavazzi Silvia	
Gregorič Asta	asta.gregoric@ijs.si
Grządziel Dominik	
Gusain Manju P.	
Gusain Om P.	
Helmut Pristacz	
Klančnik Grega	grega.klancnik@omm.ntf.uni-lj.si
Klenovšek Bojan	bojan.klenovsek@rth.si
Kniewald Goran	kniewald@irb.hr
Kochowska Elzbieta	
Kortnik Jože	joze.kortnik@ntf.uni-lj.si

Kosec Borut	borut.kosec@omm.ntf.uni-lj.si
Kosec Gorazd	
Kovačič Miha	miha.kovacic@store-steel.si
Kozak Krzysztof	
Kozamernik Mitja	
Kramar Sabina	sabina.kramar@rescen.si
Krušič Vid	vid.krusic@iskra-ae.com
Kugler Goran	goran.kugler@omm.ntf.uni-lj.si
Kumar Bhism	
Kumar Vivek	
Lajlar Bojan	bojan.lajlar@rlv.si
Lambaša Belak Živana	
Lavtar Lejla	lavtar@steel.si
Likar Jakob	jakob.likar@ntf.uni-lj.si
Lojen Sonja	sonja.lojen@ijs.si
Macuh Borut	borut.macuh@uni-mb.si
Malenković Vladimir	vladimir.malenkovic@rlv.si
Malina Jadranka	
Markoli Boštjan	bostjan.markoli@ntf.uni-lj.s
Mauko Alenka	
Mazur Jadwiga	
Medved Jožef	jozef.medved@ntf.uni-lj.si
Medved Milan	milan.medved@rlv.si
Mirtič Breda	breda.mirtic@guest.arnes.si
Mladenović Ana	ana.mladenovic@zag.si
Mrvar Primož	primoz.mrvar@ntf.uni-lj.si
Nagode Aleš	
Olarewaju, V. O.	
Olorunfemi, A. O.	
Olugbenga A. Okunlola	gbengaokunlola@yahoo.co.uk
Oluwatoyin O. Akinola	
Oyawale Festus Adekunle	

Pandey Piyush	
Panjan Matjaž	matjaz.panjan@ijs.si
Panjan Peter	peter.panjan@ijs.si
Petrović David	
Placer Ladislav	
Purandara B. K.	purandarabk@yahoo.com
Rađenović Ankica	
Rodič Tomaž	tomaz.rodic@ntf.uni-lj.si
Rogan Šmuc Nastja	nastja.rogan@guest.arnes.si
Romanowska J.	
Rotimi Oluwatosin John	orotimi@covenantuniversity.com
Senčič Sandra	sandra.sencic@kova.si
SHARMA PUNAM	
Sharma Shivesh	
Smolej Anton	anton.smolej@ntf.uni-lj.si
Sood Anchal	
Šmuc Andrej	andrej.smuc@ntf.uni-lj.si
Štrkalj Anita	strkalj@simet.hr
Šuštarič Primož	
Terčelj Milan	milan.tercelj@omm.ntf.uni-lj.si
Trkov Mitja	
Urošević Maja	
Varadarajan N.	nvarad@yahoo.com
Vassilev G.	gpvassilev@gmail.com
Vaupotič Janja	janja.vaupotic@ijs.si
Venkatesh B.	
Vodopija Josip	
Vončina Maja	maja.voncina@ntf.uni-lj.si
Vukelič Željko	zeljko.vukelic@ntf.uni-lj.si
Vukelić Željko	zeljko.vukelic@ntf.uni-.si
Žlender Bojan	bojan.zlender@uni-mb.si
Žvab Petra	petra.zvab@guest.arnes.si

RMZ MATERIALS AND GEOENVIRONMENT
Contents
Volume 57, 2010/1, 2, 3, 4

57/1

57/2

57/3

INSTRUCTIONS TO AUTHORS

RMZ-MATERIALS & GEOENVIRONMENT (RMZ- Materiali in geookolje) is a periodical publication with four issues per year (established 1952 and renamed to RMZ-M&G in 1998). The main topics of contents are Mining and Geotechnology, Metallurgy and Materials, Geology and Geoenvironment.

RMZ-M&G publishes original Scientific articles, Review papers, Preliminary notes, Professional papers **in English**. In addition, evaluations of other publications (books, monographs,...), In memoriam, Professional remarks and reviews are welcome. The Title, Abstract and Key words in Slovene will be included by the author(s) or will be provided by the referee or the Editorial Office.

**** Additional information and remarks for Slovenian authors:***
Only Professional papers, Publications notes, Events notes, Discussion of papers and In memoriam, will be exceptionally published in the Slovenian language.

Authorship and originality of the contributions. Authors are responsible for originality of presented data, ideas and conclusions as well as for correct citation of data adopted from other sources. The publication in RMZ-M&G obligate authors that the article will not be published anywhere else in the same form.

Specification of Contributions

RMZ-M&G will publish papers of the following categories:

Full papers (optimal number of pages is 7 to 15, longer articles should be discussed with Editor prior to submission). An abstract is required.

- **Original scientific papers** represent unpublished results of original research.
- **Review papers** summarize previously published scientific, research and/or expertise articles on the new scientific level and can contain also other cited sources, which are not mainly result of author(s).

- **Preliminary notes** represent preliminary research findings, which should be published rapidly.
- **Professional paper**s are the result of technological research achievements, application research results and information about achievements in practice and industry.

Short papers (the number of pages is limited to 1 for Discussion of papers and 2 pages for Publication note, Event note and In Memoriam). No abstract is required for short papers.

- **Publication notes** contain author's opinion on new published books, monographs, textbooks, or other published material. A figure of cover page is expected.
- **Event notes** in which descriptions of a scientific or professional event are given.
- **Discussion of papers (Comments)** where only professional disagreements can be discussed. Normally the source author(s) reply the remarks in the same issue.
- **In memoriam** (a photo is expected).

Supervision and review of manuscripts. All manuscripts will be supervised. The referees evaluate manuscripts and can ask authors to change particular segments, and propose to the Editor the acceptability of submitted articles. Authors can suggest the referee but Editor has a right to choose another. **The name of the referee remains anonymous.** The technical corrections will be done too and authors can be asked to correct missing items. The final decision whether the manuscript will be published is made by the Editor in Chief.

The Form of the Manuscript

The manuscript should be submitted as a complete hard copy including figures and tables. The figures should also be enclosed separately, both charts and photos in the original version. In addition, all material should also be provided in electronic form on a diskette or a CD. The necessary information can conveniently also be delivered by E-mail.

Composition of manuscript is defined in the attached Template

The original file of Template is available on RMZ-Materials and Geoenvironment Home page address:

http://www.rmz-mg.com

References - can be arranged in two ways:
- first possibility: alphabetic arrangement of first authors - in text: (Borgne, 1955), or
- second possibility: [1] numerated in the same order as cited in the text: example[1]

Format of papers in journals:

Le Borgne, E. (1955): Susceptibilite magnetic anomale du sol superficiel. *Annales de Geophysique*, 11, pp. 399–419.

Format of books:

Roberts, J. L. (1989): Geological structures, *MacMillan*, *London*, 250 p.

Text on the hard print copy can be prepared with any text-processor. The electronic version on the diskette, CD or E-mail transfer should be in MS Word or ASCII format.
Captions of figures and tables should be enclosed separately.
Figures (graphs and photos) and tables should be original and sent separately in addition to text. They can be prepared on paper or computer designed (MSExcel, Corel, Acad).
Format. Electronic figures are recommended to be in CDR, Al, EPS, TIF or JPG formats. Resolution of bitmap graphics (TIF, JPG) should be at least 300 dpi. Text in vector graphics (CDR, Al, EPS) must be in MSWord Times typography or converted in curves.
Color prints. Authors will be charged for color prints of figures and photos.
Labeling of the additionally provided material for the manuscript should be very clear and must contain at least the lead author's name, address, the beginning of the title and the date of delivery of the manuscript. In case of an E-mail transfer the exact message with above asked data must accompany the attachment with the file containing the manuscript.

Information about RMZ-M&G:
Editor in Chief prof. dr. Peter Fajfar (phone: ++386 1 4250-316) or
Secretary Barbara Bohar Bobnar, univ. dipl. ing. geol. (phone: ++386 1 4704-630),
Aškerčeva 12, 1000 Ljubljana, Slovenia
or at E-mail addresses:
peter.fajfar@ntf.uni-lj.si,
barbara.bohar@ntf.uni-lj.si

Sending of manuscripts. Manuscripts can be sent by mail to the **Editorial Office** address:

- RMZ-Materials & Geoenvironment
  Aškerčeva 12,
  1000 Ljubljana, Slovenia

or delivered to:

- **Reception** of the Faculty of Natural Science and Engineering (for RMZ-M&G)
  Aškerčeva 12,
  1000 Ljubljana, Slovenia
- E-mail - addresses of Editor and Secretary
- You can also contact them on their phone numbers.

These instructions are valid from August 2009

NAVODILA AVTORJEM

RMZ-MATERIALS AND GEOENVIRONMENT (RMZ- Materiali in geookolje) – kratica RMZ-M&G - je revija (ustanovljena kot zbornik 1952 in preimenovana v revijo RMZ-M&G 1998), ki izhaja vsako leto v štirih zvezkih. V reviji objavljamo prispevke s področja rudarstva, geotehnologije, materialov, metalurgije, geologije in geookolja.

RMZ- M&G objavlja izvirne znanstvene, pregledne in strokovne članke ter predhodne objave samo v angleškem jeziku. Strokovni članki so lahko izjemoma napisani v slovenskem jeziku. Kot dodatek so zaželene recenzije drugih publikacij (knjig, monografij …), nekrologi In Memoriam, predstavitve znanstvenih in strokovnih dogodkov, kratke objave in strokovne replike na članke objavljene v RMZ-M&G v slovenskem ali angleškem jeziku. Prispevki naj bodo kratki in jasni.

Avtorstvo in izvirnost prispevkov. Avtorji so odgovorni za izvirnost podatkov, idej in sklepov v predloženem prispevku oziroma za pravilno citiranje privzetih podatkov. Z objavo v RMZ-M&G se tudi obvežejo, da ne bodo nikjer drugje objavili enakega prispevka.

Vrste prispevkov

Optimalno število strani je 7 do 15, za daljše članke je potrebno soglasje glavnega urednika.
Izvirni znanstveni članki opisujejo še neobjavljene rezultate lastnih raziskav.
Pregledni članki povzemajo že objavljene znanstvene, raziskovalne ali strokovne dosežke na novem znanstvenem nivoju in lahko vsebujejo tudi druge (citirane) vire, ki niso večinsko rezultat dela avtorjev.
Predhodna objava povzema izsledke raziskave, ki je v teku in zahteva hitro objavo.
Strokovni članki vsebujejo rezultate tehnoloških dosežkov, razvojnih projektov in druge informacije iz prakse.
Recenzije publikacij zajemajo ocene novih knjig, monografij, učbenikov, razstav …(do dve strani; zaželena slika naslovnice in kratka navedba osnovnih podatkov - izkaznica).

In memoriam (do dve strani, zaželena slika).
Strokovne pripombe na objavljene članke ne smejo presegati ene strani in opozarjajo izključno na strokovne nedoslednosti objavljenih člankov v prejšnjih številkah RMZ-M&G. Praviloma že v isti številki avtorji prvotnega članka napišejo odgovor na pripombe.
Poljudni članki, ki povzemajo znanstvene in strokovne dogodke (do dve strani).

Recenzije. Vsi prispevki bodo predloženi v recenzijo. Recenzent oceni primernost prispevka za objavo in lahko predlaga kot pogoj za objavo dopolnilo k prispevku. Recenzenta izbere Uredništvo med strokovnjaki, ki so dejavni na sorodnih področjih, kot jih obravnava prispevek. Avtorji lahko sami predlagajo recenzenta, vendar si uredništvo pridržuje pravico, da izbere drugega recenzenta. **Recenzent ostane anonimen**. Prispevki bodo tudi tehnično ocenjeni in avtorji so dolžni popraviti pomanjkljivosti. Končno odločitev za objavo da glavni in odgovorni urednik.

Oblika prispevka

Prispevek predložite v tiskanem oštevilčenem izvodu (po možnosti z vključenimi slikami in tabelami) ter na disketi ali CD, lahko pa ga pošljete tudi prek E-maila. Slike in grafe je možno poslati tudi risane na papirju, fotografije naj bodo originalne.

Razčlenitev prispevka:

Predloga za pisanje članka se nahaja na spletni strani:

http://www.rmz-mg.com/predloga.htm

Seznam literature je lahko urejen na dva načina:
-po abecednem zaporedju prvih avtorjev ali
-po [1]vrstnem zaporedju citiranosti v prispevku.

Oblika je za oba načina enaka:
Članki:

> Le Borgne, E. (1955): Susceptibilite magnetic anomale du sol superficiel. *Annales de Geophysique*; Vol. 11, pp. 399–419.

Knjige:

ROBERTS, J. L. (1989): Geological structures, *MacMillan*, *London*, 250 p.

Tekst izpisanega izvoda je lahko pripravljen v kateremkoli urejevalniku. Na disketi, CD ali v elektronskem prenosu pa mora biti v MS Word ali v ASCII obliki.
Naslovi slik in tabel naj bodo priloženi posebej. Naslove slik, tabel in celotno besedilo, ki se pojavlja na slikah in tabelah, je potrebno navesti v angleškem in slovenskem jeziku.
Slike (ilustracije in fotografije) in tabele morajo biti izvirne in priložene posebej. Njihov položaj v besedilu mora biti jasen iz priloženega kompletnega izvoda. Narejene so lahko na papirju ali pa v računalniški obliki (MS Excel, Corel, Acad).
Format elektronskih slik naj bo v EPS, TIF ali JPG obliki z ločljivostjo okrog 300 dpi. Tekst v grafiki naj bo v Times tipografiji.
Barvne slike. Objavo barvnih slik sofinancirajo avtorji
Označenost poslanega materiala. Izpisan izvod, disketa ali CD morajo biti jasno označeni – vsaj z imenom prvega avtorja, začetkom naslova in datumom izročitve uredništvu RMZ-M&G. Elektronski prenos mora biti pospremljen z jasnim sporočilom in z enakimi podatki kot velja za ostale načine posredovanja.

Informacije o RMZ-M&G: urednik prof. dr. Peter Fajfar, univ. dipl. ing. metal. (tel. ++386 1 4250316) ali tajnica Barbara Bohar Bobnar, univ. dipl. ing. geol. (tel. ++386 1 4704630), Aškerčeva 12, 1000 Ljubljana
ali na E-mail naslovih:
peter.fajfar@ntf.uni-lj.si
barbara.bohar@ntf.uni-lj.si

Pošiljanje prispevkov. Prispevke pošljite priporočeno na naslov **Uredništva:**

- RMZ-Materials and Geoenvironment
  Aškerčeva 12,
  1000 Ljubljana, Slovenija

oziroma jih oddajte v

- **Recepciji** Naravoslovnotehniške fakultete (pritličje) (za RMZ-M&G)
  Aškerčeva 12,
  1000 Ljubljana, Slovenija
- Možna je tudi oddaja pri uredniku oziroma pri tajnici.

Navodila veljajo od avgusta 2009.

TEMPLATE

The title of the manuscript should be written in bold letters (Times New Roman, 14, Center)

Naslov članka (Times New Roman, 14, Center)

Name Surname[1], …. , & Name Surname[X] (Times New Roman, 12, Center)

[x] University of ..., Faculty of ..., Address…, Country ... (Times New Roman, 11, Center)

*Corresponding author. E-mail: ... (Times New Roman, 11, Center)

Abstract (Times New Roman, Normal, 11): The abstract should be concise and should present the aim of the work, essential results and conclusion. It should be typed in font size 11, single-spaced. Except for the first line, the text should be indented from the left margin by 10 mm. The length should not exceed fifteen (15) lines (10 are recommended).

Izvleček (Times New Roman, navadno, 11): Kratek izvleček namena članka ter ključnih rezultatov in ugotovitev. Razen prve vrstice naj bo tekst zamaknjen z levega roba za 10 mm. Dolžina naj ne presega petnajst (15) vrstic (10 je priporočeno).

Key words: a list of up to 5 key words (3 to 5) that will be useful for indexing or searching. Use the same styling as for abstract.
Ključne besede: seznam največ 5 ključnih besed (3–5) za pomoč pri indeksiranju ali iskanju. Uporabite enako obliko kot za izvleček.

Introduction (Times New Roman, Bold, 12)

Two lines below the keywords begin the introduction. Use Times New Roman, font size 12, Justify alignment.

There are two (2) admissible methods of citing references in text:

1. by stating the first author and the year of publication of the reference in the parenthesis at the appropriate place in the text and arranging the reference list in the alphabetic order of first authors; e.g.:
   "Detailed information about geohistorical development of this zone can be found in: Antonijević (1957), Grubić (1962), ..."
   "… the method was described previously (Hoefs, 1996)"
2. by consecutive Arabic numerals in square brackets, superscripted at the appropriate place in the text and arranging the reference list at the end of the text in the like manner; e.g.:
   "... while the portal was made in Zope environment. [3]"

Materials and methods (Times New Roman, Bold, 12)

This section describes the available data and procedure of work and therefore provides enough information to allow the interpretation of the results, obtained by the used methods.

Results and discussion (Times New Roman, Bold, 12)

Tables, figures, pictures, and schemes should be incorporated in the text at the appropriate place and should fit on one page. Break larger schemes and tables into smaller parts to prevent extending over more than one page.

Conclusions (Times New Roman, Bold, 12)

This paragraph summarizes the results and draws conclusions.

Acknowledgements (Times New Roman, Bold, 12, Center - optional)

This work was supported by the ****.

References (Times New Roman, Bold, 12)

In regard to the method used in the text, the styling, punctuation and capitalization should conform to the following:

FIRST OPTION - in alphabetical order

Casati, P., Jadoul, F., Nicora, A., Marinelli, M., Fantini-Sestini, N. & Fois, E. (1981): Geologia della Valle del'Anisici e dei gruppi M. Popera - Tre Cime di Lavaredo (Dolomiti Orientali). *Riv. Ital. Paleont.*; Vol. 87, No. 3, pp. 391–400, Milano.

Folk, R. L. (1959): Practical petrographic classification of limestones. *Amer. Ass. Petrol. Geol. Bull.;* Vol. 43, No. 1, pp. 1–38, Tulsa.

SECOND OPTION - in numerical order

[1] Trček, B. (2001): *Solute transport monitoring in the unsaturated zone of the karst aquifer by natural tracers.* Ph. D. Thesis. Ljubljana: University of Ljubljana 2001; 125 p.

[2] Higashitani, K., Iseri, H., Okuhara, K., Hatade, S. (1995): Magnetic Effects on Zeta Potential and Diffusivity of Nonmagnetic Particles. *Journal of Colloid and Interface Science, 172*, pp. 383–388.

Citing the Internet site:

CASREACT-Chemical reactions database [online]. Chemical Abstracts Service, 2000, updated 2. 2. 2000 [cited 3. 2. 2000]. Accessible on Internet: http://www.cas.org/CASFILES/casreact.html.

Texts in Slovene (title, abstract and key words) can be written by the author(s) or will be provided by the referee or by the Editorial Board.

PREDLOGA ZA SLOVENSKE ČLANKE

Naslov članka (Times New Roman, 14, Na sredino)

The title of the manuscript should be written in bold letters (Times New Roman, 14, Center)

Ime Priimek[1], …, Ime Priimek[X] (Times New Roman, 12, Na sredino)

[X]Univerza…, Fakulteta…, Naslov…, Država… (Times New Roman, 11, Center)

*Korespondenčni avtor. E-mail: ... (Times New Roman, 11, Center)

Izvleček (Times New Roman, Navadno, 11): Kratek izvleček namena članka ter ključnih rezultatov in ugotovitev. Razen prve j bo tekst zamaknjen z levega roba za 10 mm. Dolžina naj ne presega petnajst (15) vrstic (10 je priporočeno).

Abstract (Times New Roman, Normal, 11): The abstract should be concise and should present the aim of the work, essential results and conclusion. It should be typed in font size 11, single-spaced. Except for the first line, the text should be indented from the left margin by 10 mm. The length should not exceed fifteen (15) lines (10 are recommended).

Ključne besede: seznam največ 5 ključnih besed (3–5) za pomoč pri indeksiranju ali iskanju. Uporabite enako obliko kot za izvleček.
Key words: a list of up to 5 key words (3 to 5) that will be useful for indexing or searching. Use the same styling as for abstract.

Uvod (Times New Roman, Krepko, 12)

Dve vrstici pod ključnimi besedami se začne Uvod. Uporabite pisavo Times New Roman, velikost črk 12, z obojestransko poravnavo. Naslovi slik in tabel (vključno z besedilom v slikah) morajo biti v slovenskem jeziku.

Slika (Tabela) X. Pripadajoče besedilo k sliki (tabeli)

Obstajata dve sprejemljivi metodi navajanja referenc:

1. z navedbo prvega avtorja in letnice objave reference v oklepaju na ustreznem mestu v tekstu in z ureditvijo seznama referenc po abecednem zaporedju prvih avtorjev; npr.:

"Detailed information about geohistorical development of this zone can be found in: Antonijević (1957), Grubić (1962), ..."

"… the method was described previously (Hoefs, 1996)"

ali

2. z zaporednimi arabskimi številkami v oglatih oklepajih na ustreznem mestu v tekstu in z ureditvijo seznama referenc v številčnem zaporedju navajanja; npr.;

"... while the portal was made in Zope[3] environment."

Materiali in metode (Times New Roman, Krepko, 12)

Ta del opisuje razpoložljive podatke, metode in način dela ter omogoča zadostno količino informacij, da lahko z opisanimi metodami delo ponovimo.

Rezultati in razprava (Times New Roman, Krepko, 12)

Tabele, sheme in slike je treba vnesti (z ukazom Insert, ne Paste) v tekst na ustreznem mestu. Večje sheme in tabele je po treba ločiti na manjše dele, da ne presegajo ene strani.

Sklepi (Times New Roman, Krepko, 12)

Povzetek rezultatov in sklepi.

Zahvale (Times New Roman, Krepko, 12, Na sredino - opcija)

Izvedbo tega dela je omogočilo ……

Viri (Times New Roman, Krepko, 12)

Glede na uporabljeno metodo citiranja referenc v tekstu upoštevajte eno od naslednjih oblik:

PRVA MOŽNOST (priporočena) - v abecednem zaporedju

Casati, P., Jadoul, F., Nicora, A., Marinelli, M., Fantini-Sestini, N. & Fois, E. (1981): Geologia della Valle del'Anisici e dei gruppi M. Popera – Tre Cime di Lavaredo (Dolomiti Orientali). *Riv. Ital. Paleont.*; Vol. 87, No. 3, pp. 391–400, Milano.

Folk, R. L. (1959): Practical petrographic classification of limestones. *Amer. Ass. Petrol. Geol. Bull.;* Vol. 43, No. 1, pp. 1–38, Tulsa.

DRUGA MOŽNOST - v numeričnem zaporedju

[1] Trček, B. (2001): *Solute transport monitoring in the unsaturated zone of the karst aquifer by natural tracers.* Ph. D. Thesis. Ljubljana: University of Ljubljana 2001; 125 p.

[2] Higashitani, K., Iseri, H., Okuhara, K., Hatade, S. (1995): Magnetic Effects on Zeta Potential and Diffusivity of Nonmagnetic Particles. *Journal of Colloid and Interface Science, 172*, pp. 383–388.

Citiranje spletne strani:

CASREACT-Chemical reactions database [online]. Chemical Abstracts Service, 2000, obnovljeno 2. 2. 2000 [citirano 3. 2. 2000]. Dostopno na svetovnem spletu: http://www.cas.org/CASFILES/casreact.html.

Znanstveni, pregledni in strokovni članki ter predhodne objave se objavijo v angleškem jeziku. Izjemoma se strokovni članek objavi v slovenskem jeziku.

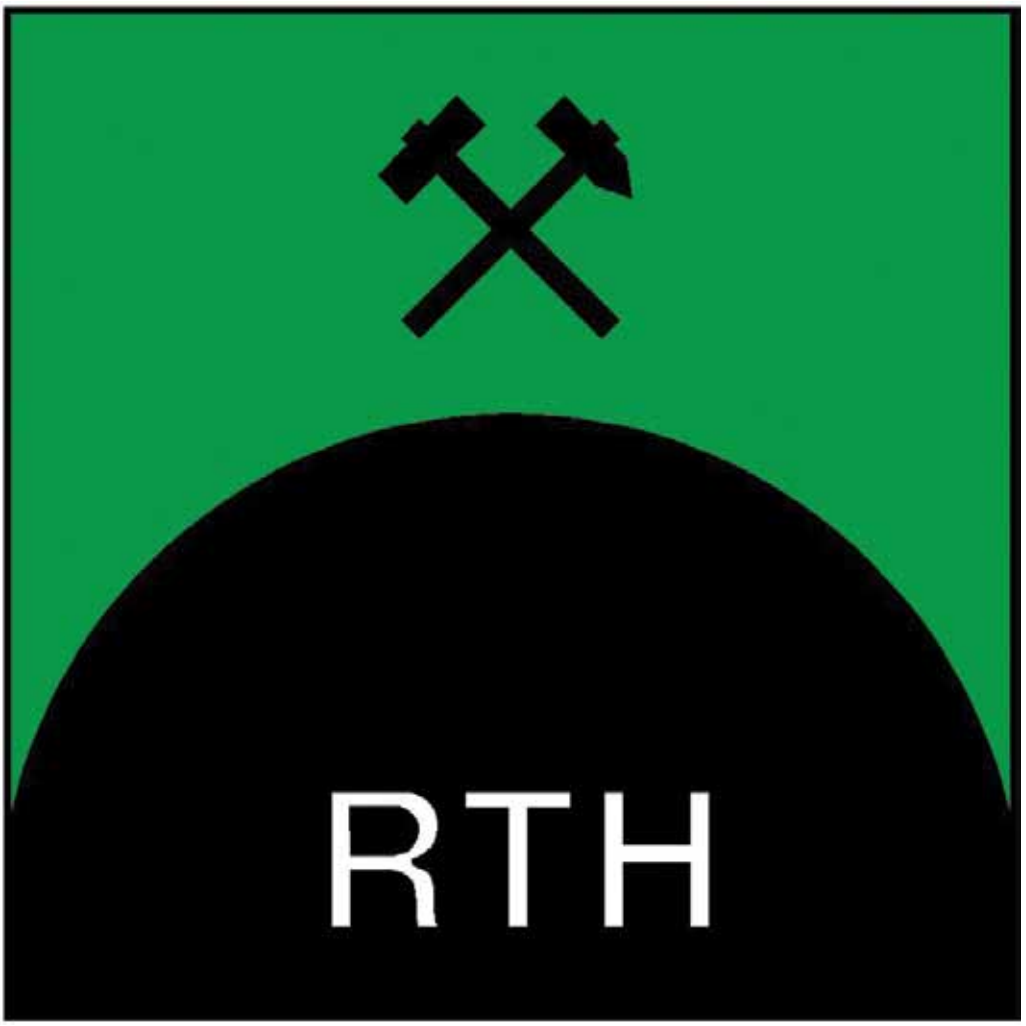
RTH

Slovenčeva 93
SI 1000 Ljubljana

tel.: +386 (1) 560 36 00
fax: +386 (1) 534 16 80
www.irgo.si

IRGO

Inženirska geologija
Hidrogeologija
Geomehanika
Projektiranje
Tehnologije za okolje
Svetovanje in nadzor

Če se premakne, boste izvedeli prvi

Leica Geosystems rešitve za opazovanje premikov

- **Geodetski senzorji**
  samodejni tahimetri, GPS in GNSS senzorji
- **Geotehnični senzorji**
  senzorji nagiba, Campbell datalogger
- **Drugi senzorji**
  meteo, senzorji nivoja
- **Programska oprema**
  za zajem in obdelavo podatkov, analizo opazovanj, alarmiranje, predstavitev rezultatov

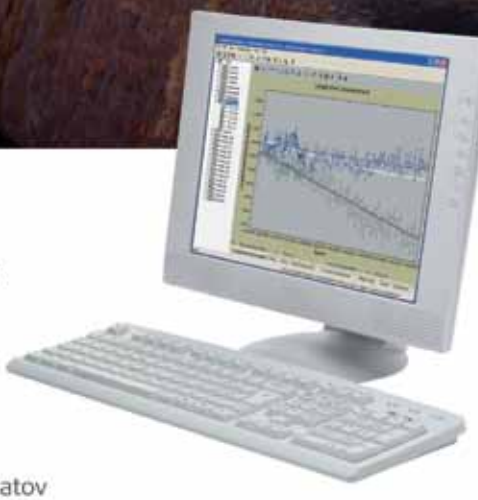

geo servis

Geoservis, d.o.o.
Litijska cesta 45, 1000 Ljubljana
t. (01) 586 38 30, i. www.geoservis.si

■ Authorized Leica Geosystems Distributor

- when it has to be **right**

Leica Geosystems